Cecilia Johanna Carneiro Håkegård

The influence of gas atmosphere on biocarbon production

June 2019

Master's thesis

2019

Cecilia Johanna Carneiro Håkegård

NTNU
Norwegian University of
Science and Technology
Faculty of Natural Sciences
Department of Biotechnology and Food Science

NTNU
Norwegian University of
Science and Technology

NTNU
Norwegian University of
Science and Technology

NTNU

Norwegian University of
Science and Technology

The influence of gas atmosphere on biocarbon production

Cecilia Johanna Carneiro Håkegård

Chemical engineering and Biotechnology
Submission date: June 2019
Supervisor: Per Bruheim, IBT
Co-supervisor: Per Carlsson, SINTEF Energy

Norwegian University of Science and Technology
Department of Biotechnology and Food Science

Preface

The research done in this master thesis was carried out for the Department of Biotechnology and Food Science at the Norwegian University of Science and Technology (NTNU) in collaboration with the Department of Thermal Energy at SINTEF Energy, spring 2019. The master thesis has taken part in PyrOPT, which is a cooperation project with SINTEF Energy and Elkem. I would like to thank my supervisors Per Bruheim and Per Carlsson for giving me the opportunity to write about replacing fossil coal with biocarbon as a reductant for silicon production. It has been inspiring to work on a project where the end goal is to create a more environmentally friendly industry. I would like to thank Per Carlsson for all the help and discussions throughout these last two semesters, and Per Bruheim for being my contact person to the institute.

I am sending my gratitude to Liang Wang at the Department of Thermal Energy at SINTEF Energy for performing the SEM analysis, and to Elin H. Albertsen at the department of Material Science at NTNU for performing the BET and pycnometer analysis.

I would also like to thank Maria N.P Olsen from the Department of Thermal Energy at SINTEF Energy, for being with me through all the experiments and for helping me whenever I had questions.

I am grateful for all the support of my friends and family throughout these past five years. A special thanks to my dad, Jan Erik, for always helping me with subjects if I needed it.

Summary

Increasing focus on sustainable metal production has brought up the possibility of replacing fossil coal as a reducing agent with biocarbon to reduce CO_2 emissions. Elkem is one of the world's leading suppliers of silicon alloys. In 2017, 21% of the reducing agent in Elkem's process was from renewable resources. The amount of biocarbon used in their process today corresponds to approximately 35000 tons/year, which will be increased to 188000 tons/year in 2030. Biocarbon is produced by thermal decomposition of biomass in the absence of oxygen, which is a process called pyrolysis. Two challenges Elkem face are that biocarbon is more expensive than fossil coal, and their process will require a significant amount of Norwegian wood dedicated to industry to meet their future goals. A promising solution to both these challenges is to increase the biocarbon yield from pyrolysis. The objective of this master thesis was to investigate the possibility of changing the gas atmosphere to increase the biocarbon yield and/or its properties. Seven different experiments were conducted, where three different carrier gases were tested; N_2 (reference), CO_2 and CO. Results from the CO experiments were compared with simulated results. The biocarbon, condensate and gas yields were determined after the experiments. Proximate analysis, thermogravimetric analysis (TGA), Brunauer–Emmett–Teller (BET) surface area, density analysis and scanning electron microscopy (SEM) were used to analyze the produced biocarbon.

The biocarbon and condensate yields were not affected by altering the carrier gas. They were found to be 29.8±0.3 wt.% and 46.0±0.5 wt.%, respectively, for experiments with hold temperature 480°C. When the pyrolysis temperature was increased to 580°C the biocarbon yield decreased to 27.1 wt.%. Proximate analysis revealed that the fixed carbon (FC) content was higher for biocarbon produced in CO_2 and CO atmosphere. The fixed carbon yield was found to be 0.227 g FC/g biomass for biocarbon produced in N_2 atmosphere at 480°C, while it was found to be 0.243 and 0.240 g FC/g biomass for biocarbon produced in CO_2 and CO atmosphere, respectively. TGA results showed that biocarbon from the reference experiment had higher mass loss between 400°C and 600°C than biocarbon from experiments with CO_2 and CO as carrier gas. SEM images revealed that when N_2 was used as carrier gas during the hold phase, the biocarbon had spiderweb-like structures in some of the pores. This was not observed in the biocarbon samples produced in pure CO_2 or CO atmosphere. The results obtained in this master thesis are contradictory, yet promising, and indicate that the biocarbon quality can be increased by changing the pyrolysis gas atmosphere, without decreasing the biocarbon yield.

Sammendrag

Fokuset på en mer bærekraftig metallindutri har økt de siste årene. Et alternativ for å redusere CO_2 utslippene er å erstatte fossilt kull som reduksjonmiddel med trekull. Elkem er verdensledende innenfor produksjon av silisium og ferrosilisium. I 2017 var 21% av reduksjonsmiddelet i Elkems prosess basert på fornybare råvarer. Mengden trekull som brukes i deres prosess i dag er ca. 35000 tonn/år, som vil øke til 188000 tonn/år i 2030. Trekull produseres ved termisk dekomponering av biomasse uten tilgang til oksygen. Denne prosessen heter pyrolyse. Overgangen fra fossilt kull til trekull byr på spesielt to utfordringer for Elkem. Fossilt kull er billigere enn trekull, og de vil trenge en stor andel av tremassen tilgjengelig for norsk industri for å produsere alt trekullet de trenger. En løsning til begge utfordringene er å øke utbyttet av trekull fra pyrolyseprosessen. Målet i denne masteroppgaven var å undersøke om endring av gassatmosfæren i pyrolysereaktoren kan øke utbyttet av trekull eller endre dens egenskaper. Syv forskjellige eksperimenter ble utført, hvor tre forskjellige gasser ble testet; N_2 (inert), CO_2 og CO. Resultatene fra CO eksperimentene ble sammenlignet med simuleringsresultater. Utbyttet av trekull, kondensat og gass ble beregnet etter hvert eksperiment. Proximate analyse, termogravimetrisk (TGA) analyse, Brunauer–Emmett–Teller (BET) overflateareals analyse, tetthetsanalyse og Scanning electron miktroskopi (SEM) analyse ble brukt for å analysere trekullet fra eksperimentene.

Utbyttet av trekull og kondensat ble ikke påvirket av å endre gassatmosfæren. De ble funnet til å være 29.8±0.3 wt.% og 46.0±0.4 wt.%, respektivt, for alle eksperimentene med hold-temperatur 480°C. For eksperimentene med hold-temperatur 580°C ble trekullutbyttet 27.1 wt%, uavhengig av gassatmosfære. Proximate analysen viste at trekullet som var produsert i CO_2 eller CO atmosfære hadde signifikant høyere fikst karbon (FC) innhold. Fikst karbon utbyttet ble funnet til å være 0.227g FC/g biomasse for trekullet som ble produsert i ren N_2 atmosfære ved 480°C, mens 0.243 og 0.240g FC/g biomasse for trekullet som ble produsert i CO_2 og CO atmosfære ved samme temperatur, respektivt. TGA resultatene viste at massetapet var større mellom 400 og 600°C for trekullet produsert i inert atmosfære enn trekullet produsert i CO_2 og CO. SEM bildene viste at trekullet som ble produsert i eksperimenter hvor N_2 var brukt under holdfasen hadde spindelvevlignende strukturer i noen av porene. Resultatene i denne masteroppgaven er lovende, men noe motsigende. De viser at det er mulig å forbedre trekullkvaliteten ved å ha CO_2 eller CO atmosfære, uten å påvirke trekullutbyttet negativt.

Contents

1 Introduction and background

The master thesis was conducted in cooperation with SINTEF Energy and Elkem and takes part in the PyrOPT research project. PyrOPT stands for Optimized biomass pyrolysis for the production of tailor-made renewable silicon reductant materials. The project is a part of Elkem's vision of a carbon-neutral metal production [1]. The focus of this report is on how process parameters such as gas atmosphere and temperature influence biocarbon production.

The metallurgical industry is energy demanding and a significant contributor to global CO_2 emissions. Due to stricter regulations, the industry has to find ways to decrease their CO_2 footprint. Elkem is one of the world's leading suppliers of metallurgical silicon and ferrosilicon [2]. In 2017, their annual global CO_2 emission was 1 773 000 tons, and their objective is to significantly reduce the CO_2 emissions generated from fossil resources [3]. The raw material in Elkem's process is quartz (SiO_2), which is reduced to silicon by carbon as reducing agent. In 2017, 21% of the reducing agent in Elkem's process was based on renewable resources. This corresponds to 135 000 tons/year reductant and consists of a mix of biocarbon and wood chips [4]. A simplified chemical reaction of the production of silicon from quartz is shown in Equation (1.1).

$$SiO_2 + C\,(s) \longrightarrow Si\,(s) + CO_2 \tag{1.1}$$

A promising alternative to reduce CO_2 emissions from the Norwegian ferrosilicon industry is by substituting fossil coal with biocarbon as reducing agent [5]. Biocarbon is produced by pyrolysis, which is the thermal decomposition of biomass in the absence of oxygen [6]. The products from pyrolysis can be categorized into three main classes; gas-phase, vapor phase and solid phase (biocarbon). The major components of the gas-phase are CO, CO_2, CH_4, H_2 and low molecular weight hydrocarbons, while the vapor phase mainly consists of water, organic acids, alcohols and other oxyanates. The amount of each phase, as well as the quality, depend on several factors such as temperature, residence time, pressure, moisture content and presence of catalyst [7–12].

As reductant biocarbon has some advantages over conventional fossil coal. It has lower sulfur, phosphor and ash content, higher porosity and high reactivity towards SiO_2 [12, 13]. Another significant positive feature is the possibility of a neutral CO_2 balance. However, fossil coal remains highly available and cheap compared to biocarbon. It is therefore crucial to find ways to make biocarbon more economically feasible.

Elkem aim to have a sustainable biocarbon production. This means that the biomass input should give maximum yield of solid carbon, that all side streams are utilized, and that the energy-demanding processes are driven by available energy sources [1]. An illustration of their vision is presented in Figure 1.1. Placing the biocarbon production (pyrolysis factory) near an existing silicon smelter would be an alternative to facilitate the integration of energy flows. Byproducts from the pyrolysis process could potentially be utilized to produce fuels and chemicals.

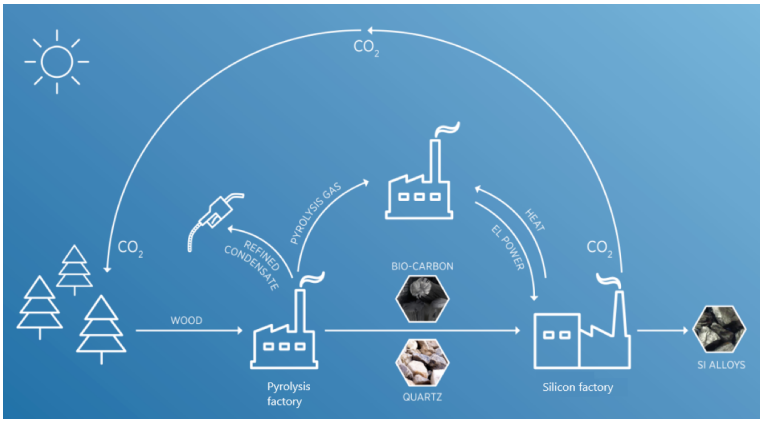

Figure 1.1: Illustration of Elkem's vision of a carbon neutral metal production [14].

Elkem's future goals are that 40% of the reducing agent in their process will be biocarbon in 2030, and 100% of the reducing agent will come from renewable resources in 2050 [14]. Today they use approximately 35 000 tons biocarbon annually for their silicon and ferrosilicon production. In 2030 the goal is to increase the amount of biocarbon to 188 000 tons/year [4]. This means that the transition from fossil coal to biocarbon is happening relatively fast. One alternative, which could make this change less challenging and more economically feasible, is to find ways to increase the product yield of biocarbon [5]. This would also decrease the need for raw material.

A specialization project was conducted prior to the master thesis to screen how different process parameters might affect the product composition from pyrolysis. Thermodynamic and kinetic simulations were performed to investigate the influence of feedstock description, temperature, gas atmosphere and moisture content by using the softwares FactSage and MATLAB. Experimental work was not performed during the specialization project.

Thermodynamic equilibrium simulations showed that a high solid carbon yield was obtained at moderate temperatures and that it decreased significantly at temperatures above 500°C. The thermodynamic study also indicated that the addition of CO or CH_4 gas to the system had promising results in regards to increasing the solid carbon yield. There will be large access of CO gas if quartz (SiO_2) is reduced to silicon in a closed furnace, which can be recycled to the pyrolysis factory. There will also be large amounts of CO_2 available as long as the silicon furnace stays open. This is also an alternative gas which can be recycled back to the pyrolysis process. The kinetic study was performed to investigate the influence of adding CO or CH_4 gas to the pyrolysis reactor during the hold phase. Due to relatively low temperatures it was considered valid to assume a reaction controlled system. Mass transfer and diffusion were therefore not taken into account in the calculations. The simulations showed that the addition of CO and CH_4 might increase the biocarbon yield, but that it greatly depends on the available surface area of the biocarbon. The reactions seemed to be very slow at moderate temperatures, and the observed effects were lower than for the equilibrium simulations.

The decomposition mechanism of biomass is complex and not well understood. The specialization project created a path for the master thesis. In this work, it will be tested if experimental results are comparable with simulated results. Based on information found in literature and results from previous work a hypothesis has been formulated. It states that CO_2 can have a positive effect on the production of biocarbon at low temperatures, but will negatively affect the biocarbon yield at higher temperatures. On the other hand, CO can have a positive effect on the biocarbon yield even at relatively high temperatures. It is therefore these two gases which will be tested experimentally and compared to experiments using inert N_2 atmosphere.

1.1 Literature study

Biocarbon has been used for centuries as fuel for cooking and was essential for the extraction of iron from iron ore in the pre-industrial era [15]. In more modern times all three product phases from pyrolysis have received increasing attention due to their contribution as renewable fuels. The gas-phase can, for example, be upgraded to syngas, a mixture of CO and H_2, which are important precursors for several chemicals. It can also be used directly as fuel. The vapor phase, bio-oil, is a promising way of converting biomass into a denser fuel. However, bio-oils tend to be too acidic and contain highly reactive oxygenated species which are not suitable for long-term storage [16]. Biocarbon is the solid product from pyrolysis, and still

serves as an essential cooking fuel in many parts of the world. However, it is also becoming an increasingly important reductant for the metallurgical industry, in addition to being used as gas adsorbent and antibacterial agent [17–19].

The product distribution from pyrolysis is affected by several factors which include both process and feedstock parameters. The focus of this report will be on the former. Some frequently discussed process parameters are temperature, pressure and carrier gas. The effects of temperature on the pyrolysis product composition are rather known in literature. There is a general agreement that increasing temperature leads to lower biocarbon yield and higher gas yield [19–21]. This is due to the fact that gasification reactions, reactions which convert char into gases, are strongly favored at high temperatures [22]. The process is called slow pyrolysis when the heating rate is less than 80°C/min and the temperature ranges between 350-750°C [23]. The main product from slow pyrolysis is biocarbon. On the contrary, the main product of fast pyrolysis is bio-oil. A higher biocarbon yield from slow pyrolysis processes is argued to be due to the longer residence time of hot vapors [24].

When it comes to the effects of pressure on the biocarbon yield, several researchers can refer to contradictory results. Skreiberg *et al.* (2018) argue that increased system pressure increases the gas residence time inside and outside the char matrix, and that this might contribute to secondary char formation. However, they point out that pressurized systems also introduce increased complexity and costs, and thereby the overall benefit is not clear [17]. Blackladder and Rensfelt (1985) reported an observed increase in biocarbon yield from 21% to 28% when the pressure was raised from 0.1MPa to 4MPa [25]. Wang *et al.* (2015) reported an observed increase from 18.89% to 24.58% in the biocarbon yield from forest residues when the pressure was raised to 2.2MPa from atmospheric pressure [26]. On the contrary, Azuara *et al.* (2017) reported a decrease in biocarbon yield from wine shoots when the pressure was raised from 0.1MPa to 1.1MPa, which is in disagreement with the above-mentioned studies [27]. Manyà *et al.* (2014) also reported a decrease in biocarbon yield from olive mill waste, when the pressure was increased from 0.1MPa to 1.0MPa. They claim that a possible explanation could be that elevated pressure might enhance the kinetics of steam gasification reactions, even at relatively low temperatures [28].

Thermodynamic equilibrium calculations indicate that biocarbon is the preferred pyrolysis product at moderate temperatures [19]. However, there is no guarantee that equilibrium will be established. Some claim that equilibrium cannot be assumed at temperatures below 500°C [29]. Although equilibrium simulations can

be useful to predict the pyrolysis yield, more precise predictions should also consider kinetics. However, this has proved to be challenging due to the complexity of biomass conversion mechanism. Several reaction mechanisms of primary pyrolysis have been proposed in literature, where two of them are one-component and multi-component mechanism. One-component mechanism usually consists of three parallel reactions, where the main product classes (biocarbon, vapors and gases) are simultaneously produced from wood/biomass. Activation energies have been purposed for one-component mechanism. At moderate temperatures, the process is more likely to be reaction limited, which means that the observed activation energy is close to the real activation energy. One-component mechanism gives the opportunity to predict the product yield and decomposition rates. However, it is argued that the assumption of one-component behavior for complex fuels, such as biomass, is too simplified and produces many inaccuracies [30]. There are fewer multi-component mechanisms suggested in literature. The work of Branca and Di Blasi from 2003, and Miller and Bellan from 1996 give two examples of multi-component mechanisms [31, 32]. The former is based on different zones in the weigh-loss curves, while the latter is based on decomposition of the pseudo-components hemicellulose, cellulose and lignin. Challenges with these two approaches were that the first approach could not predict product formation, while the second approach lacked the support of reliable and extensive experimental results [30]. These papers demonstrate some obstacles that still remain before having a generalized pyrolysis mechanism.

Kinetic studies of gasification reactions are more evolved and can be used as an alternative to generalized kinetics. Gasification of biomass means partial combustion of biomass to produce combustible gases and CO_2. As a simplification, there will be a focus on five gasification reactions in this report, which are presented in Section 2.2. Haus *et al.* (2018) studied gasification of coal by steam and CO_2, and found that steam gasification was slightly faster than CO_2 gasification. They came to the conclusion that the rate of CO_2 gasification was controlled by the chemical reaction, while the rate of steam gasification was influenced by both diffusion and the chemical reaction [33]. As early as 1946 Gadsby and co-workers established that the gasification reaction of coal and coconut char by CO_2 was retarded by partial pressure of CO and H_2 gas, which shows that kinetic studies of gasification reactions is nothing new [34]. Tomeczek and Stanislaw (2010) studied the kinetics of hydrogasification of coal, and reported that high coal conversion was only obtained at temperatures above 1200K [35]. Hydrogasification is the reaction between solid carbon and hydrogen to form methane, and is several order of magnitude slower than the two gasification reactions mentioned above [22].

These three reactions are all solid-gas reactions, and are therefore called heterogeneous reactions. They correspond to Reactions 1-3 in Section 2.2. A general rate expression for heterogeneous coal gasification has been formulated and used by some researchers [36–38]. This rate expression will be the basis for the kinetic simulations of the heterogeneous reactions in this work as well, and is presented in Section 2.2. The two remaining gasification reactions are gas-phase reactions. They are much faster than the solid-gas reactions due to mass transfer limitations for the heterogeneous reactions [22]. The water-gas shift reaction is a well known and studied chemical reaction due to its ability to form hydrogen gas from water and CO. Many rate expressions have been proposed for both high and moderate temperature intervals [39]. The second gas-phase reaction is the methane reforming reaction where CH_4 and steam reacts and form CO and H_2 gas, which are valuable industrial gases. Gasification reactions are in general favored at high temperatures. At moderate temperatures, the condensate concentration increase around the solid carbon particle and the gasification reactions cannot start until the devolatilization process is complete [22]. The rates of the five gasification reactions mentioned above have been investigated in the kinetic study and will be discussed further.

The main focus of this master thesis will be on the effects of gas atmosphere. The gas atmosphere can be manipulated by changing the carrier gas. Several researchers have compared the effects of using CO_2 as carrier gas instead of N_2. Since N_2 is an inert gas, it will only work as a gas diluting agent. Skreiberg *et al.* (2018) argue that N_2 reduces the partial pressure of CO_2 which shifts the equilibrium towards gasification of solid carbon to form more CO_2. By using CO_2 as carrier gas the equilibrium can be shifted towards more carbon staying in the solid phase. However, CO_2 will work as a gasifying agent if high temperatures are reached [17]. Liu *et al.* (2018) investigated the effects of temperature and CO_2 content on the physicochemical properties of pyrolysis biochar briquettes. They argue that increasing the CO_2 concentration of the carrier gas was beneficial for developing biocarbon with higher microporosity. However, the biocarbon yield decreased with increasing CO_2 concentration [40]. Azuara *et al.* (2017) also compared the effects having a CO_2 and N_2 atmospheres. They reported that the amount of biocarbon decreased in CO_2 atmosphere, whereas the amount of CO increased. They argued that the most likely reason was the Boudouard reaction taking place [27]. (The Boudouard reaction is presented in Section 2.2.) Zhang *et al.* (2011) investigated the effects of pyrolysis gas atmosphere, using corncobs as biomass source. They looked into the effects of CO, CH_4 and H_2 gas in addition to CO_2, and compared it to inert N_2 atmosphere. Zhang *et al.* reported that the biocarbon yield decreased

in CO_2 atmosphere compared to inert atmosphere, which is in agreement with the studies mentioned above. In addition, they reported that H_2 had a negative effect on the biocarbon yield, while CH_4 atmosphere slightly increased the yield. CO seemed to have little effect on the biocarbon yield, but gave the lowest bio-oil yield [41]. Moderate temperatures will be investigated during this master thesis. It would therefore be interesting to look into torrefaction of biomass, which has lower temperatures. Thanapal *et al.* (2014) and Bach *et al.* (2014) have investigated the effects of CO_2 atmosphere during torrefaction of woody biomass and Norwegian forest residues, respectively. Both studies used temperatures between 200-300°C. Alike some of the previous studies mentioned, they reported slightly lower biocarbon yield in CO_2 atmosphere compared to N_2 atmosphere. However, both reported an increase in fixed carbon as well as a decrease in volatile matter [42, 43]. Thanapal *et al.* studied the pore development using Scanning electron microscopy (SEM) and saw that more pores were visible for the biocarbon produced in CO_2 atmosphere. They argue that these new voids release volatile matter, which was the reason for decreased volatile matter, and increased fixed carbon [42]. On the other hand, the studies of Azuara *et al.* (2017) were conducted at 600°C, and they did not find a difference in the fixed carbon content of the biochar produced in CO_2 and N_2 atmosphere [27]. Duan *et al.* (2009) investigated coal pyrolysis in CO_2 atmosphere using TGA. They argued that CO_2 enhances volatile releasing rates even at 480°C [44]. It would therefore seem like the effects of CO_2 depends on the operating temperature. Not many have studied the effects of CO on the pyrolysis yield.

Some researchers have also investigated the effects of CO_2 atmosphere on the vapor product from pyrolysis. Liu *et al.* (2018) report that introducing CO_2 to the pyrolysis process enhances cracking of benzene rings, and fracturing of hydroxyl, methyl and methylene groups [45]. Kwon *et al.* (2012) investigated the ability of CO_2 to mitigate polycyclic aromatic hydrocarbons (PAH) during thermal decomposition of rubber. They reported that the formation of PAHs decreased considerably in CO_2 atmosphere, and dedicated it to enhanced thermal cracking [46]. However, condensate from pyrolysis of biomass at moderate temperatures does not contain much PAHs. Jindarom *et al.* (2007) looked into the effects of pyrolysing sewage sludge in CO_2 atmosphere. They analyzed the composition of the condensate and found that the condensate produced in CO_2 atmosphere had increased amount of oxygenated compounds and decreased amount of aliphatic compounds. They argue that the reason was insertion of CO_2 into the unsaturated aliphatic compounds, resulting in carboxylic- and ketone formation [47]. The gas produced from pyrolysis is also an interesting product which can be used for several

applications depending on the composition. Wang *et al.* (2018) investigated how the pyrolysis gas composition was affected by a carrier gas with increasing CO_2/N_2 ratio. They reported that introducing CO_2 to the system decreased the H_2,CH_4, and C_2H_6 yields [48].

The available surface area of biocarbon is a factor that plays a role in gasification kinetics, and thereby affects the biocarbon yield. It can vary greatly between different types of biocarbon, and the results also depend on the measurement method [49]. N_2 BET is the method recommended by the European Biochar Certificate (EBC) to measure the specific surface area of biocarbon [50]. However, the sample preparations are often not reported. Sigmund *et al.* (2017) identified that the degassing temperature at which the analysis method is conducted is crucial to determine the specific surface area and pore size. They argue that there is an urgent need to standardize measurement protocols [51]. Nevertheless, determining the BET surface area is a much-used method to analyze the reactivity of biocarbon. The importance of surface area has also been investigated during this master thesis.

1.2 Objective

The objective of this master thesis is to investigate the possibility of altering the pyrolysis gas atmosphere to increase the biocarbon yield and/or change the properties of the produced biocarbon. The kinetic model constructed in previous work will be further developed and compared with experimental results. The produced biocarbon will be analyzed using several analysis methods to investigate if altering the gas atmosphere has affected the properties of the biocarbon. Addition of CO gas will be tested based on the positive simulation results, and the fact that there will be large access to CO gas from Elkem's silicon production if the furnace is closed. CO_2 will be tested based on contradictory results found in literature.

1.3 Structure of the thesis

The master thesis is divided into three parts. First is a modeling part, which presents the simulations. Material and methods used for the simulations are explained, and the simulated results are presented and discussed. Second is the experimental work, which is the major part of the thesis. It explains which raw material was used, the apparatus, gases used for the experiments, how the experiments were performed and which analysis methods were used. All the experimental results are thereafter presented and discussed. The third part is the epilogue. Here, the practical implications of the results are presented together with how they might affect Elkem's goals in 2030. The thesis ends with a conclusion and suggestions for further work.

Part 1: Modeling

2 Materials and methods for the simulations

Simulations were performed to investigate the significance of biomass composition and to further develop a kinetic model which can be used to predict the effects of pyrolysis atmosphere. The kinetic model was used as guidance for some of the parameters of the experimental work, such as hold-time for the reaction and flow rate of added gas. From the thermodynamic and kinetic simulations performed during the specialization project it was found that addition of CO gas might have a positive effect on the biocarbon yield. CO was therefore used in the kinetic simulations during the master thesis.

2.1 Biomass composition

Different types of biomass can vary greatly in their element composition. The hydrogen-carbon (H/C) and oxygen-carbon (O/C) ratios are known to affect the solid carbon yield. Other elements such as nitrogen, sulfur and chlorine are also present, but usually in small amounts. They will form gases which dilute the gas phase to a minor extent, and do not significantly affect the fixed carbon yield [17]. Thereby, the focus has been on carbon, hydrogen and oxygen. High oxygen content is undesirable due to the formation of gases like CO and CO_2 which consume carbon. High hydrogen content is undesirable due to the formation of gases such as CH_4. Together, oxygen and hydrogen form water, which can also consume solid carbon. It then becomes clear that the presence of high amounts of both elements is negative. However, is there an optimum composition where high amounts of solid carbon are obtained besides having pure carbon from the beginning?

FactSage 7.0 was used to investigate the solution to this question. FactSage is a thermochemical software that was introduced in 2001, and is a fusion of the two software packages FACT-Win and ChemSage [52]. FactSage's Equilib module was used for the calculations. The module determines the composition of a mixture by using Gibbs' energy minimization principle. It does not take into account kinetics, which means that the software assumes that the reactions have infinite time [53]. Thereby it predicts the most likely composition at equilibrium, based solely on thermodynamic laws. The oxygen and hydrogen input parameters were varied and the simulations were run at constant temperature and pressure of 450°C and 1atm, respectively. FactPS was considered the only necessary package since only pure elements were simulated.

The amount of carbon input was constant at 49.65g for all the simulations, which is the amount of carbon given in the ultimate analysis of raw spruce chips provided by SINTEF Energy. The O/C molar ratio was varied between 0.45-0.91 moleO/-moleC, and the H/C molar ratio was varied between 0.12-3.63 moleH/moleC. The molar ratios obtained from the ultimate analysis of raw spruce chips were 0.67 and 1.48 for O/C and H/C, respectively. It was decided to investigate ratios above and below these values. The ratios used in the simulations are presented as both molar and mass ratios in Table 2.1.

Table 2.1: Simulated O/C and H/C ratios in FactSage. The carbon input was constant at 4.14moles (49.65g). For each O/C ratio all of the H/C ratios were simulated.

O/C		**H/C**	
Mole	**Mass**	**Mole**	**Mass**
0.45	0.60	0.24	0.02
0.53	0.71	0.73	0.06
0.67	0.89	1.48	0.12
0.83	1.11	2.42	0.20
0.91	1.21	3.63	0.30

The fixed carbon yield was calculated for all the H/C and O/C ratios. The fixed carbon yield is here defined as the amount of solid carbon after the simulation divided by the biomass input. The unit becomes grams of carbon per gram biomass.

2.2 Kinetics

A kinetic model was created during the specialization project. The main focus was to investigate the effects of introducing either CO or CH_4 gas to the system during the hold-phase. Here, the model has been developed further and the effects of surface area and flow rate were of interest. The available surface area of biocarbon can vary several orders of magnitude, depending on the preparation and analysis method. For the simulations the density of the solid carbon particle was varied between 50 and 150 kg/m^3 and the specific surface area was varied between 200 and 1000 m^2/g. The lowest volumetric surface area then became $0.1 \cdot 10^8$m^2/m^3 and the highest $1.5 \cdot 10^8$m^2/m^3. The carbon particle was considered a spherical particle with a constant diameter of 1cm. MATLAB was used as simulation tool.

The scripts can be found in Section A.2.1 in Appendix A. The temperature and pressure for the kinetic simulations were set to 480°C and 1 atm, respectively.

The kinetic model includes five gasification reactions. Thereof three heterogeneous reactions; Boudouard reaction, hydrogenation gasification and steam gasification, and two homogeneous reactions; methane reforming reaction and gas-shift reaction. The decomposition of biomass is complex and includes several more reactions than these five mentioned. However, global mechanisms are not well developed and simplifications were considered necessary for the scope of this project. The five gasification reactions included in the kinetic simulations are presented in Equation (2.1)-(2.5) with their corresponding heat of reaction [6].

$$\text{Boudouard reaction} : C(\text{s}) + CO_2(\text{g}) \rightleftharpoons 2CO(\text{g}), \qquad \Delta H_{rx} = 172.4 \frac{\text{kJ}}{\text{mol}} \quad (2.1)$$

$$\text{Hydrogenation reaction} : C(\text{s}) + 2H_2(\text{g}) \rightleftharpoons CH_4(\text{g}), \qquad \Delta H_{rx} = -74.8 \frac{\text{kJ}}{\text{mol}} \quad (2.2)$$

$$\text{Steam gasification} : C(\text{s}) + H_2O(\text{g}) \rightleftharpoons CO(\text{g}) + H_2(\text{g}), \Delta H_{rx} = 131.3 \frac{\text{kJ}}{\text{mol}} \quad (2.3)$$

$$\text{Methane reforming} : CH_4(\text{g}) + H_2O(\text{g}) \rightleftharpoons CO(\text{g}) + 3H_2(\text{g}), \Delta H_{rx} = 206.1 \frac{\text{kJ}}{\text{mol}} \quad (2.4)$$

$$\text{Water-gas shift} : CO(\text{g}) + H_2O(\text{g}) \rightleftharpoons CO_2(\text{g}) + H_2(\text{g}), \quad \Delta H_{rx} = -41.1 \frac{\text{kJ}}{\text{mol}} \quad (2.5)$$

The five reactions presented above have been extensively studied, and several kinetic parameters have been purposed. The kinetic data used in this thesis have been described by Yan *et al* [37]. It has been assumed that the system is reaction controlled, which is considered a valid assumption due to low temperatures. Thus, only the reaction rate constants have been included, while gas diffusion and ash-film diffusion constants have been excluded. The general rate expressions for the heterogeneous and homogeneous reactions used for the simulations are presented in Equation (2.6) and Equation (2.7), respectively.

$$R_s = k_s(p_i - p_i^*) \tag{2.6}$$

$$R = k_+ P_1^{p1} P_2^{p2} - k_- R_1^{r1} R_2^{r2} \tag{2.7}$$

R_s is the reaction rate of the heterogeneous reactions, k_s is the reaction rate constant, $(p_i - p_i^*)$ is the effective partial pressure of the gases, R is the reactions rate of the homogeneous reactions, k_+ and k_- are the reaction rate constants, P_1, P_2, R_1 and R_2 are the concentrations of products and reactants, respectively, with their corresponding stoichiometric coefficients $p1$, $p2$, $r1$ and $r2$. The kinetic data for the heterogeneous and homogeneous reactions are presented in Table 2.2 and Table 2.3, respectively.

Table 2.2: Kinetic correlation for heterogeneous gasification reactions [37].

Reaction	**Kinetic correlation**	**Unit**
$\mathrm{C(s) + CO_2 \rightleftharpoons 2\,CO}$	$k_s = 247\exp(\frac{-21060}{T})$	$\mathrm{g/cm^2/atm/s}$
	$p_i - p_i^* = p_{\mathrm{CO_2}}$	atm
$\mathrm{C(s) + 2\,H_2 \rightleftharpoons CH_4}$	$k_s = 0.12\exp(\frac{-17921}{T})$	$\mathrm{g/cm^2/atm/s}$
	$p_i - p_i^* = p_{\mathrm{H_2}} - \sqrt{\frac{p_{\mathrm{CH_4}}}{K_{eq}}}$	atm
	$\mathrm{K}_{eq} = \frac{0.175}{34713}\exp(\frac{18400}{1.8T})$	$\mathrm{atm^{-1}}$
$\mathrm{C(s) + H_2O \rightleftharpoons CO + H_2}$	$k_s = 247\exp(\frac{-21060}{T})$	$\mathrm{g/cm^2/atm/s}$
	$p_i - p_i^* = p_{\mathrm{H_2O}} - \frac{p_{\mathrm{H_2}} p_{CO}}{K_{eq}}$	atm
	$\mathrm{K}_{eq} = \exp(17.644 - \frac{30260}{1.8T})$	atm

Table 2.3: Kinetic correlations for homogeneous gasification reactions [37].

Reaction	**Kinetic correlations**	**Units**
$CH_4 + H_2O \rightleftharpoons CO + 3\,H_2$	$R_4 = k_4(\frac{p_{CH_4}}{RT})(\frac{p_{H_2O}}{RT})\text{-}k_{-4}(\frac{p_{CO}}{RT})(\frac{p_{H_2}}{RT})^3$	$mol/m^3/s$
	$k_4 = 312\exp(\frac{-2.0*10^4}{RT})$	$m^3/mol/s$
	$K_{eq} = 6.7125*10^{-24}\exp(\frac{27020}{RT})*(RT)^2$	$(mol/m^3)^2$
	$k_{-4} = \frac{k_4}{K_{eq}}$	$(m^3/mol)^3 s^{-1}$
$CO + H_2O \rightleftharpoons CO_2 + H_2$	$R_5 = k_5(\frac{p_{CO}}{RT})(\frac{p_{H_2O}}{RT})\text{-}k_{-5}(\frac{p_{CO_2}}{RT})(\frac{p_{H_2}}{RT})$	$mol/m^3/s$
	$k_5 = 2.75*10^3\exp(\frac{-8.36*10^4}{RT})$	$m^3/mol/s$
	$K_{eq} = 2.65*10^{-5}\exp(\frac{3956}{T})$	-
	$k_{-5} = \frac{k_5}{K_{eq}}$	$m^3/mol/s$

A reaction matrix was constructed to simulate the heterogeneous and homogeneous reactions in MATLAB. The matrix shows how each species contribute to the five reactions. It can be seen that the units for the heterogeneous reactions in Table 2.2 are $g/cm^2/s$, while for the homogeneous reactions in Table 2.3 are $mol/m^3/s$. A couple of conversions were therefore necessary before adding the reactions in the matrix. The molar mass of each species was used to convert grams to moles, and the volumetric surface area mentioned at the beginning of this section was used to convert cm^2 to m^3. By multiplying the heterogeneous reactions with the particle volume and the homogeneous reactions with the reactor volume, the final unit became mol/s. The reaction matrix used for the simulations is presented in Equation (2.8).

$$\begin{pmatrix} -1 & -1 & -1 & 0 & 0 \\ -1 & 0 & 0 & 0 & 1 \\ 2 & 0 & 1 & 1 & -1 \\ 0 & 1 & 0 & -1 & 0 \\ 0 & -2 & 1 & 3 & 1 \\ 0 & 0 & -1 & -1 & -1 \end{pmatrix} \begin{pmatrix} R_1 \\ R_2 \\ R_3 \\ R_4 \\ R_5 \end{pmatrix} = \begin{pmatrix} \frac{dC}{dt} \\ \frac{dCO_2}{dt} \\ \frac{dCO}{dt} \\ \frac{dCH_4}{dt} \\ \frac{dH_2}{dt} \\ \frac{dH_2O}{dt} \end{pmatrix} \tag{2.8}$$

R1 represents the Boudouard reaction, R2 the hydrogenation reaction, R3 the steam gasification reaction, R4 the methane reforming reaction and R5 the gas-shift reaction. The reactor was simulated as a continuous stirred tank reactor (CSTR) with gas purging to keep the pressure constant at 1 atm. Equations showing how the reactor was simulated can be found in Section A.2 in Appendix A.

The dependence of solid carbon yield on the available surface area was investigated

by altering the volumetric surface area and plotting the conversion of solid carbon as function of time. The conversion was defined as the increase in solid carbon from equilibrium state. The volumetric surface area was altered by varying the density of the solid carbon particle between 50 and 150kg/m^3, and the specific surface area between 200 and 1000m^2/g, and multiplying them. Since the addition of CO gas showed the most promising results in the specialization project all the simulations were based on addition of this gas. In addition, the derivative of the conversion was plotted as a function of time. By plotting the derivative it was possible to see at which time the change in conversion was most significant, and equally as important, where the change in conversion decreased. This would give an indication of how long the pyrolysis hold-time should last. If the change in conversion was low after a certain time it could be an alternative to stop the process at that time instead of continuing. The flow rate of CO was set to 2L/min per 100g biomass for these simulations.

The effects of altering the flow rate of CO were also investigated. The temperature of the added gas was set to 20°C, and the investigated flow rates were 1, 2, 3, 4 and 5L/min CO per 100g biomass. The conversion and the derivative of the conversion were plotted as functions of time. For these simulations the solid carbon density and specific surface area were set to 100kg/m^3 and 1000m^2/g, respectively.

3 Simulation results and discussion

The effects of biomass composition, surface area and gas flow rate of CO were investigated by thermodynamic equilibrium simulations and kinetic simulations. The results from the simulation will be compared with experimental results in Part 2: Experimental work.

3.1 Biomass composition

The biomass composition can greatly affect the carbon yield from pyrolysis. Here the focus has been on the most abundant elements in biomass, which are carbon, hydrogen and oxygen. The H/C and O/C ratios were varied, and the carbon yield at equilibrium was calculated using FactSage. The results are presented in Figure 3.1.

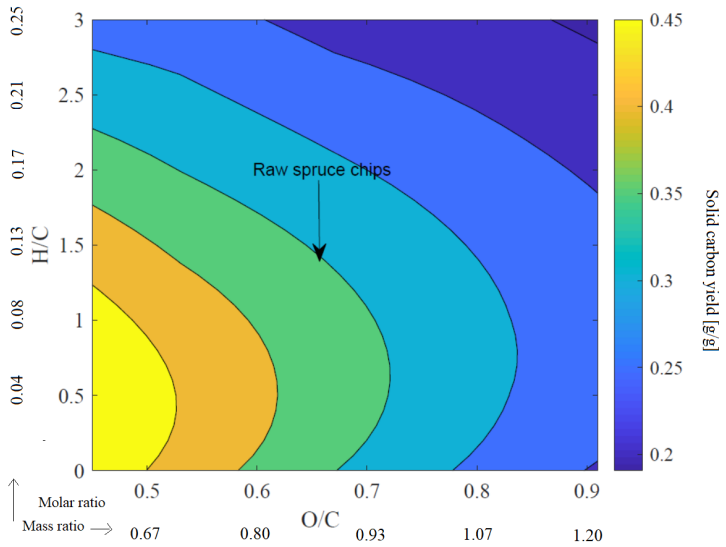

Figure 3.1: Contour plot of solid carbon yield as function of H/C and O/C ratios. Molar ratios are shown closest to the plot, and mass ratios further out. The color bar represents the carbon yield in grams carbon per gram biomass. T=450°C, P=1atm for the simulations.

The results in Figure 3.1 are shown as a contour plot. It can be seen that the O/C ratio has a strictly negative effect on the carbon yield. The higher the oxygen content, the lower the carbon output. However, this does not apply for hydrogen. It can be seen that the curve has an optimum that is greater than zero for the H/C ratio. This shows that as long as there is oxygen in the raw material, which is always the case for biomass, the optimal H/C ratio seems to be between 0.25 and 1.0 mole H/mole C. The contour plot shows that at this H/C ratio, a higher O/C ratio can be tolerated to get high carbon yield. The ultimate analysis of raw spruce chips informed that the H/C and O/C molar ratios were 1.48 and 0.67, respectively. Equilibrium simulations calculated a solid carbon yield of 0.34g solid carbon/g biomass for the raw spruce chips when the temperature and pressure were 450°C and 1 atm, respectively.

The reason that the presence of oxygen is undesirable is that it promotes the production of CO and CO_2 gases which consume carbon. High hydrogen content is also undesirable due to formation of CH_4. The tolerance for low levels of hydrogen is most likely due to hydrogen reacting with oxygen to form water. This reaction uses some of the highly reactive oxygen that would otherwise consume solid carbon. This would explain why the system tolerates higher O/C ratios when there is some hydrogen present. However, water can also consume solid carbon during steam gasification (Equation (2.3)). The optimal raw material would purely contain carbon, but this is not the case for biomass. Attempts have been made to pretreat biomass by torrefaction. This would increase the quality of the biomass, and have some benefits when it comes to hydrophobicity, grindability and space requirements. It does also decrease the O/C ratio [54–56]. However, there is a challenge when it comes to removing oxygen from the feedstock, without also removing carbon. Pretreatment of biomass is an interesting field of study, but goes beyond the scope of this thesis.

3.2 Kinetic model

The effects of surface area and gas flow rate were investigated by kinetic simulations. The density of the solid carbon particles was varied between 50 and 150kg/m^3, and the specific surface area was varied between 200 and 1000 m^2/g. The conversion of solid carbon, which here is defined as the increase in solid carbon from equilibrium state, was plotted as a function of time. The results are presented in Figure 3.2. A CO flow rate of 2L/min per 100g biomass was set when investigating the effects of surface area.

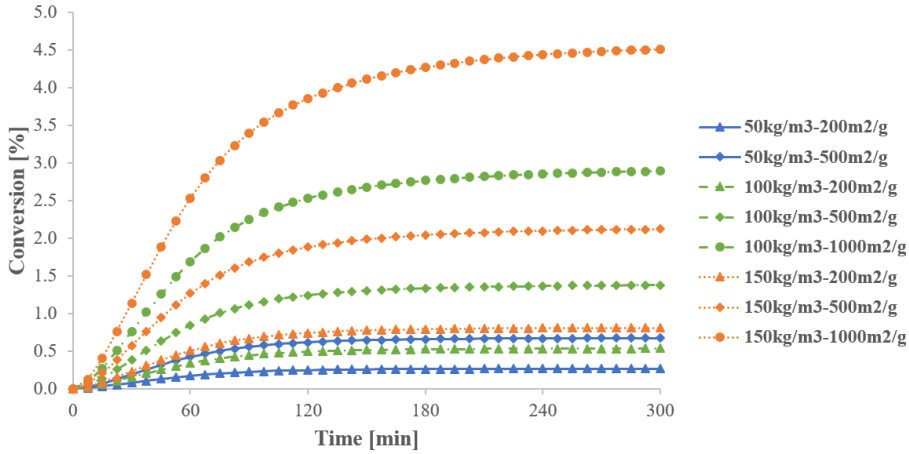

Figure 3.2: Conversion of solid carbon as function of time at 2L/min added CO gas. T = 480°C, P = 1atm.

It can be seen from Figure 3.2 that the conversion increased with increasing surface area. The trend was the same for all the investigated surface areas, where the increase seemed to be largest at the beginning and stagnated after approximately 120 minutes. To better see the behavior of the incline, the derivative of the conversion was plotted as a function of time. The results are presented in Figure 3.3.

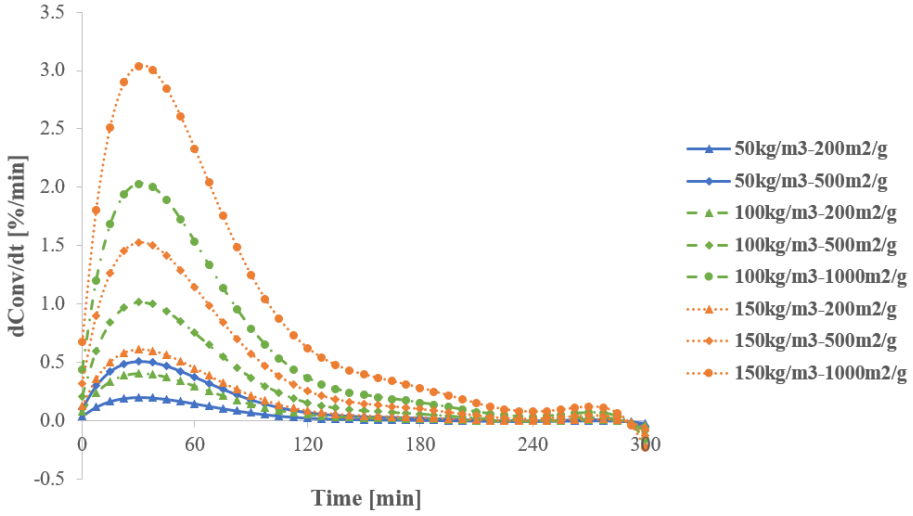

Figure 3.3: The derivative of the solid carbon conversion plotted as function of time.

As predicted from Figure 3.2 it can be seen from Figure 3.3 that the conversion per time had its peak at approximately 30-60 minutes for all the surface areas. At 120 minutes the conversion rate was significantly lower than the peak. These results indicate that there might be little to gain in form of higher solid carbon yield if the hold-time for the pyrolysis process surpasses two hours at 2L/min added CO per 100g biomass. This applies especially for the simulations with lower surface areas.

The effect of flow rate was investigated for 1,2,3,4 and 5L/min of CO per 100g biomass. The gas had a simulated input temperature of 20°C. The results are presented in Figure 3.4. The specific surface area and density were set to 1000m^2/g and 150kg/m^3, respectively.

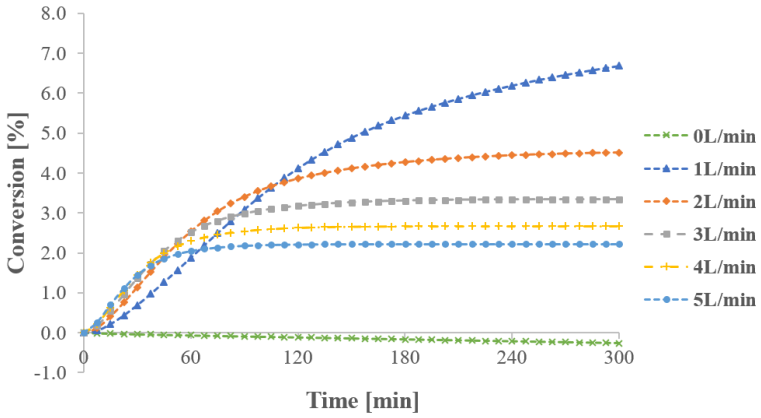

(a) Solid carbon conversion as function of time

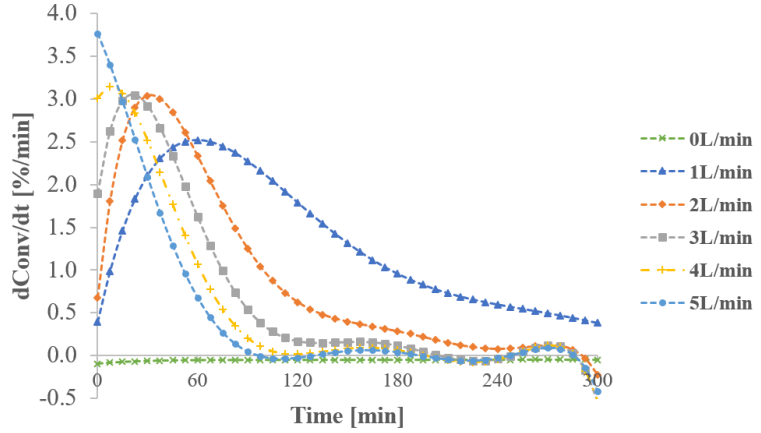

(b) Derivative of carbon conversion as function of time

Figure 3.4: Simulated influence of different CO flow rates on the conversion of solid carbon and its derivative. Density and specific surface area were set to 150kg/m^3 and 1000m^2/g, respectively. T = 480°C, P = 1atm.

The conversion decreases at 0L/min CO, which shows that there was an offset from equilibrium conditions. This had most likely to do with the kinetic constants not fully matching the equilibrium data from FactSage, which were used as starting

conditions. However, the offset was -0.26% after 300 minutes, and was considered acceptable. It can be seen from Figure 3.4a that the conversion of solid carbon increased with decreasing flow rate of CO for the rest of the flow rates. The conversion was highest for 1L/min CO after 120 minutes. Higher flow rates gave a steeper slope at the beginning which bent off earlier as the flow rate increased. This can also be observed in Figure 3.4b. The top peak was earlier as the flow rate increased. For 5L/min CO the conversion rate decreased from the beginning and was close to zero after approximately 90 minutes. The peaks shifted to the right as the flow rate decreased, as well as becoming wider. The simulation with 1L/min CO had the lowest peak, however, it spanned a much wider range than the other flow rates. The results from Figure 3.4 thereby indicate that a low flow rate of CO is desired to get a higher conversion of solid carbon. However, the hold time should be longer at lower flow rates.

The change in gas components during the simulations was also investigated. The mole fractions of the five gas species were plotted as a function of time for 1, 3, and 5L/min CO per 100g biomass. The results are presented in Figure 3.5.

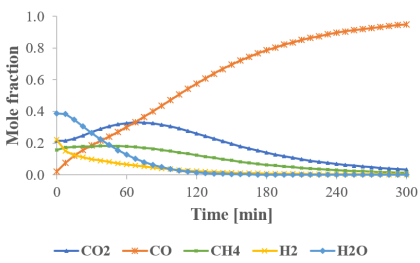

(a) Mole fraction at 1L/min CO.

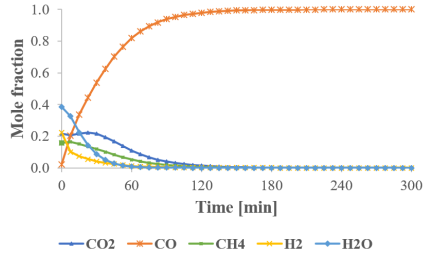

(b) Mole fraction at 3L/min CO.

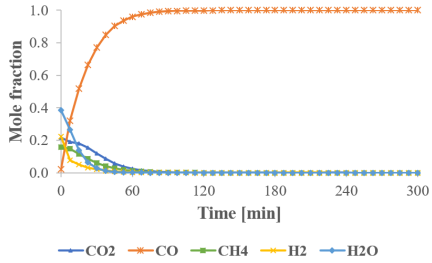

(c) Mole fraction at 5L/min CO.

Figure 3.5: Simulated mole fraction of gas components.

It can be seen from Figure 3.5 that the mole fraction of CO eventually reached approximately 1.0 for all three flow rates. The higher the flow rate, the faster the

CO mole fraction reaches 1.0. This shows that higher gas flows had more rapidly a diluting effect. By comparing Figure 3.5 with Figure 3.4b it can be seen that the conversion rate peaked at the same time as when the CO_2 mole fraction was at its highest level. For 1L/min CO this corresponded to approximately 60 minutes, while 30 minutes for 3L/min CO and almost instantaneously for 5L/min CO. The conversion rate dropped when the mole fraction of CO became the dominant gas in the reactor. This would correspond to the time when CO had a diluting effect on the system.

The results obtained from the kinetic simulations indicate that the surface area mainly affects the degree of conversion. The highest conversion rate was obtained at the same time, independent of the available surface area. However, the gas flow rate of CO determined when the highest conversion rate took place, and gave an indication of how long the hold time should last. The highest conversion was reached for the lowest simulated gas flow, which was also when the presence of other gases was longest. This has to do with the fact that when the flow rate increases the residence time of the gases in the reactor decreases. However, this does not explain why the conversion of solid carbon stopped when the system only experienced CO gas. The results indicate that the conversion rate increased when the CO/CO_2 ratio stayed relatively low, and dropped significantly as the concentration of CO became much greater than CO_2. From literature it can be found that the Boudouard reaction is slow at temperatures below 700°C [57]. Based on this information and the obtained results it can be assumed that the Boudouard reaction is not the dominant reaction in this system at 480°C. CO is involved in four of the five reversible reactions presented in Section 2.2. High flow rates of CO have a diluting effect on the system, and the absence of other gases seems to slow down the conversion rate. There are three reactions besides the Boudouard reaction where CO participate; steam gasification, methane reforming and water-gas shift. In these reactions CO reacts with either H_2 or H_2O. When the diluting effect becomes large, the molar fractions of H_2 and H_2O approach zero. This means that there will not be much left to react with CO to form other gases and drive the system forward. When there is no H_2 in the system steam gasification cannot be reversed to produce more carbon. The methane reforming reaction will not be reversed either, and there will be little production of CH_4. If there is no H_2O in the system the water-gas shift reaction will not be able to proceed, which is an important reaction to balance the whole system. This means that the system will stagnate, which is observed from Figure 3.4 and Figure 3.5. Gupta *et al.* (2019) investigated how experimental process parameter could be optimized for pyrolysis of teak sawdust. They looked into the effects of gas flow

rate (here N_2) and found that the biocarbon yield decreased with increasing flow rate. They argue that the reason is a reduction in vapor residence time inside the reactor, and that the vapors get pushed out of the reaction zone which stops secondary reactions [58]. This is in agreement with the simulated results, and indicates that the flow rate should be low in the experimental work. However, it should be kept in mind that lower flow rates also indicated that the hold time for the process should be longer.

Part 2: Experimental work

4 Materials and methods for the experiments

The experimental work was the major part of the master thesis. Seven different experiments were conducted; two references with N_2 as carrier gas, three experiments with CO_2 and two experiments with CO. The main focus of the experimental work was to investigate the effects of altering the gas atmosphere on the pyrolysis products.

4.1 Biomass feedstock

The biomass used for the experiments was raw spruce chips provided by SINTEF Energy. The spruce chips were dried at 105°C for approximately 16 hours before each experiment. Ultimate and proximate analysis of the dried biomass have been performed by Belab AB, and are presented in Table 4.1.

Table 4.1: Ultimate and proximate analysis of dried spruce chips used for the experiments. db stands for dry basis.

Analysis	**wt.%**	**Norm**
Moisture, 105°C	1.1	SS-EN ISO 18134-1:2015/-2:2017
Ash, 550°C db	0.7	SS-EN ISO 18122:2015
Volatile matter, db	81.4	SS-EN ISO 18123:2015
Fixed carbon, db	17.9	Calculated
Carbon (C), db	49.6	SS-EN ISO 16948:2015
Hydrogen (H), db	6.1	SS-EN ISO 16948:2015
Nitrogen (N), db	<0.1	SS-EN ISO 16948:2015
Oxygen (O), db	43.9	Calculated
Chlorine (Cl), db	<0.01	SS-EN ISO 16994:2016
Sulfur (S), db	<0.012	SS-EN ISO 16994:2016

The size and shape of the spruce chips varied greatly. The length varied between approximately 2-10cm, and the width varied between approximately 1-3cm. The difference in size and shape could affect product composition. Larger pieces were therefore avoided to try to have as uniform biomass input as possible. Pieces of bark were also excluded. A picture taken of the raw spruce chips is presented in Figure 4.1.

Figure 4.1: Picture of raw spruce chips used as biomass in the experiments.

4.2 Apparatus and gases

The apparatus used for the experiments belonged to the Department of Thermal energy at SINTEF Energy. It consisted of a pyrolysis reactor, cooler, two filters and a gas meter. The apparatus was connected to gas bottles which could inject the desired gas into the reactor. The reactor tube was 500mm long, with an inner diameter of 125mm. A furnace from Entech AB surrounded the reactor tube and consisted of three individual heater sections with a maximum temperature of 1100°C. The cooler was connected to the pyrolysis reactor to condense the tarry vapors developed in the process. The working medium of the cooler was propylene glycol at 5°C. Two filters were connected to the cooler to trap aerosols

developed during the process. Uncondensed gas which passed through the filters was measured by a gas meter and thereby analyzed by a Varian CP 4900 micro-GC. A safety valve was connected to the reactor, and was set to open if the gauge pressure in the reactor surpassed 0.7-1.0 bars. An illustration of the apparatus is presented in Figure 4.2.

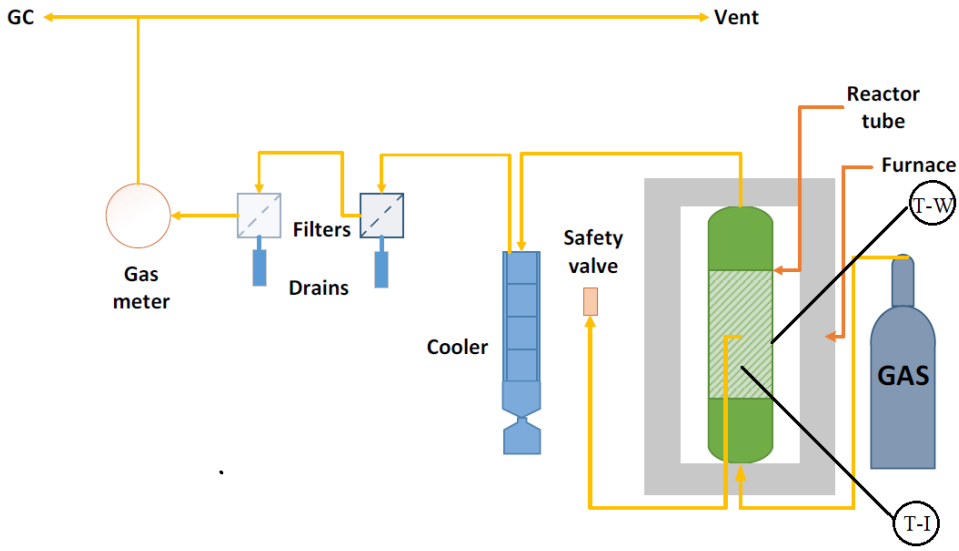

Figure 4.2: Illustration of the apparatus used for the experiments. T-I: internal temperature in the reactor, T-W: wall temperature.

The carrier gases used in the experiments were N_2 (inert gas), CO_2 and CO. All gases were delivered by AGA. The N_2 and CO_2 gases held industry quality ($\geq$ 99.6% N_2 and $>$ 99.7% CO_2 [59, 60]), and the CO gas held an instrument quality. CO is a toxic gas and demands special precautions before use [61]. Fresh air gas masks were used during all experiments involving CO, extra ventilation was installed over the CO flask and each operator wore gas detectors.

4.3 GC calibration

The GC was calibrated before starting the experiments. The back gases were argon and helium which held a pressure of 21 PSI. The columns used for the analysis were CP-4900 Backflush Column Module, 10m PPQ which had a temperature of 50°C and CP-4900 Backflush Column Module, 10m MMS which had a temperature of

120°C. Five different gases were used for the calibrations; air, pure N_2, pure CO_2, pure CO and a calibration gas. The composition of the calibration gas can be found in Table 4.2.

Table 4.2: Composition of calibration gas used to calibrate GC.

Gas	Acetylene (C_2H_2)	Ethane (C_2H_6)	Ethene (C_2H_4)	Hydrogen (H_2)	Methane (CH_4)	Nitrogen (N_2)	Carbonmonoxide (CO)	Carbondioxide (CO_2)
Vol%	0.5	1.5	0.5	4.0	15.0	16.5	30.0	32.0

4.4 Experiments

Seven different experiments were conducted to investigate the impact of different carrier gases on the pyrolysis products. The experiments using N_2 as carrier gas were set as references. Two of the experiments (one reference- and one CO_2 experiment) were repeated twice due to errors in the GC analysis. However, this only affected the gas analysis, and the biocarbon and condensate could still be used for further analysis. The experimental work consisted of three main steps; preparation of the experiments, the experiments and analysis of the products.

4.4.1 Preparation

Raw spruce chips was used as biomass for all the experiments. The preparation phase consisted of drying the biomass in a Termaks 9000-er serie furnace for 16 hours at 105°C. The dried spruce chips were thereafter weighed and placed into the reactor tube. 700±40g of dried biomass was used for all the experiments. The reactor tube was heated to 120°C and held there for one hour with N_2 purge to ensure that no oxygen was present in the reactor, and to further dry the biomass. The gas flow rate was set to approximately 1.4L/min, which was the lowest stable flow manageable. After the drying process was finished the furnace temperature was set to 480°C/580°C, depending on the desired hold temperature. The GC was turned on and put on continuous sampling mode.

4.4.2 The experiment

The experiments consisted of two main phases; a heat-up phase and a hold phase. The heating rate was set to 13°C/min for all the experiments, and the heat-up phase started when the three heating regions on the furnace was changed from

120°C to 480°C/580°C. The hold phase started when all three heater sections reached the desired hold temperature (480°C/580°C), and lasted for three hours. An illustration of how the temperature developed during these two phases, and at what time the gases were added, is presented in Figure 4.3.

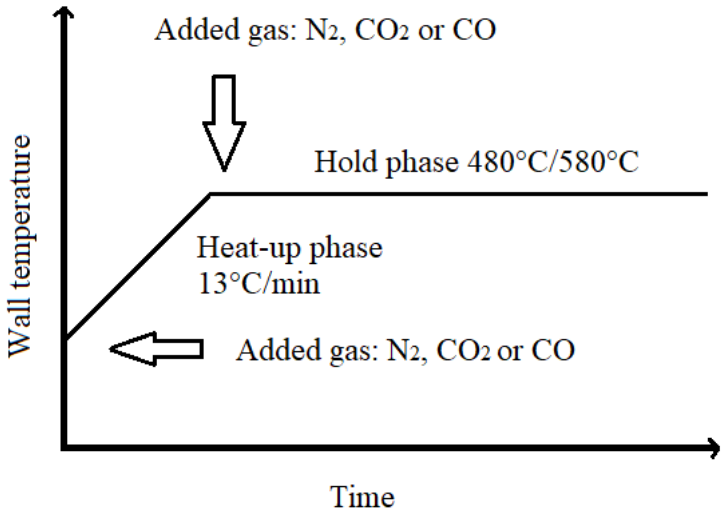

Figure 4.3: Illustration of heat-up and hold phase. Hold phase started when the wall temperature reached desired hold temperature.

Different carrier gases were added to the heat-up and hold phase. An overview of the gases used in each experiment is presented in Table 4.3. The names given for the different experiments will be used further in the Results and Discussion section. N_2 was used as carrier gas throughout the two reference experiments with different hold temperatures. CO_2 was used as carrier gas during only the heat-up phase in one experiment, and throughout the entire experiment at two different hold temperatures. CO was used as carrier gas throughout one experiment, while only during the hold phase during another. The gas flow into the reactor was set to approximately 1.4L/min for all the experiments, which was the same as the N_2 purge during the preparations. The internal temperature in the reactor was logged every 5 seconds during the entire experiment. The gas flow through the gas meter, the temperature of the furnace (wall temperature) and the gauge pressure in the reactor were manually registered every minute during the heat-up phase and for 1.5 hours after hold temperature was reached. They were thereafter registered every 5 minutes for 1 hour and every 10 minutes for the last 30 minutes.

After three hours of carbonization the heaters were turned off and a N_2 purge of 2L/min was set to cool down the system. One experiment lasted shorter than the others. The experiment with N_2 during heat-up and CO during the hold phase was stopped 40 minutes earlier than the others due to detection of CO gas in the room. The hold phase lasted therefore two hours and twenty minutes instead of three hours.

Table 4.3: Overview of which gases were added at which phase during the different experiments. Two different hold temperatures were investigated with N_2 and CO_2 as carrier gas.

Experiment name	**Gas during heat-up**	**Gas during hold phase**	$\mathbf{T_{hold}}$ **[°C]**
N_2N_2480	N_2	N_2	480
N_2N_2580	N_2	N_2	580
CO_2N_2480	CO_2	N_2	480
CO_2CO_2480	CO_2	CO_2	480
CO_2CO_2580	CO_2	CO_2	580
COCO480	CO	CO	480
N_2CO480	N_2	CO	480

After the experiments, biocarbon and condensate were removed from the reactor tube and cooler tank and weighed to find the biocarbon and bio-oil yield, respectively. The produced biocarbon was separated into three groups depending on where it was placed in the reactor. This was to investigate if there were any differences in the biocarbon from the top, middle and bottom of the reactor. The gas yield was calculated based on the registered volume from the gas meter and the GC analysis. After the experiment was finished and the equipment was cooled down, the apparatus was dissembled and cleaned. Samples of the produced biocarbon were thereafter analyzed.

4.5 Analysis

The product yields were calculated directly after each experiment, and several analysis methods were used to investigate the properties of the produced biocarbon. The analysis methods consisted of proximate analysis, thermogravimetric analysis (TGA), pycnometer analysis, Brunauer–Emmett–Teller (BET) surface area analysis and scanning electron microscope (SEM) analysis.

4.5.1 Product yield

The biocarbon and condensate mass yields were calculated directly after the experiments by weighing the products and dividing by the initial biomass weight. The gas yield was determined by using the gas volume which had passed through the gas meter and the GC analysis. The GC detected N_2, O_2, CO_2, CH_4, CO, H_2, C_2H_2/C_2H_4 and C_2H_6. The mass development of each of these gases was calculated based on the registered volumetric flow each minute and the volume percentages provided by the GC. It was assumed that the gas held room temperature and atmospheric pressure through the gas meter and into the GC device. These assumptions were considered valid due to the fact that it was an open system out to the ventilation system, and it was checked and confirmed that the pipes into the gas meter were not warm. The molar gas yield of each gas was determined by using that the molar volume of an ideal gas at 0°C and 1 atm is 22.4L and correcting for the temperature. The mass yield was thereby calculated by using the individual molar masses.

4.5.2 Proximate analysis

Proximate analysis is used to determine the moisture, volatile matter, fixed carbon and ash content of a sample. This can be used to determine the quality of the produced biocarbon [62]. The proximate analysis of biocarbon was conducted in compliance with the procedure used in the PyrOPT project. Nine biocarbon samples, taken from the middle region of the reactor, were analyzed. Experiments with N_2 and CO_2 at T_{hold} 480°C were performed twice, which was the reason that there where nine biocarbon samples even though there were seven different experiments. The samples were grounded by using a mill with a sieve size of 1mm. Crucibles were labeled and weighed with and without lid on before the analysis started. 1±0.1g of grounded sample was added in the crucibles. Three replicates were prepared for each sample. A muffle furnace was used for the analysis. The furnace was first set to 105°C to determine the moisture content. The samples were placed in the furnace with the lid on, and stayed overnight to ensure that all the available moisture had evaporated. The next day the samples were weighed and the moisture content was determined by using Equation (4.1).

$$\text{Moisture}\% = \frac{A - B}{A} * 100\% \tag{4.1}$$

Here A is the initial mass of biocarbon and B is the mass of the sample after

staying in the furnace overnight at 105°C. After determining the moisture content the furnace was heated to 950°C. The samples were placed with the lid on into the furnace and held there for 15 minutes. As the furnace door was open to place the samples, the temperature decreased to approximately 750°C. The samples experienced therefore 950°C only the last 5 minutes. After the total 15 minutes had passed the samples were taken out and cooled down to room temperature before weighed. The volatile content was determined bu using Equation (4.2).

$$\text{Volatile\%} = \frac{B - C}{B} * 100\% \tag{4.2}$$

Here C is the weight of the sample after 15 minutes at 950°C. After determining the volatile matter the furnace was set to 750°C. The samples were placed without lid in the furnace and left there overnight. The samples were thereafter taken out and weighed for the last time. The ash content was determined by using Equation (4.3).

$$\text{Ash\%} = \frac{D}{B} * 100\% \tag{4.3}$$

Here D is the weight of the residue left in the crucible. The raw data for the proximate analysis can be found in Section B.3 in Appendix B. The fixed carbon content, FC, was determined based on the results obtained from the proximate analysis. The fixed carbon is the remaining percentage when subtracting moisture, volatiles and ash. This is illustrated in Equation (4.4).

$$\text{FC\%} = 100\% - \text{Moisture\%} - \text{Volatile\%} - \text{Ash\%} \tag{4.4}$$

Finally, the fixed carbon yield, y_{FC}, could be calculated from the char yield obtained from the experiments and the fixed carbon contents found from the proximate analysis. The unit becomes grams of fixed carbon per gram biomass. The fixed carbon yield was calculated by using Equation (4.5).

$$y_{\text{FC}} = \frac{m_{\text{char}}}{m_{\text{biomass}}} * \frac{\text{FC\%}}{100\%} \tag{4.5}$$

4.5.3 TGA

Thermogravimetric analysis (TGA) is a common technique for determining thermal decomposition behavior of fuel samples at low heating rates. There are no heat and mass-transfer limitations, and the results can be used to determine reactivity and mass loss kinetics [63]. Here there will be a focus on the thermal decomposition behavior and the mass loss curves. TGA was performed on the biocarbon produced from all the experiments in addition to dried biomass. A Q600 SDT Quickstart TA instrument was used to analyze the samples, which were the same as the grounded samples used for the proximate analysis. Before starting the analysis of the samples a baseline was created with an empty crucible. Thereafter 5.5±0.5mg of sample was added to the crucibles, which were placed in the furnace of the TA instrument. A N_2 purge of 200mL/min was set for all the analysis to ensure inert atmosphere. First, the furnace was heated up to 100°C with a heating rate of 20°C/min, and held there for 15 minutes to remove moisture. Thereafter the furnace was heated up to 1200°C with a heating rate of 10°C/min. As the temperature increased the weight loss of the sample was registered by the software. When the furnace temperature reached 1200°C the analysis was over and the instrument cooled down. When the temperature was below 50°C the N_2 purge was decreased to 5mL/min.

4.5.4 Density and BET surface area analysis

Density and Brunauer–Emmett–Teller (BET) analysis were performed by the Department of Material Science at the Norwegian University of technology and science (NTNU). Density measurements were conducted for biocarbon produced in experiments N_2N_2480, N_2N_2580, CO_2CO_2480, CO_2CO_2580 and COCO480. The BET surface areas were determined for biocarbon produced from experiments N_2N_2480, CO_2CO_2480 and COCO480. The biocarbon densities were measured using AccuPyc II 1340 V2.01 pycnometer, which is a gas displacement pycnometer. It measures the absolute volume of solids by inserting an inert gas (He or N_2) in a sealed chamber with a known volume where the solid is placed. The gas is thereby expanded into another chamber, and the pressure before and after expansion is measured to find the volume of the sample. The density is determined by dividing the weight of the sample by its volume [64]. Before the analysis started all the samples were placed 30 minutes in a furnace at 100°C to release moisture. 5.5±0.5g of biocarbon was placed in the pycnometer chamber. Helium was used as analysis gas. Ten purges were conducted for each sample, and the average of the three last densities was used for the results. 3Flex version 5.00 was used for the BET analysis. The surface area is determined by calculating the amount of adsorbate gas corresponding to a monomolecular layer on the surface of the material. The technique includes both external- and pore area evaluations to determine the total specific surface area [65]. Before the analysis, the samples were pulverized using mortar and pestle and degassed for 7 hours at 250°C. The analysis adsorptive was N_2 gas, and the analysis bath temperature was -196°C. Different analysis times were used for different samples. Biocarbon from N_2N_2480, CO_2CO_2480 and COCO480 were analyzed for 19h and 19minutes, 7h and 19min, and 6h and 21min, respectively.

4.5.5 SEM analysis

Scanning electron microscope (SEM) is used to scan surfaces using a focused electron beam to create images. The electrons interact with the surface, creating secondary electrons, backscattered electrons and X-rays. By collecting the signals, detectors are able to form images which can be used to obtain information about the topography and composition of the surface [66]. The analysis was performed by the department of Thermal Energy at SINTEF Energy Research. Field Emission Scanning Electron Microscope (FE-SEM, Zeiss Supra 55) was used to analyze the biocarbon. It was operated at secondary electron imaging mode to investigate the apparent microstructure and morphology of the samples. To be able to examine in more detail the microstructure, the samples were sliced vertically and the cross-section area was scanned. An illustration is shown in Figure 4.4.

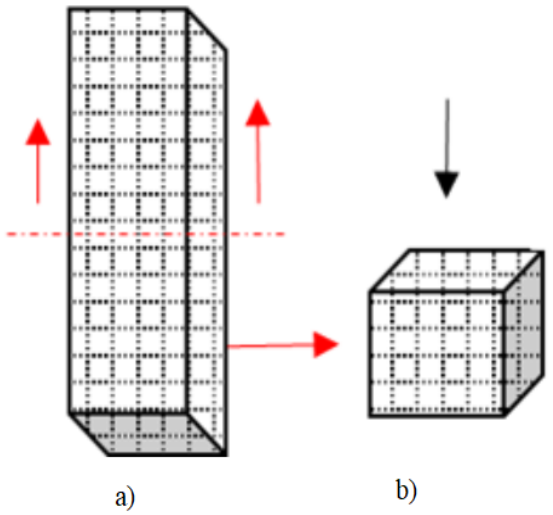

Figure 4.4: Illustration of the how the biocarbon piece was analyzed. a) Vertically cross-section of one biocarbon sample. b) Top view of cross-section.

5 Experimental results and discussion

Seven different experiments were conducted where all three product yields were calculated; two experiments with N_2 as carrier gas, three with CO_2 and two with CO. For the experiments with N_2 and CO_2, one experiment of each was performed at 580°C in addition to 480°C, which was the base case for the other experiments. More information about the different experiments can be found in Table 4.3 in Section 4.4. The aim was to investigate if altering the gas atmosphere influenced the product yield and/or properties of the produced biocarbon. The presentation of the experimental results starts with the product yields, which were obtained right after each experiment. Following are the results from the proximate analysis and TGA, which both give information about the biocarbon behavior during different temperatures ranges. Lastly are the results from the analysis which study the structure of the biocarbon. First, the measured densities and surface areas, thereafter images of the carbon structure by SEM analysis.

5.1 Product yield

The biocarbon, condensate and gas yields obtained from the seven different experiments are presented in Table 5.1. The reason that N_2N_2480 and CO_2CO_2480 have uncertainties added to the biocarbon and condensate yield is that both experiments were conducted twice. However, the gas compositions were only obtained for one of each experiment due to an error in the GC analysis. It should be noted that the calculated losses from experiment CO_2CO_2580 were significantly higher than the other experiments. This was most likely related to the low condensate yield and will be further discussed in Section 5.1.2

Table 5.1: Product yield obtained from the experiments.* significantly higher losses than the other experiments.

Yield [wt.%]	N_2N_2480	CO_2N_2480	CO_2CO_2480	COCO480	N_2CO480	N_2N_2580	CO_2CO_2580
Biocarbon	29.8±0.3	29.8	29.6±0.2	29.5	29.6	27.1	27.1
Condensate	45.6±0.1	45.8	45.3±0.4	45.8	45.1	46.4	39.5
Gas	19.9	20.6	19.3	18.8	19.9	19.8	23.0
Losses	4.4	3.8	5.6	5.9	5.4	6.7	10.4*

5.1.1 Biocarbon yield

It can be seen from Table 5.1 that the biocarbon yield was not significantly affected by changing the carrier gas, but rather the temperature. When T_{hold} was 480°C the biocarbon yield became slightly lower than 30 wt.%, independent of the carrier gas. When T_{hold} was 580°C the biocarbon yield became 27 wt.% for both the N_2 and CO_2 experiments. Several researchers have reported that CO_2 as carrier gas decreases the biocarbon yield, even at low temperatures [41–43]. However, from these results it seems like CO_2 does not affect the biocarbon yield at temperatures up to 580°C compared to N_2. The biocarbon was separated into three groups (top, middle, bottom) depending on its placement in the reactor. It was observed that the conversion of biocarbon differed in the three groups. Pictures taken of biocarbon from the bottom region of the reactor are presented in Figure 5.1.

(a) Biocarbon from bottom of reactor after exp. COCO480.

(b) Biocarbon from bottom of reactor after exp. CO_2CO_2480

Figure 5.1: Pictures of poorly converted biocarbon from the bottom region of the reactor after experiments with CO and CO_2 as carrier gas at T_{hold} 480°C.

It can be seen in both Figure 5.1a and 5.1b that parts of the biocarbon have not been fully pyrolyzed. This was observed for all experiments with T_{hold} 480°C. The reason is most likely that the bottom of the reactor is cooled down by incoming gas which had room temperature. The biocarbon retrieved from the top of the reactor

seemed fully converted for all the experiments. Thereby it can seem like the heat was not equally distributed throughout the reactor, and that all of the biocarbon did not experience the same conditions. This is a challenge that should be dealt with in future work. However, in Elkems case this might not be a challenge. If the gas is circulated back from the smelter furnace it would have a high temperature. Thereby the biocarbon in the bottom would most likely not experience these different conditions.

5.1.2 Condensate yield

The condensate yield did not differ significantly between the experiments. It was found to be 46.0±0.5 wt% and seems independent of the carrier gas, alike the biocarbon yield. The condensate was the main product from the pyrolysis process. In Elkem's vision of a sustainable biocarbon production they mention that this includes utilizing all side streams [1]. Some options for the condensate are the production of green chemicals and biofuels, or to be burned to produce heat. Several other solutions are also possible.

One experiment deviated from the rest. The experiment with CO_2 as carrier gas at 580°C had a much lower calculated condensate yield. One reason was that a large amount of condensate was left in the apparatus after the experiment, which was difficult to include in the calculations. The filters and filter drains were weighed to obtain the weight of condensate which had passed the cooler. However, there was much condensate left around the filters and in the cooler which was not accounted for in the calculations.

Some of the visible losses from the experiment with CO_2 at 580°C are shown in Figure 5.2.

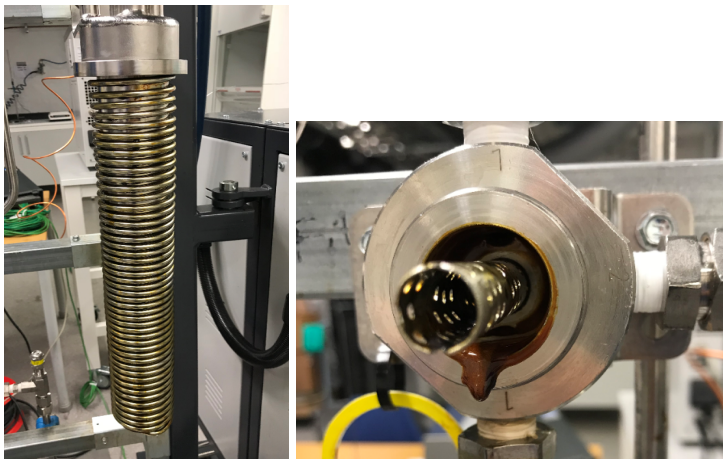

(a) Condensate left on the cooler

(b) Condensate left after the filter is removed.

Figure 5.2: Pictures taken after experiment CO_2CO_2580. Condensate which was left in/on the apparatus contributed to losses.

It can be seen from Figure 5.2 that there were significant losses of condensate, and that the yield should have been higher. An interesting observation was that the condensate on the filters had a much lighter color when CO_2 was used as carrier gas. Both at 480°C and 580°C the experiments with CO_2 produced condensate with a lighter color at the filters. Experiments with N_2 and CO produced dark condensate with a seemingly thinner consistency.

Pictures were taken of the condensate left on the first filter after the cooler, and are presented in Figure 5.3.

(a) Condensate from exp. N_2N_2580.

(b) Condensate from exp. COCO480.

(c) Condensate from exp. CO_2CO_2580.

Figure 5.3: Pictures of condensate at the first filter after the cooler for experiments with N_2, CO and CO_2 as carrier gas. Notice the lighter color of the condensate on the picture to the right.

It can be seen from Figure 5.3 that the condensate left on the filter was lighter when CO_2 was used as carrier gas. From previously discussed results it can seem like pyrolysis under CO_2 atmosphere did not affect the biocarbon yield at 480°C/580°C compared to N_2 and CO atmosphere, nor the condensate mass yield. However, the composition of the condensate seems to be altered during experiments with CO_2. Since it has not been performed an analysis of the condensate during this master thesis, this cannot be confirmed. Nevertheless, researchers have reported that CO_2 can affect cracking behavior and devolatilization during pyrolysis and gasification [45, 46, 67]. Altering the composition of the condensate can be a promising solution to making the product more directly applicable in the industry, and it would be interesting to explore this more in future work.

5.1.3 Gas yield

The gas yield was calculated based on data from the GC and the registered gas flow through the gas meter. It was assumed that the gas flow into the reactor kept stable throughout the experiments. It should be noted that there are two different temperature expressions; internal temperature and wall temperature. The internal temperature was the temperature within the reactor which was logged ever 5 seconds. The wall temperature was the temperature shown on the three heater sections of the furnace. The gases were switched between the heat-up phase and the hold phase when the wall temperature reached the desired hold temperature. However, the internal temperature was significantly lower.

It can be seen from Table 5.1 that the calculated gas yields varied from 18.8% to 23.0%. There were no clear trends regarding the gas yield. The mass development of CO_2, CO, CH_4, H_2, C_2H_2/C_2H_4 and C_2H_6, as well as the internal temperature, were plotted as functions of time. The results from experiment N_2N_2480 are presented in Figure 5.4.

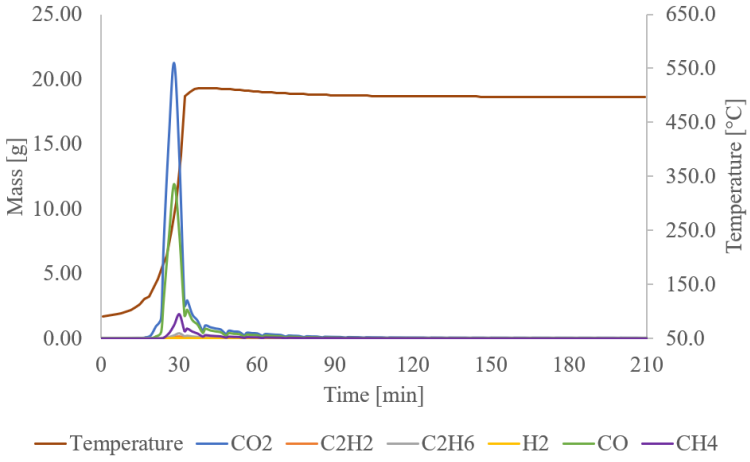

Figure 5.4: Mass development of CO_2, CO, CH_4, H_2, C_2H_2/C_2H_4 and C_2H_6 during the reference experiment with T_{hold} 480°C. The recorded internal temperature is also shown on the right axis.

The accumulated gas development for the major and minor gases from experiment N_2N_2480 are presented in Figure 5.5 and 5.6, respectively.

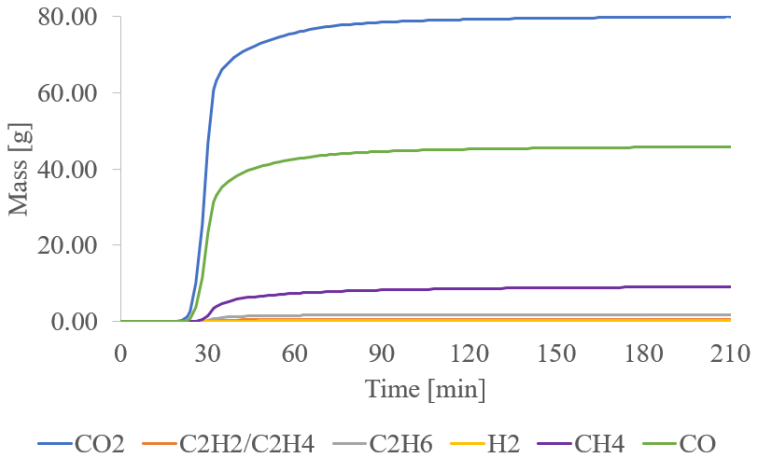

Figure 5.5: Accumulated mass development of CO_2, CO, CH_4, H_2, C_2H_2/C_2H_4 and C_2H_6 during the reference experiment with T_{hold} 480°C.

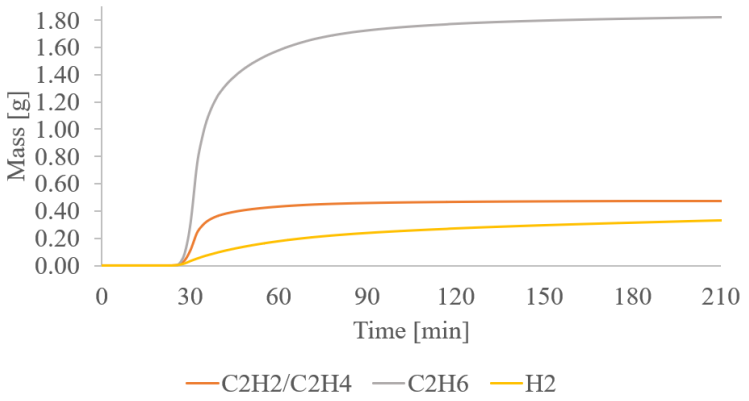

Figure 5.6: Accumulated mass development of H_2, C_2H_2/C_2H_4 and C_2H_6 during the reference experiment with T_{hold} 480°C.

The gas development trends (Figure 5.4) were similar for all seven experiments. CO_2 started to develop first and had the highest peak after around 30 minutes, followed by CO and CH_4. These were also the gases which were produced in highest amounts, and accounted for the majority of the gas produced in the pyrolysis

process (Figure 5.5 and 5.6). The minor gases were C_2H_6, C_2H_2/C_2H_4 and H_2. They were produced in much smaller amounts (on mass basis), which can be seen in Figure 5.6. Plots of the gas development for all the other experiments can be found in Section B.2 in Appendix B. When CO_2 was used as carrier gas the development of C_2H_6 and H_2 decreased, which was also reported by Wang *et al.* [48]. The highest amount of CO gas was produced in experiment CO_2CO_2580, where T_{hold} was 580°C. This is in agreement with the studies of Azuara *et al.* which had a peak temperature of 600°C. They argued that the reason most likely was the promotion of the Boudouard reaction [27]. Different results were found for the CO experiments. Like the CO_2 experiments, the development of C_2H_6 decreased when CO was used as carrier gas. However, the development of H_2 increased compared to the reference and CO_2 experiments, and surpassed the amount of C_2H_2/C_2H_4. The amount of H_2 produced in experiment COCO480 was approximately 33% and 63% higher than N_2N_2480 and CO_2CO_2480, respectively. Experiment N_2N_2480 had the highest production of CH_4 of all the experiments with T_{hold} 480°C, followed by experiments using CO_2 and CO. The gas yield increased when T_{hold} was increased from 480°C to 580°C, which was expected. The production of H_2 increased significantly for both N_2N_2580 and CO_2CO_2580 compared to N_2N_2480 and CO_2CO_2480. This is in agreement with literature where it can be found that gasification reactions are favored at higher temperatures. Development of CH_4 also increased for experiments N_2N_2580 and CO_2CO_2580.

Most of the gas development happened during the first 60 minutes. The internal temperature was also stable from that point. The gas development was therefore also plotted as a function of internal temperature during the first 120 minutes of the experiments. The results from all seven experiments are presented in Figure 5.7.

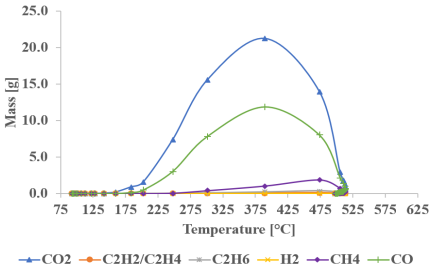

(a) Gas development for N_2N_2480

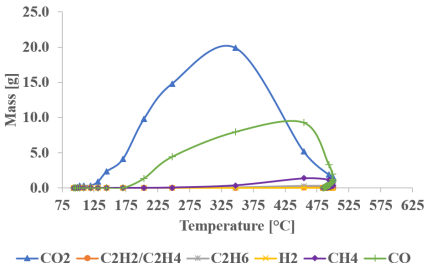

(b) Gas development for CO_2N_2480

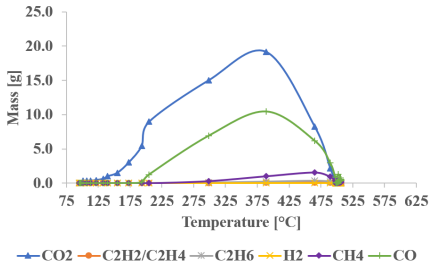

(c) Gas development for CO_2CO_2480

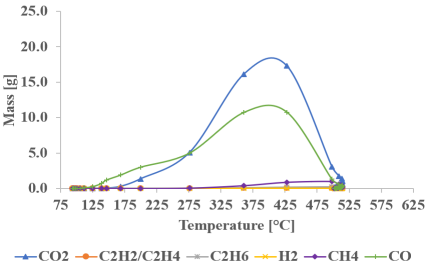

(d) Gas development for COCO480

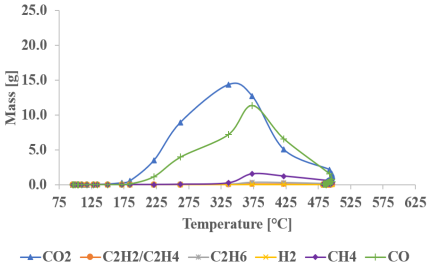

(e) Gas development for N_2CO480

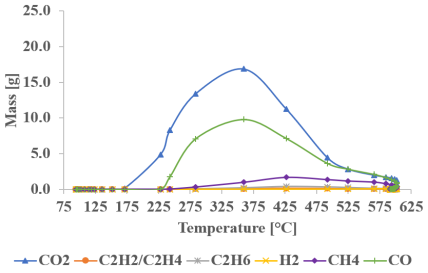

(f) Gas development for N_2N_2580

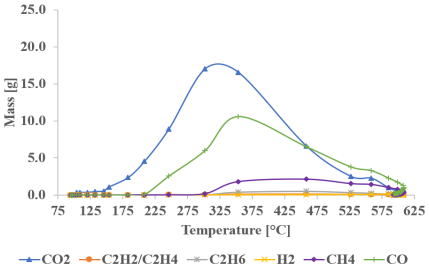

(g) Gas development for CO_2CO_2580

Figure 5.7: Gas development as function of internal temperature the first 120 minutes.

Even though the gas developments as function of time were similar for all experiments, it can be seen from Figure 5.7 that the gas developments as functions of internal temperature were not. The gas production peaked at different temperatures for the different gas species. Production of CO_2 and CO peaked between 300°C and 425°C for all experiments, except CO_2N_2480 where CO peaked much later than CO_2. Production of CH_4 and the minor gases peaked between 375°C and 475°C. The gas development as function of internal temperature for the minor gases can be found in Section B.2 in Appendix B. It can be seen that both experiments with N_2 as the only carrier gas (Figure 5.7a and 5.7f) had the most symmetrical gas development. When the gas was changed between the heat-up phase and the hold phase it seems to suppress the development of CO_2 at higher temperatures, and promote the production of CO. It can be observed that the three experiments where the development of CO surpassed CO_2 at high temperatures were when the carrier gas was changed during the experiment (Figure 5.7b and 5.7e) and when CO_2 was used as carrier gas at T_{hold} 580°C (Figure 5.7g). The last observation is in agreement with the simulated results, that the forward Boudouard reaction, Equation (2.1), is favoured at higher temperatures. In Figure 5.7e it can be seen at which internal temperature the gas was changed from N_2 to CO by the sudden increase of CO at 336°C. Since the gas flow was changed manually it cannot be said with certainty exactly the amount of CO added to the system, which might explain this effect. The gas was changed when the wall temperature was 480°C. However, the internal temperature was almost 150°C lower. This shows that even though the heating rate of the furnace was 13°C/min, the internal temperature could not keep up with the wall temperature during the heat-up phase.

The results indicate that the carrier gas affected the gas product composition during the first 120 minutes (heat-up phase plus approximately 90 minutes hold time). Higher temperatures and CO as carrier gas gave higher production of H_2, which is a valuable industrial gas. However, it is challenging to see any trends between the different experiments. Of all the calculated mass yield, the highest uncertainty lays in the gas yield. Firstly, the gas volume that passed the gas meter was manually registered every minute. There is uncertainty when it comes to correctly register the amount of gas which was developed. Secondly, it was assumed that the gas flow into the reactor was stable throughout the experiments. Most likely the gas flow was altered when the type gas was changed (experiments CO_2N_2480 and N_2CO480), but there was no way of checking during the experiment. Thirdly, when calculating the gas development from the process, the added gas had to be subtracted. Not knowing exactly the flow makes this a significant uncertainty.

5.2 Proximate analysis and FC yield results

Proximate analysis was performed to determine the moisture, volatile matter, ash and fixed carbon contents of the produced biocarbon. Experiments with N_2 and CO_2 as carrier gas throughout the experiment with T_{hold} 480°C (N_2N_2480 and CO_2CO_2480) were performed twice, which gave the chance to analyze two independent biocarbon samples that had been produced under same process conditions. These results would indicate how reproducible the experiments and analysis were. All the biocarbon samples were taken from the middle region of the reactor. Raw data from the proximate analysis can be found in Table B.2 in Appendix B.

Table 5.2: Results from proximate analysis in wt.%. VM - volatile matter, FC - fixed carbon, VM:FC - volatile matter fixed carbon ratio. * on dry ash free basis

Experiment	Moisture	VM	Ash	FC	VM:FC*
$N_2N_2480.1$	1.2±0.1	22.8±0.6	1.5±0.1	74.4±0.6	0.30±0.01
$N_2N_2480.2$	1.5±0.3	20.9±0.1	2.1±0.3	75.5±0.6	0.28±0.01
CO_2N_2480	1.2±0.1	17.8±0.1	1.9±0.1	79.0±0.1	0.23±0.01
$CO_2CO_2480.1$	0.6±0.1	15.9±0.3	1.5±0.2	81.9±0.4	0.19±0.01
$CO_2CO_2480.2$	1.0±0.2	17.1±0.1	1.0±0.2	80.9±0.4	0.21±0.00
$COCO480$	0.7±0.2	17.7±0.5	1.1±0.1	80.6±0.7	0.22±0.01
N_2CO480	0.6±0.1	16.3±0.7	2.0±0.2	81.0±0.6	0.20±0.01
N_2N_2580	0.2±0.2	11.8±0.3	1.1±0.1	86.9±0.1	0.14±0.01
CO_2CO_2580	1.0±0.1	11.2±0.1	1.5±0.1	86.3±0.2	0.13±0.00

It can be seen that the results from $N_2N_2480.1$ and $N_2N_2480.2$, as well as $CO_2CO_2480.1$ and $CO_2CO_2480.2$, differed slightly. This indicates that there were some differences in the biocarbon produced in these experiments, even though they experienced same process conditions. Due to the fact that biocarbon can absorb moisture before being analyzed, the VM-FC ratio should be compared since it is on dry basis. These values differed as well, which shows that it was not solely the moisture content that was different. The selected biocarbon pieces might be different even though they were selected from the same region of the reactor and according to their appearance. Deviation in the volatile matter and fixed carbon content can therefore be related to the heterogeneity of the selected biocarbon samples. Nevertheless, the results from both experiments N_2N_2480 and CO_2CO_2480 were comparable, and do not deviate from the rest of the trends.

Very interesting results were obtained from the proximate analysis. From Table 5.1 it can be seen that the biocarbon yield was not significantly affected by changing the gas atmosphere. However, from Table 5.2 it can be seen that the fixed carbon content and volatile matte were affected for experiments with T_{hold} 480°C. The biocarbon produced in experiments $N_2N_2480.1$ and $N_2N_2480.2$ had an average fixed carbon content of 75.0±1.5%. For experiments with CO_2 as carrier gases it was found that the fixed carbon content had increased significantly. They were found to be 79.0±0.1% and 81.4±0.9% (average value) for experiments CO_2N_2480 and CO_2CO_2480, respectively. CO_2 was added to the system during the heat-up phase, which lasted for approximately 30 minutes, in experiment CO_2N_2480, while during the entire experiment in CO_2CO_2480. It can be seen that the fixed carbon content was higher for experiment CO_2CO_2480. However, even when CO_2 was added to the system during only the heat-up phase, the fixed carbon content became higher than the reference. The internal temperature was 309°C when the gas was switched from CO_2 to N_2 in experiment CO_2N_2480. This indicates that a significant part of the effect on the volatile matter and fixed carbon content happened at low temperatures. These temperatures can be compared to torrefaction temperatures. Both Thanapal *et al.* (2014) and Bach *et al.* (2014) reported an increase in fixed carbon after torrefaction of woody biomass and Norwegian forest residues, respectively, in CO_2 atmosphere compared to N_2 atmosphere [42, 43]. Nevertheless, the volatile content was lower when CO_2 was added to the system during the entire experiment. This is in compliance with the studied of Duan *et al.* (2009) which reported that CO_2 enhances the release of volatile matter even at 480°C [44]. This can also be seen from the VM-FC ratio, which was calculated on dry ash free basis. Biocarbon produced in CO_2 atmosphere at T_{hold} 480°C had significantly lower VM-FC ratio than the biocarbon produced in N_2 atmosphere.

The fixed carbon content did not increase for experiment CO_2CO_2580 compared to N_2N_2580. Both these experiments had T_{hold} 580°C. This is in agreement with the studies of Azuara *et al.* which did not obtain higher fixed carbon content after pyrolysis of wine shoots in CO_2 atmosphere at 600°C [27]. The VM-FC ratios were also approximately the same for the two experiments. These results indicate that CO_2 affects the properties of biocarbon at low temperatures, while at higher temperatures these effects decrease significantly. Thanapal *et al.* (2014) argue that CO_2 increase the microporosity of biocarbon, which release volatiles and thereby increase the fixed carbon content at low temperatures [42]. Another theory is that CO_2 forms a layer that surrounds the biocarbon particles at low temperatures, which increases the gas residence time within the particle and increases the fixed carbon content [68]. At higher temperatures, this effect will not be present and

CO_2 will work as a gasifying agent.

The experiments with CO as carrier gas also produced biocarbon with higher fixed carbon compared to the reference. The fixed carbon content was found to be 80.6±0.6 and 81.0±0.6 for experiments COCO480 and N_2CO480, respectively. Since the error limits overlap it cannot be assumed that there were any differences between the results. Experiment COCO480 had CO as carrier gas throughout the whole experiment, while N_2CO480 had N_2 as carrier gas during the heat-up phase and CO during the hold phase. Experiment N_2CO480 was shorter than the others due to detection of CO gas in the room. However, it can seem like this did not affect the results. Contrary to the findings for CO_2, these results indicate that CO mainly affects the biocarbon properties during the hold phase. Not many have studied the effects of CO gas on the pyrolysis product composition. It is known that CO_2 works as a gasifying agent at high temperatures. However, CO is usually produced in gasification reactions (see Equation (2.1) and (2.3)). Nevertheless, these results suggest that CO might work in the same manner as CO_2 when it comes to decreasing the volatile content of biocarbon and increasing the fixed carbon content.

It was interesting to see that CO_2 had a different effect on the biocarbon quality, depending on the temperature. The fixed carbon content was thereby plotted as a function of temperature to illustrate the effect. The results are shown in Figure 5.8. Linear regression was added for the reference and CO_2 experiments, even though there were only two measured points (at temperature 480°C and 580°C). To be certain that there is a linear trend there should be three or more points. However, a linear trend was assumed here, with the knowledge that more experiments at different temperatures have to be conducted to validate the assumption. The outer points were found by using the equation from the linear regression.

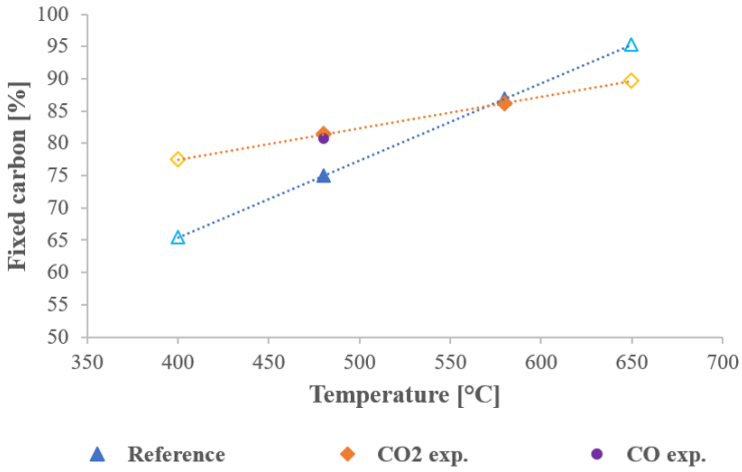

Figure 5.8: Fixed carbon as function of temperature for experiments N_2N_2480, N_2N_2580, CO_2CO_2480, CO_2CO_2580 and COCO480. Linear regression was added to the N_2 and CO_2 experiments, and gave the equations y = 0.1191x + 17.822 and y = 0.0488x + 57.952, respectively. The outer points were found by using the equation given by the linear regressions.

Linear regression gave the equations $y = 0.1191x+17.822$ and $y = 0.0488x+57.952$ for the N_2 and CO_2 experiments, respectively. If the assumption of linearity is correct this means that temperature has a significantly lower effect on the fixed carbon content when CO_2 is used as carrier gas. It can be seen that the slope is much steeper between the N_2 experiments. At higher temperatures this means that biocarbon produced in inert atmosphere obtains higher quality than biocarbon produced in CO_2 atmosphere. However, at lower temperatures it would be the opposite. This is very interesting results because different metallurgical industries have different requirements when it comes to quality and fixed carbon content. If the process tolerates lower fixed carbon contents, the use of CO_2 as carrier gas instead of N_2 leads to the possibility of lowering the process temperature. Elkem's requirement is that the biocarbon must have 76% fixed carbon [4]. The process temperature could then be 400°C if CO_2 is used as carrier gas (and still fulfill the requirement), while it would have to be 488°C if N_2 is used instead. This is of course if the assumption of linearity is valid. It was mentioned in the literature study that there is a general agreement when it comes to the effects of temperature on biocarbon yield [19–21]. If the pyrolysis temperature can be lowered in CO_2 atmosphere, the biocarbon yield will become higher. However, more experiments have to be conducted to investigate the relationship between carrier gas, temper-

ature and fixed carbon yield. Both CO experiments were performed at 480°C, and it can therefore not be said if the trend is the same as for CO_2. What can be said is that also CO seems to have a positive effect on the quality of the produced biocarbon at 480°C. Both these gases will be available from Elkem's silicon production. Lowering the pyrolysis temperature would have several positive effects; energy consumption would be lower, the biocarbon yield would increase and the demand for raw material would decrease (as a direct consequence of higher biocarbon yield). These findings are therefore very promising.

The fixed carbon yield was calculated by combining the results from the product yields and proximate analysis, see Equation (4.5). The results are presented in Table 5.3. The fixed carbon contents used for the calculations were on dry basis, and average values were used for experiments N_2N_2480 and CO_2CO_2480.

Table 5.3: Fixed carbon yield and the difference between the references (N_2N_2480 and N_2N_2580) and the other experiments with same temperature. * average values used.

Experiment	$y_{\mathbf{FC}}$ **[g FC/g biomass]**	**Difference [%]**
N_2N_2480	0.227*	-
CO_2N_2480	0.238	4.85
CO_2CO_2480	0.243*	7.05
COCO480	0.240	5.73
N_2CO480	0.241	6.17
N_2N_2580	0.236	-
CO_2CO_2580	0.236	0.00

From Table 5.1 it was established that the biocarbon yield did not differ significantly between the experiments. It is therefore the fixed carbon content that mostly contributes to the differences in fixed carbon yield. It can be seen from Table 5.3 that the biocarbon produced in experiment CO_2N_2480 differed the least from the biocarbon produced in N_2N_2480. However, the fixed carbon yield was still 4.85% higher than the fixed carbon yield from the reference. The highest fixed carbon yield was obtained from experiment CO_2CO_2480. This indicates that even though a large part of the effects of CO_2 happened at low temperature, it still contributed to a positive effect at temperatures up to 500°C. It can also be seen that there was no difference in the fixed carbon yield between experiments N_2N_2580 and CO_2CO_2580. This means that the positive effects of CO_2 at low temperatures have been outweighed. The fixed carbon yields from the CO ex-

periments were between the two CO_2 experiments. The result from experiment N_2CO480 was slightly higher than the results from experiment COCO480. More experiments and analysis should be conducted before establishing if the difference is significant, but the results do indicate that CO has a greater affect when it is applied at higher temperatures.

From the equilibrium simulations it was found that the fixed carbon yield of raw spruce chips was 0.34 g FC/g biomass. This is significantly higher than the fixed carbon yield obtained in the experiments. There are at least two reasons for this. One, the temperature of the equilibrium simulations was 450°C, which was lower than for the experiments. Lowering the hold temperature to 450°C during the experiments would result in higher biocarbon yield, but lower fixed carbon content. It is therefore not certain that this would greatly affect the fixed carbon yield. However, since the simulations and experiments did not have the same temperature, it makes it challenging to directly compare the results. Two, it cannot be assumed that equilibrium was established in the reactor. It was seen that the biocarbon was unevenly converted throughout the reactor, and it was thereby expected that the actual fixed carbon yield would be lower than the simulated value. The equilibrium simulations do not take into account time, which could also be a factor that contributes to the difference.

5.3 TGA results

TGA was performed for all seven experiments in addition to the dried spruce chips. Weight loss curves were constructed for all samples, and the results are presented in Figure 5.9-5.11.

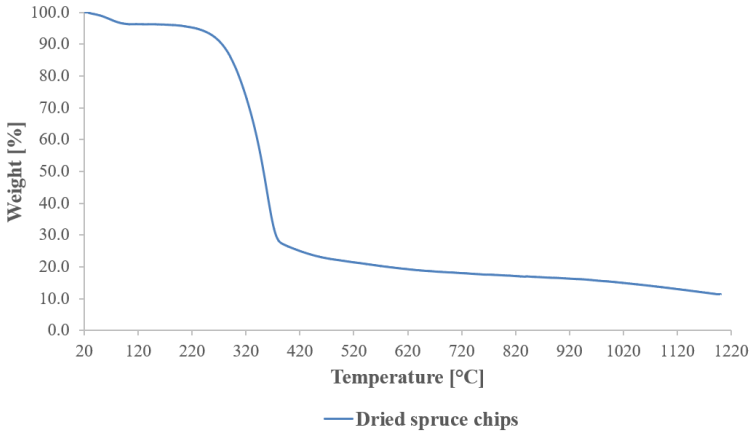

Figure 5.9: Weight loss curve of dried spruce chips.

The weight loss curve for the dried spruce chips is presented in Figure 5.9. The weight loss between 20°C and 120°C corresponds to loss of moisture, which was low. The curve has a plateau between approximately 120°C and 220°C which shows that the drying process was over and that there was little loss of other components in this temperature range. Between 300°C and 400°C the weight loss went from 5% to 75%, which corresponds to loss of volatile matter. This was the major contributor to the weight loss, and is in compliance with the proximate analysis in Table 4.1. Volatile components continued to be released until 1200°C was reached.

The weight loss curves of biocarbon produced from experiments with T_{hold} 480°C were plotted together in Figure 5.10. To get a reminder of the different experiments see Table 4.3 in Section 4.4.

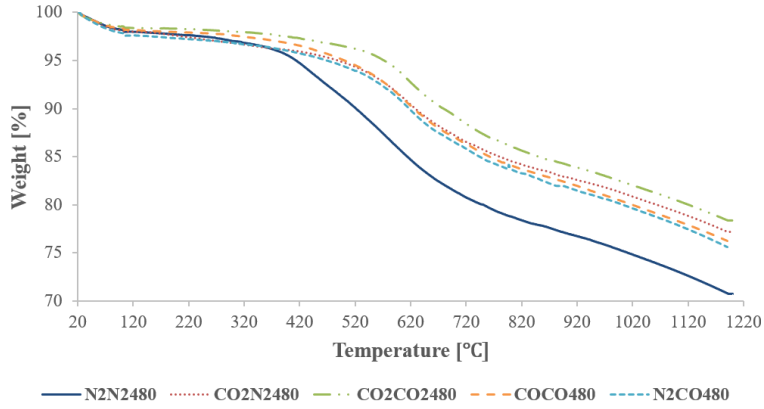

Figure 5.10: Weight loss curves of biocarbon produced in experiments with T_{hold} 480°C.

The weight loss due to moisture was similar for all five biocarbon samples. However, unlike for the biomass, these curves did not have a plateau which clearly showed where the drying process was finished. This indicates that there were losses of other components at very low temperatures, which overlapped with the drying process. It would be more accurate to directly compare the samples by excluding the drying process and normalizing the remaining results. However, since there is an overlap between drying and weight loss of other components, it cannot be said with certainty where the drying process stopped. Nevertheless, it can be seen that the major differences between the curves did not lay in the temperature range 20-200°C, and the results were therefore compared without excluding the weight loss due to water.

The main differences in weight loss were between 400°C and 700°C, which corresponds to the major loss of volatile matter. N_2N_2480 experienced the largest weight loss, and confirms that the biocarbon produced in N_2 atmosphere had higher amount of volatiles than biocarbon produced in CO_2 and CO atmosphere. Again, this is in agreement with the studies of Thanapal *et al.* (2014) and Bach *et al.* (2014) [42, 43]. The TGA results show that the release of volatiles from biocarbon produced in experiments CO_2N_2480, COCO480 and N_2CO480 was similar, and that the biocarbon produced in experiment CO_2CO_2480 had the lowest mass loss (which corresponds to less volatiles being present). Results from the

proximate analysis (Table 5.2) on the other hand suggested that the amount of volatile matter was the same in biocarbon produced in CO_2CO_2480, $COCO480$ and N_2CO480, due to overlapping uncertainties. It would be expected that the proximate analysis posed the largest uncertainty because of some differences in sample-time in the muffle furnace. Nevertheless, both analysis show that biocarbon produced in CO_2 or CO atmosphere at T_{hold} 480°C had higher quality than biocarbon produced in N_2 at T_{hold} 480°C. The weight loss after 800°C seems to be similar for all experiments.

The weight loss curves of biocarbon produced from experiments with T_{hold} 580°C were plotted together in Figure 5.11.

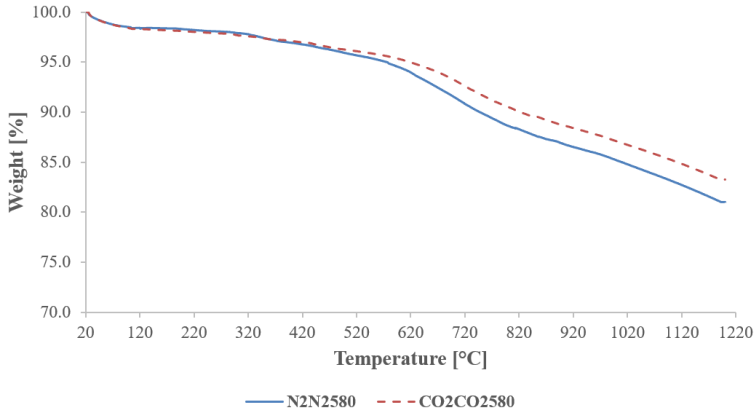

Figure 5.11: Weight loss curves of biocarbon produced in experiments with T_{hold} 580°C.

The weight loss from biocarbon produced in experiments N_2N_2580 and CO_2CO_2580 were approximately the same up to 580°C. Also here it can be observed that there was no plateau which clearly showed when the drying process finished. This indicates that there were components in the biocarbon that upon cooling and reheating was released at lower temperatures. From the proximate analysis it was found that there were no significant differences in the biocarbon produced under N_2 and CO_2 atmosphere at T_{hold} 580°C. However, the TGA results show that the biocarbon produced in N_2N_2480 had higher weight loss between 620°C and 820°C than the biocarbon produced in CO_2CO_2580. This indicates that the properties of the biocarbon might have been altered also at 580°C.

In addition to plotting the TGA results as a function of temperature, the derivative (DTG) was also plotted as a function of temperature to find the weight loss rate. The results are presented in Figure 5.12.

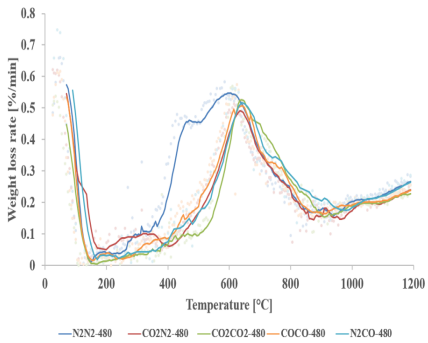

(a) DTG curves from exp. with T_{hold} 480°C

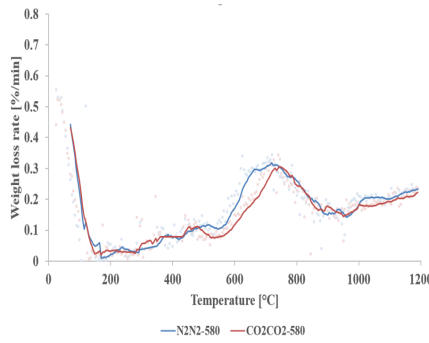

(b) DTG curves from exp. with T_{hold} 580°C

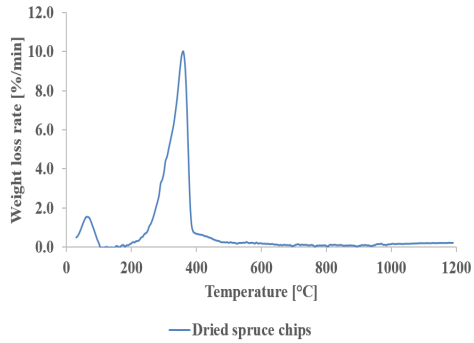

(c) DTG curve of biomass.

Figure 5.12: Weight loss rate of biocarbon produced in all the experiments in addition to dried spruce chips.

The weight loss rate for biocarbon samples produced at T_{hold} 480°C are presented in Figure 5.12a. It can be seen that the beginning and the end of the curves are relatively similar. The weight loss rate was above zero between 200°C and 400°C, which in theory it should not have been since the biocarbon was produced at 480°C. However, between the production and the analysis of the biocarbon it was cooled down. Some components might have been absorbed or attached to the structure, which were thereby released at low temperatures when the biocarbon was reheated during the analysis. The main difference between the curves in Figure 5.12a was between 400-700°C, which was also seen in Figure 5.10. The DTG curves for

biocarbon produced in CO_2 or CO atmosphere have one distinctive peak around 700°C, while the biocarbon produced in N_2 atmosphere has two (one around 450°C and one at around 600°C). From the proximate analysis it was found that N_2N_2480 produced biocarbon with more volatile matter than the other experiments. Since the volatile content was not the same in all experiments, caution should be made when comparing the weight loss rate directly. However, since the DTG curve of N_2N_2480 has two peaks, it can be assumed that the first peak represents the extra volatile matter (which would be released earlier) and that the second peak is more comparable with the peaks from the other experiments. Even when the first peak is not accounted for, it can be seen that the releasing rate of volatile matter happened earlier for the biocarbon produced in N_2N_2480. The four other curves had the same trends throughout the analysis. This indicates that CO_2 and CO atmosphere had similar effect on the biocarbon properties when it was produced at 480°C. Since there was little difference between CO_2N_2480 and CO_2CO_2480 it can again seem like the major effect of CO_2 was during low temperatures. This is in agreement with the results from the proximate analysis. There were even less differences between the TG and DTG curves for COCO480 and N_2CO480, which indicates that the addition of CO during the heat-up phase had little effect.

The weight loss rate for biocarbon samples produced at T_{hold} 580°C are presented in Figure 5.12b. The curves can be compared more directly due to similar composition of moisture and volatile matter found in the proximate analysis. The beginning and end of the curves are approximately the same. However, also here the main peak was postponed for biocarbon produced in CO_2 atmosphere. It was not found that there were significant differences in the fixed carbon content between the biocarbon samples. Nevertheless, it seems like the postponing effect on the mass loss for biocarbon produced in CO_2 atmosphere is present at both 480°C and 580°C. This was also observed in the TG curves in Figure 5.10 and 5.11.

The weight loss rate of dried spruce chips is presented in Figure 5.12c. The curve shows two distinctive peaks. First, the drying peak, which is followed by the rate almost becoming zero. This corresponds to the plateau which was observed in the TG curve of dried spruce chips, but not for the biocarbon samples. The second peak represents loss of volatile matter. These results are in agreement with the results of Ibrahim *et al.* (2013) which investigated the physicochemical characterization of torrefied biomass using TGA. They reported that the DTG curve of agricultural biomass, such as switchgrass and timothy, have two peaks in the area where volatiles are released, while forestry biomass have one peak [69]. When there are two peaks the first represents the degradation of hemicellulose, and the second represents the degradation of cellulose. Spruce is forestry biomass, and

the DTG curve had thereby one peak. The highest mass loss rate was obtained at 360°C.

5.4 Density and BET surface area results

Pycnometer analysis was performed to investigate how carrier gas and temperature affected the biocarbon density. The analyzed biocarbon samples were produced in experiments N_2N_2480, CO_2CO_2480, COCO480, N_2N_2580 and CO_2CO_2480. By using AccuPyc II 1340, the absolute volume was measured. Absolute volume is lower than apparent volume because it does not include the space between particles. This means that the obtained densities were of the solid carbon, without the pores being accounted for. The BET surface area analysis was performed on biocarbon produced in experiments N_2N_2480, CO_2CO_2480 and COCO480. Previous results from the kinetic simulation showed that available surface area might have a significant effect of the solid carbon yield. It was therefore interesting to investigate these characteristics. The results from both analyses are presented in Table 5.4.

Table 5.4: Results from density and BET analysis. The BET analysis contains inconsistencies which are discussed below.

Experiment	N_2N_2480	CO_2CO_2480	COCO480	N_2N_2580	CO_2CO_2580
Absolute density [g/cm^3]	1.386	1.384	1.395	1.472	1.492
BET surface area [m^2/g]	98.07	131.08	1.04	-	-

It can be seen that all the densities were higher than 1g/cm^3, which means that they were higher than the density of water. The results show that temperature affects the density of the carbon structure more than the gas atmosphere. biocarbon produced at T_{hold} 580°C had 5-7% higher absolute density than biocarbon produced at T_{hold} 480°C. The gas atmosphere did not affect the density significantly at T_{hold} 480°C, while biocarbon produced in CO_2 atmosphere seems to have slightly higher density compared to biocarbon produced in N_2 atmosphere at T_{hold} 580°C. It makes sense that the biocarbon produced at higher temperatures have higher absolute density. To illustrate, the density of graphite is 2.26g/cm^3, which is pure carbon [70]. Since biocarbon produced at higher temperatures obtain higher fixed carbon content and less volatile matter, the absolute density

would be expected to increase. It would also be expected that the biocarbon has a higher degree of microporosity, but this would not affect the absolute density. Previous results from the proximate analysis showed that there were no significant differences between the biocarbon produced at 580°C in N_2 and CO_2 atmosphere. The difference in density can therefore not be said to be because of different fixed carbon contents between these samples.

The results from the BET analysis varied greatly between the samples. All three of the obtained surface areas were lower than expected, and the value from experiments COCO480 is most likely incorrect due to the high deviance. However, very small BET surface areas have been reported for ground biocarbon. Thanapal *et al.* (2014) obtained a small BET surface area for their ground torrefied biocarbon. They reported that the surface areas of biocarbon produced from Juniper and Mesquite in CO_2 atmosphere were 55% and 29% higher, respectively than biocarbon produced in N_2 atmosphere [42]. Biocarbon from torrefied biomass is expected to have lower surface area than biocarbon from pyrolyzed biomass, but the results are comparable with the results obtained in this analysis. The biocarbon produced in CO_2CO_2480 had 34% higher surface area compared to biocarbon produced in N_2N_2480. It should be noted that the analysis times were not the same for all three samples, which have to be kept in mind when comparing the results. Gupta *et al.* (2019) reported a BET surface area of 2.4 and 6.9m^2/g for biocarbon produced from Teak sawdust at 400 and 500°C, respectively. They argue that such low values were due to incomplete carbonization and remaining volatile matter [58]. If there is remaining volatile matter in the pores of the biocarbon, this could freeze when using LN2 and give lower apparent surface area than the actual surface area. A solution can be to degas the samples for a longer time [71]. Since the obtained result from experiment COCO480 deviates significantly from the others, the uncertainty is regarded as too large for a comparison to be made.

The simulated results in Section 3.2 were based on the product between the density (in kg/m^3) and the available surface area (in m^2/g). The obtained density from the pycnometer analysis was much larger than the simulated densities, due to the fact that the simulated values were based on apparent densities and the measured values were absolute densities. The BET surface area from the experiment with CO as carrier gas was unrealistically low compared to the others. However, if it is assumed that the other surface areas were correct and that the actual surface area of the biocarbon produced in CO atmosphere was approximately the same as the other two, for example 100m^2/g, the product between the density and the surface area becomes comparable with the simulated values. The largest simulated values were

150kg/m^3 and 1000m^2/g, which gave $1.5 \cdot 10^8 m^2/m^3$. The product of 1395kg/m^3 and 100m^2/g becomes approximately $1.4 \cdot 10^8 m^2/m^3$. From the simulated results it was seen that the solid carbon yield could increase with 4.3% and 5.4% at hold time 3 hours and CO flow rates of 2 and 1L/min per 100g biomass, respectively. The flow rate in the experiments was set to approximately 1.4L/min, which is much lower than the simulated flow rates per biomass weight. 1.4L/min for the experiments corresponds to approximately 0.2L/min per 100g biomass. The fixed carbon yield of the biocarbon produced in N_2N_2480 and COCO480 were 0.227g FC/g biomass and 0.240g FC/ g biomass, respectively (see Table 5.3). The fixed carbon yield increased thereby with 5.73% in the CO experiment compared to the reference. These results indicate that even though the kinetic model is vastly simplified, it might predict correct trends when CO is used as carrier gas. However, to have more precise results more analysis should be performed. The BET analysis should be repeated to obtain a more reasonable surface area for the biocarbon produced in CO atmosphere.

5.5 SEM results

SEM was used to investigate if changing the gas atmosphere affected the microstructures of the biocarbon. The results are presented in Figure 5.13 and 5.14. White boxes indicate the area which got further magnified. The first four pictures in Figure 5.13 (a-d) are SEM images of biocarbon produced in experiment N_2N_2480, followed by biocarbon produced in experiments CO_2N_2480 (e-h), CO_2CO_2480 (i-l), COCO480 (m-p) and N_2CO480 (q-t).

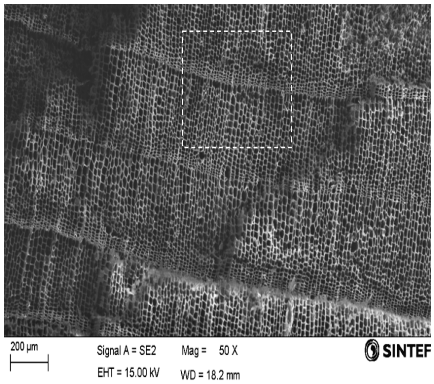

(a) N_2N_2480, 50X

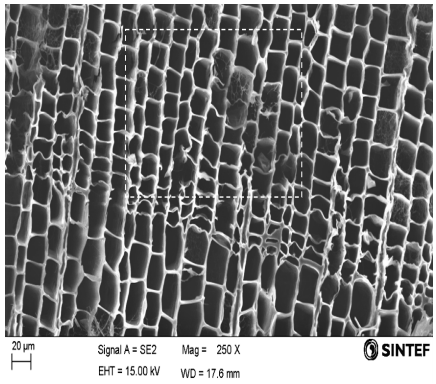

(b) N_2N_2480, 250X

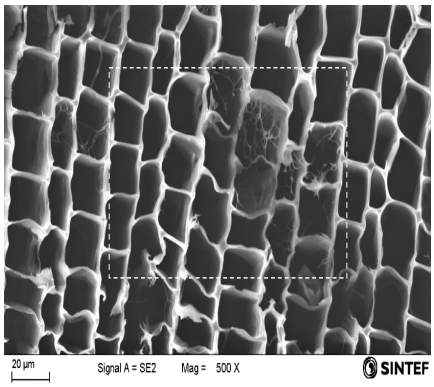

(c) N_2N_2480, 500X

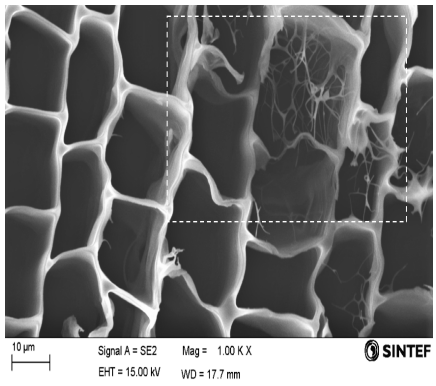

(d) N_2N_2480, 1000X

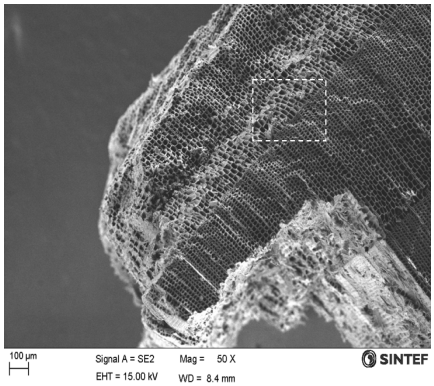

(e) CO_2N_2480, 50X

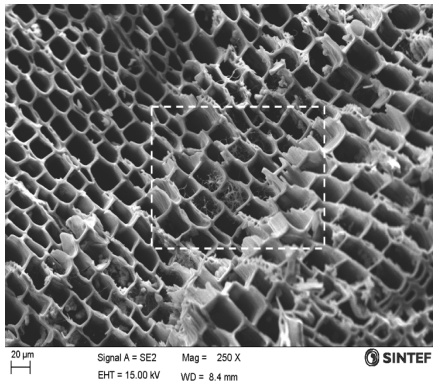

(f) CO_2N_2480, 250X

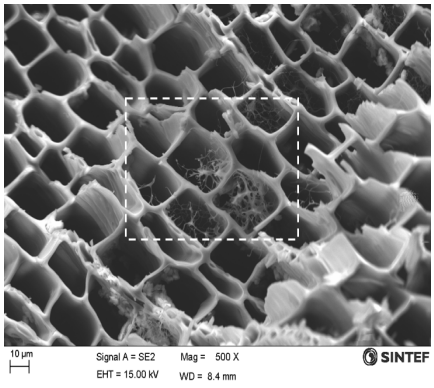

(g) CO_2N_2480, 500X

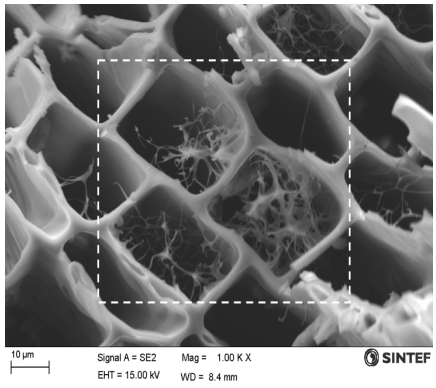

(h) CO_2N_2480, 1000X

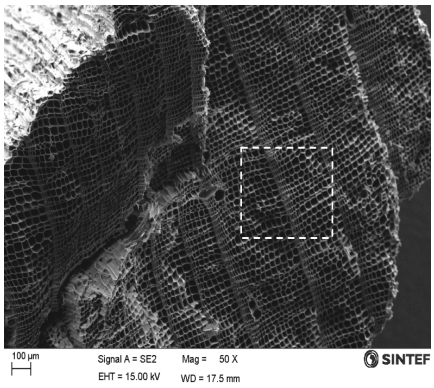

(i) CO_2CO_2480, 50X

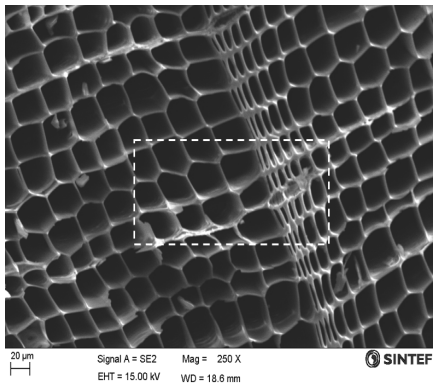

(j) CO_2CO_2480, 250X

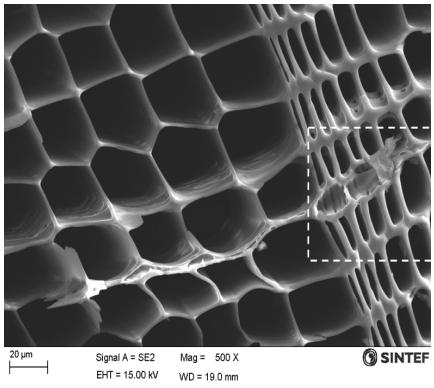

(k) CO_2CO_2480, 500X

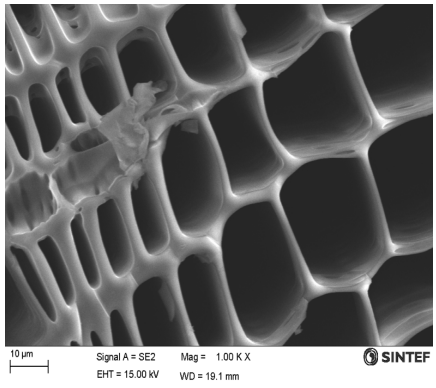

(l) CO_2CO_2480, 1000X

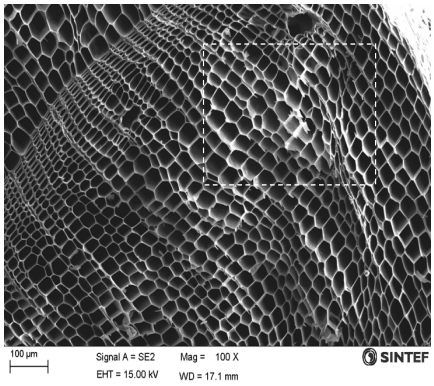

(m) COCO480, 100X

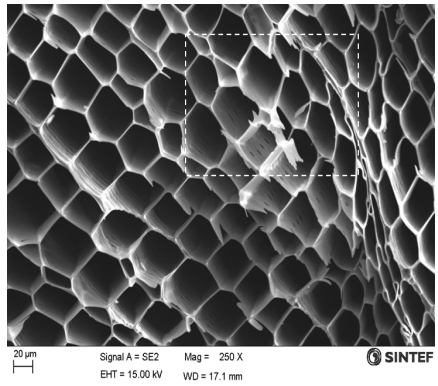

(n) COCO480, 250X

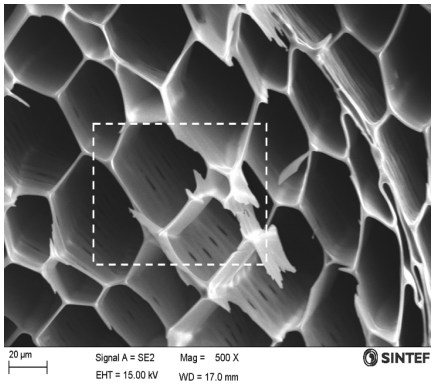

(o) COCO480, 500X

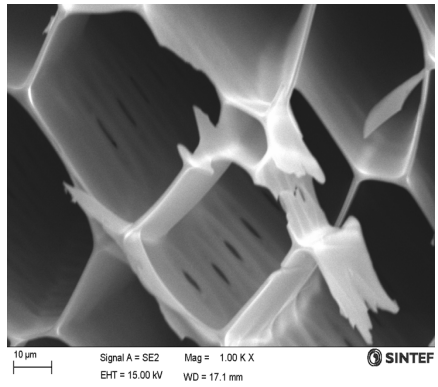

(p) COCO480, 1000X

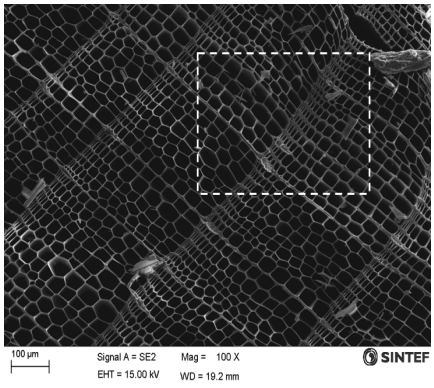

(q) N_2CO480, 100X

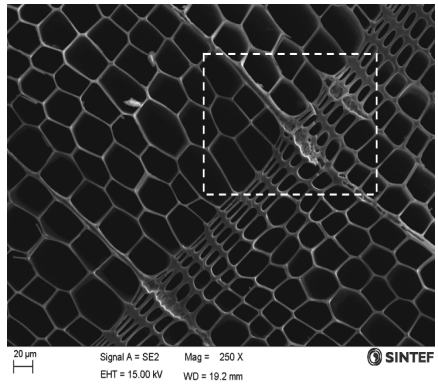

(r) N_2CO480, 250X

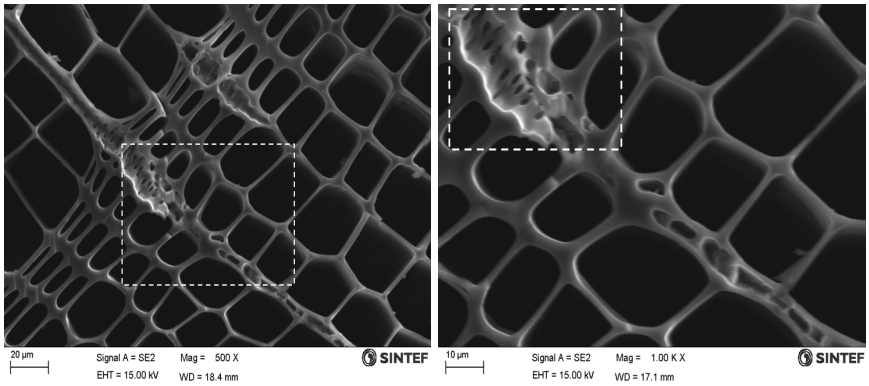

(s) N_2CO480, 500X (t) N_2CO480, 1000X

Figure 5.13: SEM images of biocarbon produced at T_{hold} 480.

Kwon *et al.* (2009) studied the transition characteristics of the cell wall during pyrolysis of wood under different temperatures using SEM. They reported that the cell wall retained its fibrous structure up to 300°C, while above 350°C it obtained an amorphous-like structure with no cell wall layering [72]. Qi *et al.* (2016) studied the carbonization characteristics of tension wood and compression wood at carbonization temperatures 400, 600 and 800°C. They reported that the primary and secondary layers of the cell wall were not identified after carbonization due to degradation of cellulose and hemicellulose, along with rearrangement of carbon into graphite structure [73]. It can be seen from all the SEM images that the carbon structures have obtained a smooth amorphous, honeycomb structure. However, there are several differences between the results. The biocarbon produced in experiments N_2N_2480 and CO_2N_2480 (Figure 5.13a-5.13h) have a spiderweb-like filling in some of the pores. As far as the author is aware of, it has not been reported such results in literature. Based on the fact that the biocarbon from these two experiments have the highest level of volatiles, it could be possible that the fillings are volatile matter. However, the fixed carbon yield was substantially higher for the biocarbon produced in experiment CO_2N_2480 than N_2N_2480, which could indicate that the filling is something else. Further analysis is therefore necessary to get a better understanding of the structure. Biocarbon produced in experiments CO_2CO_2480, $COCO480$ and N_2CO480 did not have these structures within the pores. Thanapal *et al.* (2014) reported an increase in porosity in biocarbon produced in CO_2 atmosphere [42]. They argued that these new voids released volatiles, and therefore the biocarbon had higher fixed carbon content. The biocarbon produced in pure CO_2 atmosphere seem to have larger and more pores

than the biocarbon produced in pure N_2 atmosphere (Figure 5.13i-5.13l). This was also the case for the biocarbon produced in CO atmosphere (Figure 5.13m-5.13t). It can be seen that small pores have been created within the larger pores in the biocarbon produced in experiment COCO480 (Figure 5.13o and 5.13p). This strongly indicates that the BET surface area reported for this biocarbon was not correct, and should be larger. From these SEM results, it can look like the biocarbon produced in CO atmosphere had openings with the largest diameter and the most porous structure. The fact that the biocarbon yield was the same for all experiments, but that the biocarbon seems to be more porous when produced in CO_2 and CO atmosphere is contradictory. If the theory about new voids releasing volatile matter is correct, it would be expected that the biocarbon yield decreased.

SEM images of biocarbon samples produced in N_2 and CO_2 atmosphere at T_{hold} 580°C are presented in Figure 5.14. The first four images (a-d) represent biocarbon produced in experiment N_2N_2580 and thereafter the biocarbon produced in experiment CO_2CO_2580 (e-h).

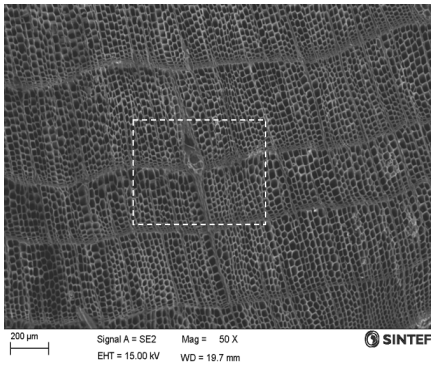

(a) N_2N_2580, 50X

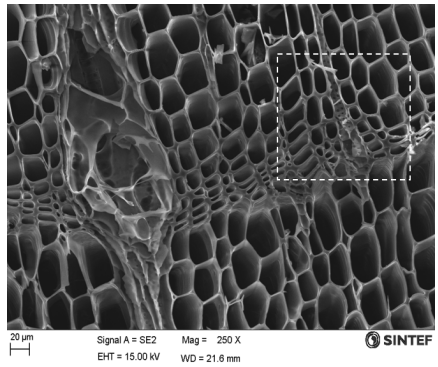

(b) N_2N_2580, 250X

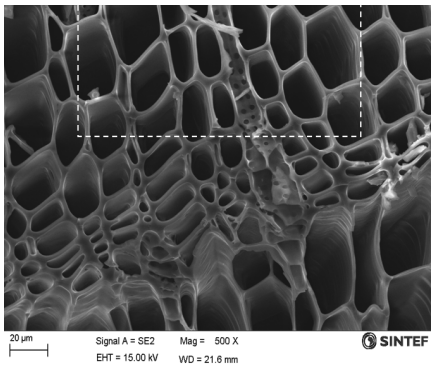

(c) N_2N_2580, 500X

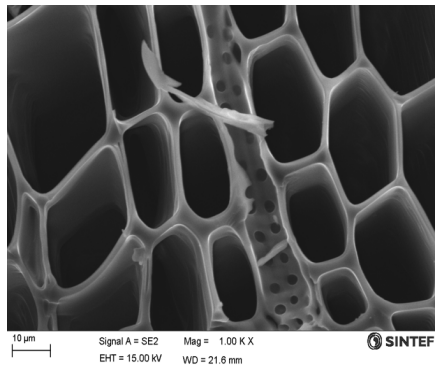

(d) N_2N_2580, 1000X

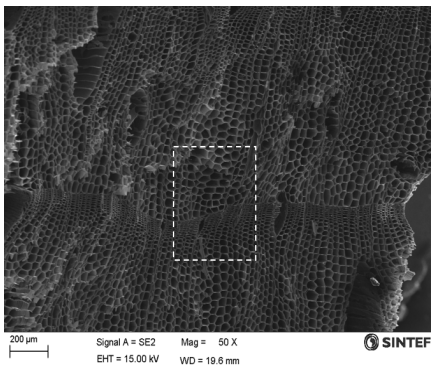

(e) CO_2CO_2580, 50X

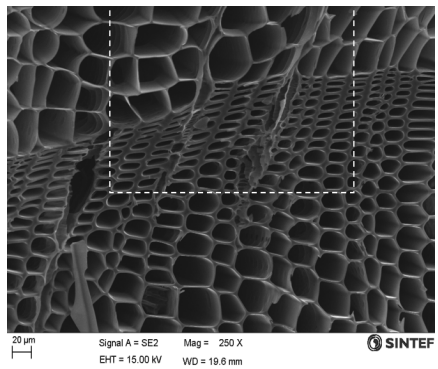

(f) CO_2CO_2580, 250X

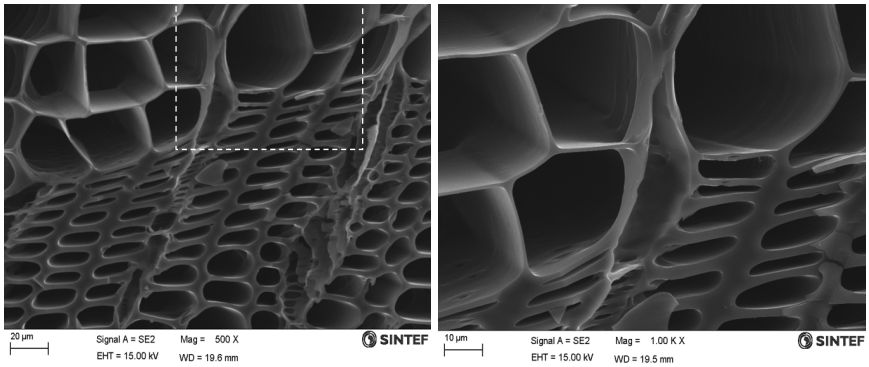

(g) CO_2CO_2580, 500X (h) CO_2CO_2580, 1000X

Figure 5.14: SEM images of biocarbon produced at T_{hold} 580°C.

It can be seen that the spiderweb-like filling found in the biocarbon sample produced at 480°C in N_2 atmosphere was not present when the temperature was increased to 580°C. The pores size seems to have increased as well for the biocarbon produced in N_2. Both biocarbon samples have a large number of macropores which create a honeycomb structure. The biocarbon produced at T_{hold} 580°C in N_2 and CO_2 atmosphere were much more alike than the biocarbon produced at T_{hold} 480°C. This is in agreement with previous results from the proximate analysis, which showed that the properties of the biocarbon were approximately the same for these experiments.

Part 3: Epilogue

6 Overall impact towards 2030

The objective of this master thesis was to investigate the possibility of increasing the biocarbon yield, or its properties, by altering the gas atmosphere during pyrolysis. A hypothesis was established, which stated that the addition of CO_2 as carrier gas could have a positive effect on the biocarbon yield at low temperatures, while the addition of CO as carrier gas could have a positive effect on the biocarbon yield at high temperatures. The results from the modelling part showed that the fixed carbon yield at equilibrium conditions was 0.34g FC/g biomass at 450°C. The kinetic simulations showed that available surface area and flow rate of carrier gas could potentially affect the system significantly. It was found that the increase of solid carbon was greatest when the diluting effect of CO was low and the available surface area was high. The temperature for the kinetic simulations was 480°C, which was also set as base case for the experimental work.

Seven experiments were conducted where the gas atmosphere was altered. The experimental results showed that the biocarbon and condensate yields were not affected by changing the gas atmosphere. The gas yield did not show any clear trends between the experiments. Based solely on these results it can seem like altering the carrier gas only had a diluting effect. However, the proximate analysis showed that the biocarbon produced in CO_2 and CO atmosphere at T_{hold} 480°C had significantly higher fixed carbon content than the biocarbon produced in pure N_2 atmosphere. The fixed carbon yield varied from 0.227g FC/g biomass (N_2 during entire experiment) to 0.243g FC/g biomass (CO_2 during entire experiment). This was lower than the simulated value of 0.34g FC/g biomass, which was expected since equilibrium is not established during the experiments. The fixed carbon yield was the same for biocarbon produced in CO_2 and N_2 atmosphere at T_{hold} 580°C. This indicated that the effect of CO_2 was mainly at low temperatures, which supports the hypothesis. The fixed carbon yield was higher for biocarbon produced in experiment N_2CO480 than COCO480. This could indicate that CO effected the biocarbon properties at high temperatures, and that the effect was low at lower temperatures. But what are the practical implications of these results?

Today Elkem use approximately 35 000 tons/year of biocarbon for their production of silicon alloys. Their goal is to increase the amount to 188 000 tons/year in 2030, and their quality requirement for the biocarbon is 76 wt.% fixed carbon [4]. From the experimental results it was found that the fixed carbon yield of biocarbon produced in pure N_2, CO and CO_2 atmosphere were 0.227, 0.240 and 0.243g FC/g dried spruce chips, respectively. The amount of dry raw material can thereby be calculated by multiplying the amount of biocarbon with the fixed

carbon requirement, and dividing by the fixed carbon yield. The amount of dry spruce chips needed in 2030 is $6.29 \cdot 10^5$ tons/year if the biocarbon is produced in pure N_2 atmosphere. If the production is in CO or CO_2 atmosphere, the demand for dried spruce chips would be $5.95 \cdot 10^5$ and $5.88 \cdot 10^5$ tons/year, respectively. This would mean a reduction of $0.34 \cdot 10^5$ and $0.41 \cdot 10^5$ tons/year, which corresponds to 5.4 and 6.5%, respectively. The results obtained in this master thesis are thereby very promising. If further research confirms that both CO_2 and CO can have such positive effects on the biocarbon properties it could have a significant impact on the metallurgical industry. The reduction of raw material would also affect the size requirements for the pyrolysis factory. In addition to decreasing the need for raw material, the results also indicate that the pyrolysis temperature could be reduced. The biocarbon would still fulfill the requirement of 76% fixed carbon with notably lower temperatures if CO or CO_2 are used as carrier gases instead of N_2. Nevertheless, more research is necessary to obtain a better understanding of the mechanism which can explain these results.

7 Conclusion

Modeling, experimental and analytical work have been performed to investigate if altering the gas atmosphere during pyrolysis affects the biocarbon yield and/or biocarbon properties. The results show that the biocarbon yield was not affected by changing the carrier gas from N_2 to CO_2 or CO. However, the properties of the biocarbon were affected. Biocarbon produced in CO_2 and CO atmosphere had significantly higher fixed carbon yield than biocarbon produced in N_2 atmosphere at T_{hold} 480°C. TGA results showed that the mass loss increased at lower temperatures for the biocarbon produced in N_2 at both hold temperatures, compared to biocarbon produced in CO_2 and CO atmospheres. SEM images showed that when N_2 was used as carrier gas throughout the experiment or during the hold phase (at T_{hold} 480°C), the produced biocarbon had spiderweb-like structures in some of the pores. This was not present when CO_2 and CO were used as carrier gas at same hold temperature. The results in this master thesis are contradictory, yet promising, and indicate that the biocarbon quality can be increased by changing the pyrolysis gas atmosphere, without decreasing the biocarbon yield. The results also indicate that the hypothesis formulated during the introduction might be correct. The effects of CO_2 seem to be dominating at low temperatures, while the effects of CO seem to be dominating at high temperatures. If these results are confirmed in future work, it will have the possibility to significantly affect several aspects of Elkem's goal towards a carbon-neutral metal production. Nevertheless, many of the obtained results are challenging to explain, and further research is recommended to gain more understanding.

8 Further work

There is much further work that can and should be done in this project. All experiments should be performed again to obtain parallels, which ensure that the experiments are reproducible. The condensate can be analyzed to see if the composition was altered when CO_2 was used as carrier gas. It was seen that the conversion degree of biocarbon differed significantly between the layers in the reactor due to incoming gas with low temperature. Effort should be made to minimize this effect. As mention in the report, this might not be a problem in Elkem's process, since the gas will have a much higher temperature when it leaves the silicon furnace before being circulated back to the pyrolysis process.

From the results of the proximate analysis, it was presented a scenario which illustrated the effects CO_2 compared to N_2 at different temperatures. Since only two temperatures were tested it cannot be said with much certainty that the trend is linear, which in this case was assumed. Therefore, more experiments with different temperatures should be conducted. From the proximate analysis and TGA it was also found that CO has a positive effect on the fixed carbon yield. More experiments with different temperatures should also be performed with CO as carrier gas and compared with the effects of CO_2.

The SEM analysis showed that biocarbon produced in N_2 atmosphere had structures within the pores which were not present in the biocarbon produced in CO_2 and CO atmosphere. These structures were assumed to be volatile matter. However, the structure should be further analyzed to confirm its composition. Determining the actual surface area of the biocarbon would also be interesting to see if the microporosity has increased, or if more carbon structures have been created and decreased the available surface area.

References

1. Elkem ASA. *Pyrolysis of wood optimised for production of energy and tailor-made biochar for silicon production* Accessed 28.01.2019 [online] at. 2019. https://www.elkem.com/innovation/research-projects/pyropt/.
2. Elkem. *Elkem Silicon Materials* Accessed 24.09.18 [online] at. https://www.elkem.com/no/about-elkem/business-areas/elkem-silicon-materials/.
3. Elkem. *Råvare for produksjon av biokarbon i Norge* Report obtained by Geir J. Andersen from Elkem. 2018.
4. Andersen, G. J. . "Elkems målsetning mot 2030." Message to Cecilia Håkegård 28.05.19. E-mail.
5. Monsen, B. *et al.* Bruk av biokarbon i norsk ferrolegeringsindustri. Feasibilitystudie 1999. doi:10.13140/RG.2.2.29766.88640 (1999).
6. Brown, R. C. & Brown, T. R. in *Biorenewable Resources* 2nd ed., 195–236 (John Wiley & Sons, 2014).
7. Fassinou, W. F., Van de Steene, L., Toure, S., Volle, G. & Girard, P. Pyrolysis of Pinus pinaster in a two-stage gasifier: Influence of processing parameters and thermal cracking of tar. *Fuel Processing Technology* **90,** 75–90 (2009).
8. Elyounssi, K., Collard, F.-X., Mateke, J.-a. N. & Blin, J. Improvement of charcoal yield by two-step pyrolysis on eucalyptus wood: A thermogravimetric study. *Fuel* **96,** 161–167 (2012).
9. Agirre, I., Griessacher, T., Rösler, G. & Antrekowitsch, J. Production of charcoal as an alternative reducing agent from agricultural residues using a semi-continuous semi-pilot scale pyrolysis screw reactor. *Fuel Processing Technology* **106,** 114–121 (2013).
10. Adrados, A., De Marco, I., Lopez-Urionabarrenechea, A., Solar, J. & Caballero, B. Avoiding tar formation in biocoke production from waste biomass. *Biomass and Bioenergy* **74,** 172–179 (2015).
11. Adrados, A. *et al.* Hydrogen rich reducing gases generation in the production of charcoal from woody biomass carbonization. *Energy Conversion and Management* **148,** 352–359 (2017).
12. Solar, J., Caballero, B., De Marco, I., López-Urionabarrenechea, A. & Gastelu, N. Optimization of Charcoal Production Process from Woody Biomass Waste: Effect of Ni-Containing Catalysts on Pyrolysis Vapors. *Catalysts* **8,** 191 (2018).
13. Van Wesenbeeck, S. *et al.* Charcoal "mines" in the Norwegian Woods. *Energy and Fuels* **30,** 7959–7970 (2016).

14. Elkem. *Important milestone on the road to carbon-neutral metal production* Accessed 24.09.18 [online] at. `https://www.elkem.com/sustainability/carbon-netural-metal-production-charchoal/`.
15. Basu, P. *Biomass gasification, pyrolysis and torrefaction : practical design and theory* 147–176. ISBN: 9780123964885 (Academic Press, 2013).
16. Tarves, P. C., Mullen, C. A. & Boateng, A. A. Effects of Various Reactive Gas Atmospheres on the Properties of Bio-Oils Produced Using Microwave Pyrolysis. *ACS Sustainable Chemistry & Engineering* **4,** 930–936 (2016).
17. Skreiberg, O., Wang, L., Bach, Q. & Gronli, M. Carbonization pressure influence on fixed carbon yield. *Chemical Engineering Transactions* **65,** 7–12 (2018).
18. Yang, F.-C. *et al.* Preparation and Antibacterial Effect of Bamboo Charcoal/Ag on Staphylococcus Aureus and Pseudomonas Aeruginosa. *Journal of the Chinese Chemical Society* **56,** 327–334 (2009).
19. Antal, M. J. & Gronli, M. The art, science, and technology of charcoal production. *Ind. Eng. Chem,* 1619–1640 (2003).
20. Solar, J. *et al.* Influence of temperature and residence time in the pyrolysis of woody biomass waste in a continuous screw reactor. *Biomass and Bioenergy* **95,** 416–423 (2016).
21. Lin, S. H., Hsu, L. Y., Chou, C. S., Jhang, J. W. & Wu, P. Carbonization process of Moso bamboo (Phyllostachys pubescens) charcoal and its governing thermodynamics. *Journal of Analytical and Applied Pyrolysis* **107,** 9–16 (2014).
22. Higman, C. & Van der Burgt, M. *Gasification* 2nd ed., 36 (Gulf Professional Publishing, 2008).
23. Nachenius, R. W., Ronsse, F., Venderbosch, R. H. & Prins, W. *Biomass Pyrolysis* 1st ed., 75–139 (Elsevier Inc., 2013).
24. Chen, W.-H. & Lin, B.-J. Characteristics of products from the pyrolysis of oil palm fiber and its pellets in nitrogen and carbon dioxide atmospheres. *Energy* **94,** 569–578 (2016).
25. Blackadder, W. & Rensfelt, E. in *Fundamentals of Thermochemical Biomass Conversion* 747–759 (Springer Netherlands, Dordrecht, 1985).
26. Skreiberg, O., Gronli, M. G., Antal, M. J., Wang, L. & Higashi, C. *Charcoal production from forest residues* in *Processing of the 23rd European Biomass Conference and Exhibition* (Vienna, 2015).
27. Azuara, M., Sáiz, E., Manso, J. A., García-Ramos, F. J. & Manyà, J. J. Study on the effects of using a carbon dioxide atmosphere on the properties of vine shoots-derived biochar. *Journal of Analytical and Applied Pyrolysis* **124,** 719–725 (2017).

28. Manya, J. J., Laguarta, S., Ortigosa, M. A. & Manso, J. J. Biochar from Slow Pyrolysis of Two-Phase Olive Mill Waste: Effect of Pressure and Peak Temperature on its Potential Stability. *Energy & Fuels* **28,** 3271–3280 (2014).
29. Xing, P. *et al.* The use of equilibrium thermodynamic models for the prediction of inorganic phase changes in the co-firing of wheat straw with El Cerrejon coal. *Journal of the Energy Institute.* doi:10.1016/J.JOEI.2018.02.003 (2018).
30. Di Blasi, C. Modeling chemical and physical processes of wood and biomass pyrolysis. *Progress in Energy and Combustion Science* **34,** 47–90 (2008).
31. Branca, C. & Di Blasi, C. Kinetics of the isothermal degradation of wood in the temperature range 528–708 K. *Journal of Analytical and Applied Pyrolysis* **67,** 207–219 (2003).
32. Miller, R. S. & Bellan, J. A Generalized Biomass Pyrolysis Model Based on Superimposed Cellulose. *Combustion Science and Technology* **126,** 97–137 (1997).
33. Haus, J., Goltzsche, M., Hartge, E.-U., Heinrich, S. & Werther, J. Gasification kinetics of lignite char in a fluidized bed of reactive oxygen carrier particles. *Fuel* **236,** 166–178 (2018).
34. Gadsby, J., Hinshelwood, C. N. & Sykes, K. W. The Kinetics of the Reactions of the Steam-Carbon System. *Proceedings of the Royal Society A: Mathematical, Physical and Engineering Sciences* **187,** 129–151 (1946).
35. Tomeczek, J. & Gil, S. The kinetics of coal chars hydrogasification. *Fuel Processing Technology* **91,** 1564–1568 (2010).
36. Wen, C. Y. & Chaung, T. Z. Entrainment Coal Gasification Modeling. *Industrial & Engineering Chemistry Process Design and Development* **18,** 684–695 (1979).
37. Yan, L. *et al.* Kinetic model and prediction for coal hydrogasification. *International Journal of Hydrogen Energy* **38,** 4513–4523 (2013).
38. Liu, X. J., Zhang, W. R. & Park, T. J. Modelling coal gasification in an entrained flow gasifier. *Combustion Theory and Modelling* **5,** 595–608 (2001).
39. Smith J, B. R., Loganathan, M. & Shekhar Shantha, M. A Review of the Water Gas Shift Reaction Kinetics A Review of the Water Gas Shift Reaction Kinetics. *International Journal of Chemical Reactor Engineering.* doi:10.2202/1542-6580.2238 (2010).
40. Liu, Z. *et al.* Pyrolysis/gasification of pine sawdust biomass briquettes under carbon dioxide atmosphere: Study on carbon dioxide reduction (utilization) and biochar briquettes physicochemical properties. *Bioresource Technology* **249,** 983–991 (2018).

41. Zhang, H. *et al.* Biomass fast pyrolysis in a fluidized bed reactor under N2, CO2, CO, CH4 and H2 atmospheres. *Bioresource Technology* **102,** 4258–4264 (2011).
42. Thanapal, S. S. *et al.* Carbon Dioxide Torrefaction of Woody Biomass. *Energy & Fuels* **28,** 1147–1157 (2014).
43. Bach, Q.-V., Tran, K.-Q., Skreiberg, Ø. & Khalil, R. A. Effects of CO2 on Wet Torrefaction of Biomass. *Energy Procedia* **61,** 1200–1203 (2014).
44. Duan, L., Zhao, C., Zhou, W., Qu, C. & Chen, X. Investigation on Coal Pyrolysis in CO 2 Atmosphere. *Energy & Fuels* **23,** 3826–3830 (2009).
45. Liu, Z., Hu, J., Ba, F., Yuan, X. & Zhang, K. Experimental Investigation on Pyrolysis of Pine Sawdust Biomass Briquettes to Make Biochar Briquettes in CO2/N2 Atmosphere. *Proceedings of the Chinese Society of Electrical Engineering* **38,** 3281–3288 (2018).
46. Kwon, E. E., Yi, H. & Castaldi, M. J. Utilizing Carbon Dioxide as a Reaction Medium to Mitigate Production of Polycyclic Aromatic Hydrocarbons from the Thermal Decomposition of Styrene Butadiene Rubber. *Environmental Science & Technology* **46,** 10752–10757 (2012).
47. Jindarom, C., Meeyoo, V., Rirksomboon, T. & Rangsunvigit, P. Thermochemical decomposition of sewage sludge in CO 2 and N 2 atmosphere. *Chemosphere* **67,** 1477–1484 (2007).
48. Wang, Q. *et al.* Effects of CO2 atmosphere on slow pyrolysis of high-ash lignite. *Carbon Resources Conversion* **1,** 94–103 (2018).
49. Marsh, H. & Rodríguez-Reinoso, F. *Activated carbon* ISBN: 0080455964 (Elsevier, 2006).
50. Schmidt, H.-P. *European Biochar Certificate (EBC) - guidelines version 6.1* tech. rep. (2015). doi:10.13140/RG.2.1.4658.7043.
51. Sigmund, G., Hüffer, T., Hofmann, T. & Kah, M. Biochar total surface area and total pore volume determined by N2 and CO2 physisorption are strongly influenced by degassing temperature. *Science of The Total Environment* **580,** 770–775 (2017).
52. Bale, C. *et al.* FactSage thermochemical software and databases. *Calphad* **26,** 189–228 (2002).
53. Bale, C. *et al.* FactSage thermochemical software and databases, 2010–2016. *Calphad* **54,** 35–53 (2016).
54. Jian, J., Lu, Z., Yao, S., Li, X. & Song, W. Comparative Study on Pyrolysis of Wet and Dry Torrefied Beech Wood and Wheat Straw. *Energy & Fuels* **33,** 3267–3274 (2019).

55. Mei, Y. *et al.* Low temperature deoxidization of biomass and its release characteristics of gas products. *Industrial Crops and Products* **123,** 142–153 (2018).
56. Chen, Z. *et al.* Biomass torrefaction: A promising pretreatment technology for biomass utilization. *IOP Conference Series: Earth and Environmental Science* **113,** 012201 (2018).
57. Hunt, J. *et al.* Microwave-Specific Enhancement of the Carbon-Carbon Dioxide (Boudouard) Reaction. *J. Phys. Chem C.* **117,** 26871–26880 (2013).
58. Gupta, G. K., Gupta, P. K. & Mondal, M. K. Experimental process parameters optimization and in-depth product characterizations for teak sawdust pyrolysis. *Waste Management* **87,** 499–511 (2019).
59. AGA. *Nitrogen flaske* Accessed 16.04.19 [online] at. `https://shop.aga.no/shop/no/no-ig/nitrogen-ind-50-l-100256-106`.
60. AGA. *Karbondioksid flaske* Accessed 16.04.19 [online] at. `https://shop.aga.no/shop/no/no-ig/gass-gas/rene-gasser-ig-pure-gas/karbondioksid-flaske-1214-106#product1`.
61. AGA. *Sikkerhetsdatablad Karbonmonoksid* Released 16.01.13. Updated 03.07.2017. Accessed 18.02.19 [online] at. `https://www.aga.no/no/images/Karbonmonoksid_1.0_NO_tcm639-445183.pdf`.
62. Yin, C.-Y. Prediction of higher heating values of biomass from proximate and ultimate analyses. *Fuel* **90,** 1128–1132 (2011).
63. Skreiberg, A., Skreiberg, Ø., Sandquist, J. & Sørum, L. TGA and macro-TGA characterisation of biomass fuels and fuel mixtures. *Fuel* **90,** 2182–2197 (2011).
64. Micromeritics Instrument. *AccuPyc II 1340 Gas Displacement Pycnometry System* Accessed 14.05.2019 [online] at. `https://www.micromeritics.com/Repository/Files/AccuPyc_Final_0.pdf`.
65. Micromeritics Instrument. *Surface area instruments* Accessed 14.04.2019 [online] at. `https://www.micromeritics.com/Product-Showcase/Surface-Area.aspx`.
66. NanoScience Intruments. *Scanning Electron Microscopy* Accessed 07.05.2019 [online] at. `https://www.nanoscience.com/techniques/scanning-electron-microscopy/`.
67. Kwon, E. E., Jeon, Y. J. & Yi, H. New candidate for biofuel feedstock beyond terrestrial biomass for thermo-chemical process (pyrolysis/gasification) enhanced by carbon dioxide (CO2). *Bioresource Technology* **123,** 673–677 (2012).
68. Skreiberg, Ø. . Personal communication, 10.05.2019.

69. Ibrahim, R. H., Darvell, L. I., Jones, J. M. & Williams, A. Physicochemical characterisation of torrefied biomass. *Journal of Analytical and Applied Pyrolysis* **103,** 21–30 (2013).
70. Poco Graphite Inc. *PROPERTIES AND CHARACTERISTICS OF GRAPHITE* Accessed 28.05.2019 at. `http://poco.com/Portals/0/Literature/Semiconductor/IND-109441-0115.pdf`.
71. Wielechowski, H. A. . "Problem med kull prøver, haster med svar, oppdrag." Message to Elin H. Albertsen. 08.05.2019. E-mail.
72. Kwon, S.-M., Kim, N.-H. & Cha, D.-S. An investigation on the transition characteristics of the wood cell walls during carbonization. *Wood Science and Technology* **43,** 487–498 (2009).
73. Qi, Y. *et al.* Carbonization of reaction wood from Paulownia tomentosa and Pinus densiflora branch woods. *Wood Science and Technology* **50,** 973–987 (2016).

Appendices

A Modeling

Raw material for the simulation results, explanation on how the CSTR reactor was simulated and the MATLAB scrips are presented in this section.

A.1 Biomass composition

The raw data corresponding to Figure 3.1 are presented in Table A.1. The fixed carbon yield correspond to the solid carbon obtained after the simulation divided on the biomass input.

Table A.1: Raw data from simulation of different biomass composition. O/C and H/C molar ratios. Unit of fixed carbon yield (y_{FC}) is g FC/g biomass

O/C 0.45		**O/C 0.53**		**O/C 0.67**		**O/C 0.83**		**O/C 0.91**	
H/C	$y_{\mathbf{FC}}$	**H/C**	$y_{\mathbf{FC}}$	**H/C**	$y_{\mathbf{FC}}$	**H/C**	$y_{\mathbf{FC}}$	**H/C**	$y_{\mathbf{FC}}$
0.24	0.49	0.24	0.44	0.24	0.37	0.24	0.29	0.24	0.26
0.73	0.49	0.73	0.44	0.73	0.37	0.73	0.30	0.73	0.27
1.48	0.43	1.48	0.39	1.48	0.34	1.48	0.29	1.48	0.26
2.42	0.33	2.42	0.32	2.42	0.28	2.42	0.24	2.42	0.22
3.63	0.21	3.63	0.20	3.63	0.19	3.63	0.17	3.63	0.16

A.2 Kinetics

The reactor was simulated as a continuous stirred tank reactor (CSTR) to be able to investigate the influence of adding gas to the system. A general mass balance was formulated for the system, and is shown in Equation (A.1).

$$F_{i,\text{in}} - F_{i,\text{out}} + R_i V = \frac{dX_i}{dt} \tag{A.1}$$

$F_{i,\text{in}}$ is the molar flow of component i into the reactor, $F_{i,\text{out}}$ is the molar flow out of the reactor, R_i is moles of i generated in the reactor, V is the reactor volume or carbon particle volume depending on if the reaction is homogeneous or

heterogeneous, respectively, and dX_i/dt is the accumulated moles of i. The molar flow into the reactor was set, while the molar flow out of the reactor was calculated on the basis of having constant temperature, pressure and reactor volume. In order to keep all those parameters constant the number of gas molecules also had to be constant. A mass balance for the change in number of moles is presented in Equation (A.2).

$$\frac{dn_{\text{gas}}}{dt} = \sum F_{\text{gas,in}} - F_{\text{out}} + \big(\sum R_{\text{gas}}\big)V = 0 \tag{A.2}$$

dn_{gas}/dt is the change in gas molecules in the reactor due to inlet and outlet flow of gas ($F_{\text{gas,in}}$ and F_{out}), and chemical reactions that either produce or reduce the amount of moles (R_{gas}). This change equals zero when temperature, volume and pressure are constant, and the total molar outflow could thereby be calculated as the sum of inflow of gas and the change in moles due to chemical reactions. To calculate the outflow of each individual gas species, the total flow was multiplied with the mole fraction of each gas specie.

A.2.1 MATLAB scripts

Script 1: ODE function

```
clear all
clc
close all

%Inital conditions
Species.Initial_conditions=[2.841, 0.7095, 0.0677, 0.5159,
    0.7374, 1.2766];
Species.speciesnames={'C' 'CO2' 'CO' 'CH4' 'H2' 'H2O'};

%Time for the simulation
tspan=0:900:3600*5;

%Simulation temp
Temp=480+273;

%Arrhenius coefficients for the reactions

%C(s)+ CO2 -> 2CO R=[g/cm2/s]
Reaction.A(1)    = 247;
Reaction.E(1)    = 21060;
Reaction.Keq(1) =exp(17.644-(30260/(1.8*Temp)));

%C(s) + 2H2 -> CH4 R=[g/cm2/s]
Reaction.A(2)    = 0.12;
Reaction.E(2)    = 17921;
Reaction.Keq(2) =0.175/34713*exp(18400/(1.8*Temp));

%C(s) + H2O -> H2 + CO R= [g/cm2/s]
Reaction.A(3)    = 247;
Reaction.E(3)    = 21060;
Reaction.Keq(3) =exp(17.644-30260/(1.8*Temp));

%CH4 + H2O -> CO + 3H2 R=[mol/m3/s]
R = 8.314; %J/K/mol
Reaction.A(4)    = 312;
```

```
Reaction.E(4)     = 20000/R;
Reaction.Keq(4)  =6.7125e-24*exp(27020/Temp)*(R*Temp)^2;

%CO + H2O -> CO2 + H2 R=[mol/m3/s]
R = 8.314; %J/K/mol
Reaction.A(5)     = 2.75e3;
Reaction.E(5)     = 8.36e4/R;
Reaction.Keq(5)  =2.65e-2*exp(3956/Temp);

Species.y=[];
Species.t=[];
ode = @(t,y) Reactions_CSTR_S(t,y,Reaction.A,Reaction.E,
    Reaction.Keq,Temp);
[Species.t,Species.y] = ode15s(ode, tspan, Species.
    Initial_conditions);

close all
figure(1)
subplot(1,3,1)
plot(Species.t/3600,Species.y(:,2:1:6))
legend(Species.speciesnames(2:1:6))
xlabel('Time [h]')
ylabel('moles')

n = length(Species.y);
for i = 1:n
    Convy(i) = (Species.y(i,1)./Species.y(1,1)-1)*100;
end

subplot(1,3,2)
plot(Species.t/3600,Species.y(:,1))
legend(Species.speciesnames(1))
xlabel('Time [h]')
ylabel('mol solid carbon')

CO_added = {'1L/s'};
subplot(1,3,3)
plot(Species.t/60, Convy)
legend(CO_added)
```

```
72 xlabel('Time [h]')
73 ylabel('Conversion [%]')
74
75 x_CO2 = Species.y(:,2)./(Species.y(:,2)+Species.y(:,3)+...
76     Species.y(:,4)+ Species.y(:,5)+Species.y(:,6));
77 x_CO = Species.y(:,3)./(Species.y(:,2)+Species.y(:,3)+...
78     Species.y(:,4)+ Species.y(:,5)+Species.y(:,6));
79 x_CH4 = Species.y(:,4)./(Species.y(:,2)+Species.y(:,3)+...
80     Species.y(:,4)+Species.y(:,5)+Species.y(:,6));
81 x_H2 = Species.y(:,5)./(Species.y(:,2)+Species.y(:,3)+...
82     Species.y(:,4)+Species.y(:,5)+Species.y(:,6));
83 x_H2O = Species.y(:,6)./(Species.y(:,2)+Species.y(:,3)+...
84     Species.y(:,4)+Species.y(:,5)+Species.y(:,6));
85
86 x_gas = [x_CO2, x_CO, x_CH4, x_H2, x_H2O];
87
88 subplot(1,3,3)
89 plot(Species.t/3600, x_gas)
90 xlabel('Time [h]')
91 ylabel('Mole fraction')
92
93 figure(2)
94 plot(Species.t/60, Species.y)
95 legend(Species.speciesnames)
96 xlabel('Time [min]')
97 ylabel('Amount [moles]')
```

Script 1: Modeling CSTR

```
function [y,Temp] = Reactions_CSTR_S_report(t,y,A,b,Eq,Temp)
m_C = y(1);
n_CO2 = y(2);
n_CO= y(3);
n_CH4 = y(4);
n_H2 = y(5);
n_H2O = y(6);

P_tot = 1; %atm
n_tot = n_CO2 + n_CO + n_CH4 + n_H2 + n_H2O;

%mole fractions of gas
x_CO2 = n_CO2/n_tot;
x_CO = n_CO/n_tot;
x_CH4 = n_CH4/n_tot;
x_H2 = n_H2/n_tot;
x_H2O = n_H2O/n_tot;

x_gas = [x_CO2, x_CO, x_CH4, x_H2, x_H2O];
%partial pressure atm
p_CO2 = P_tot * x_CO2;
p_CO = P_tot * x_CO;
p_CH4 = P_tot * x_CH4;
p_H2 = P_tot * x_H2;
p_H2O = P_tot * x_H2O;

%Flow into reactor mol/s
v_in = 1; %L/min
n_in = v_in/(22.4*(20+273)/273)/60; %mol/s
F_0 = [0,n_in, 0, 0, 0];


% Assume particle diameter
d_p = 1; %cm
V_p = 4/3*pi*(0.01*d_p/2)^3; % m3 volume of coal particle
a_p = 1000; % m2/g
```

```
rho_p = 150; %g/dm3
Rho_p = rho_p *1000; %g/m3
A_p = a_p*Rho_p; %m2/m3 surface area per volume
T = Temp; %K
V_r = 0.0057; % m3 reactor volume

% Rate constant
k(1) = A(1)*exp(-b(1)/T)*1e4*A_p;          %gC/atm/m3_particle/s
k(2) = A(2)*exp(-b(2)/T)*1e4*A_p;          %gC/atm/m3_particle/s
k_eq(2) = Eq(2);
k(3) = A(3)*exp(-b(3)/T)*1e4*A_p;          %gC/atm/m3_particle/s
k_eq(3) = Eq(3);
k(4)= A(4)*exp(-b(4)/T);                   %m3_reactor/mol/s
k_eq(4) = Eq(4);
k(5) = A(5)*exp(-b(5)/T);                  %m3_reactor/mol/s
k_eq(5) = Eq(5);

R = 8.314;
%Rate expressions
R1 = k(1)*(p_CO2); % gC/m3_particle/s
R2 = k(2)*(p_H2-sqrt(p_CH4/k_eq(2)));% gC/m3_particle/s
R3 = k(3)*(p_H2O-(p_CO*p_H2/k_eq(3))); % gC/m3_particle/s
R4 = k(4)*(p_CH4*1.013e5/R/T*p_H2O*1.013e5/R/T- 1/k_eq(4)*p_CO*...
    1.013e5/R/T*(p_H2*1.013e5/R/T)^3); %mol/m3_reactor/s
R5 = k(5)*(p_CO*1.013e5/R/T*p_H2O*1.013e5/R/T - 1/k_eq(5)*p_CO2*...
    1.013e5/R/T*p_H2*1.013e5/R/T); %mol/m3_reactor/s

%Flow out mol/s
F = sum(F_0) + (R1-R2+R3)/12*V_p + 2*R4*V_r;
%reactions which change the number of gas molecules
%(To have constant pressure the numer of moles have to be constant)

F_CO2 = F*x_gas(1); %molCO2/s out
```

```
70 F_CO = F*x_gas(2);   %molCO/s out
71 F_CH4 = F*x_gas(3); %molCH4/s out
72 F_H2 = F*x_gas(4);   %molH2/s out
73 F_H2O = F*x_gas(5); %molH2O/s out
74
75 %Change in composition
76 dC_dt = (-R1 -R2 -R3)/12*V_p; % mol C/s
77 dCO2_dt = F_0(1)-F_CO2 -R1/12*V_p + R5*V_r; %mol CO2/s
78 dCO_dt = F_0(2)-F_CO + (2*R1/12 + R3/12)*V_p + (R4 - R5)*
       V_r; %mol CO/s
79 dCH4_dt =  F_0(3)-F_CH4 + R2/12*V_p - R4*V_r; %mol CH4/s
80 dH2_dt =  F_0(4)-F_H2 + (-R2/12 + R3/12)*V_p + (3*R4 + R5)*
       V_r;%mol H2/s
81 dH2O_dt =  F_0(5)-F_H2O - R3/12*V_p + (- R4 - R5)*V_r;%mol
       H2O/s
82
83
84 y = [dC_dt; dCO2_dt; dCO_dt; dCH4_dt; dH2_dt; dH2O_dt];
85
86
87 end
```

A.2.2 Raw data

Raw data corresponding to Figure 3.2 is presented in Table A.2. The conversion shows the simulated increase in % of solid carbon compared to equilibrium state.

Table A.2: Conversion of solid carbon at different particle density and surface area. Flow rate of CO 2L/min per 100g biomass.

Density [kg/m^3]	50			100			150		
Surface area [g/m^2]	200	500	1000	200	500	1000	200	500	1000
Time [min]	**Conversion %**								
0	0	0	0	0	0	0	0	0	0
30	0.076	0.190	0.380	0.152	0.380	0.758	0.228	0.569	1.135
60	0.168	0.421	0.842	0.336	0.842	1.686	0.505	1.263	2.531
90	0.221	0.555	1.114	0.443	1.114	2.250	0.667	1.681	3.401
120	0.245	0.615	1.241	0.491	1.241	2.530	0.740	1.881	3.856
150	0.254	0.642	1.301	0.512	1.301	2.678	0.773	1.983	4.111
180	0.259	0.656	1.334	0.522	1.334	2.765	0.790	2.040	4.270
210	0.261	0.663	1.352	0.527	1.352	2.820	0.799	2.075	4.373
240	0.262	0.666	1.363	0.530	1.363	2.855	0.804	2.097	4.440
270	0.263	0.668	1.370	0.532	1.370	2.877	0.806	2.110	4.483
300	0.263	0.670	1.374	0.532	1.374	2.890	0.808	2.118	4.509

Raw data corresponding to Figure 3.4 is presented in Table A.3. The conversion represents the increase in solid carbon in % compared to equilibrium state.

Table A.3: Conversion [%] of solid carbon at different flow rates of CO. Density 150kg/m^3, specific surface area 1000m^2/g.

	Flow rate of CO [L/min]					
Time [min]	**0**	**1**	**2**	**3**	**4**	**5**
0	0	0	0	0	0	0
15	-0.021	0.215	0.404	0.539	0.634	0.697
30	-0.038	0.691	1.135	1.358	1.442	1.443
45	-0.053	1.263	1.883	2.042	1.989	1.854
60	-0.066	1.876	2.531	2.509	2.294	2.046
75	-0.079	2.494	3.034	2.800	2.456	2.135
90	-0.092	3.087	3.401	2.979	2.545	2.179
105	-0.104	3.633	3.664	3.094	2.596	2.201
120	-0.117	4.115	3.856	3.171	2.627	2.211
135	-0.129	4.530	4.000	3.224	2.645	2.216
150	-0.142	4.883	4.111	3.261	2.655	2.218
165	-0.154	5.183	4.200	3.287	2.661	2.219
180	-0.166	5.439	4.270	3.305	2.664	2.219
195	-0.179	5.662	4.327	3.317	2.665	2.219
210	-0.191	5.858	4.373	3.325	2.666	2.219
225	-0.203	6.033	4.410	3.330	2.666	2.219
240	-0.215	6.189	4.440	3.333	2.666	2.219
255	-0.227	6.331	4.464	3.335	2.666	2.219
270	-0.239	6.459	4.483	3.336	2.666	2.219
285	-0.251	6.575	4.498	3.336	2.666	2.219
300	-0.263	6.682	4.509	3.337	2.666	2.219

Raw data corresponding to Figure 3.5 are presented in Table A.4-A.6.

Table A.4: Mole fraction of the five gas species at 1L/min CO per 100g biomass added to the system.

Time [min]	**CO_2**	**CO**	**CH_4**	**H_2**	**H_2O**
0	0.215	0.020	0.156	0.223	0.386
15	0.228	0.122	0.177	0.125	0.348
30	0.269	0.187	0.180	0.099	0.264
45	0.306	0.242	0.182	0.082	0.188
60	0.327	0.301	0.179	0.066	0.127
75	0.330	0.366	0.171	0.052	0.080
90	0.317	0.436	0.158	0.041	0.048
105	0.293	0.507	0.142	0.031	0.028
120	0.261	0.576	0.124	0.023	0.016
135	0.228	0.639	0.107	0.018	0.009
150	0.195	0.695	0.091	0.014	0.005
165	0.166	0.744	0.076	0.011	0.003
180	0.140	0.786	0.064	0.008	0.002
195	0.117	0.821	0.053	0.007	0.001
210	0.098	0.851	0.044	0.006	0.001
225	0.082	0.875	0.037	0.005	0.001
240	0.069	0.896	0.030	0.004	0.001
255	0.058	0.913	0.025	0.004	0.000
270	0.048	0.928	0.021	0.003	0.000
285	0.040	0.940	0.017	0.003	0.000
300	0.034	0.950	0.014	0.002	0.000

Table A.5: Mole fraction of the five gas species at 3L/min CO per 100g biomass added to the system.

Time [min]	**CO_2**	**CO**	**CH_4**	**H_2**	**H_2O**
0	0.215	0.020	0.156	0.223	0.386
15	0.217	0.336	0.150	0.073	0.224
30	0.215	0.539	0.119	0.042	0.086
45	0.166	0.701	0.083	0.023	0.027
60	0.110	0.818	0.052	0.012	0.008
75	0.067	0.893	0.031	0.007	0.002
90	0.040	0.938	0.018	0.004	0.001
105	0.023	0.964	0.010	0.002	0.000
120	0.013	0.979	0.006	0.001	0.000
135	0.008	0.988	0.003	0.001	0.000
150	0.004	0.993	0.002	0.001	0.000
165	0.003	0.996	0.001	0.000	0.000
180	0.001	0.998	0.001	0.000	0.000
195	0.001	0.999	0.000	0.000	0.000
210	0.001	0.999	0.000	0.000	0.000
225	0.000	1.000	0.000	0.000	0.000
240	0.000	1.000	0.000	0.000	0.000
255	0.000	1.000	0.000	0.000	0.000
270	0.000	1.000	0.000	0.000	0.000
285	0.000	1.000	0.000	0.000	0.000
300	0.000	1.000	0.000	0.000	0.000

Table A.6: Mole fraction of the five gas species at 5L/min CO per 100g biomass added to the system.

Time [min]	**CO_2**	**CO**	**CH_4**	**H_2**	**H_2O**
0	0.215	0.020	0.156	0.223	0.386
15	0.181	0.517	0.115	0.049	0.138
30	0.120	0.771	0.061	0.020	0.028
45	0.058	0.902	0.027	0.008	0.005
60	0.025	0.960	0.011	0.003	0.001
75	0.010	0.984	0.004	0.001	0.000
90	0.004	0.994	0.002	0.001	0.000
105	0.002	0.997	0.001	0.000	0.000
120	0.001	0.999	0.000	0.000	0.000
135	0.000	1.000	0.000	0.000	0.000
150	0.000	1.000	0.000	0.000	0.000
165	0.000	1.000	0.000	0.000	0.000
180	0.000	1.000	0.000	0.000	0.000
195	0.000	1.000	0.000	0.000	0.000
210	0.000	1.000	0.000	0.000	0.000
225	0.000	1.000	0.000	0.000	0.000
240	0.000	1.000	0.000	0.000	0.000
255	0.000	1.000	0.000	0.000	0.000
270	0.000	1.000	0.000	0.000	0.000
285	0.000	1.000	0.000	0.000	0.000
300	0.000	1.000	0.000	0.000	0.000

B Experimental

Raw data for the product yields and proximate analysis, and data sheets with the different gas development trends from all the experiment are presented in this section.

B.1 Product yield

Raw data corresponding to Table 5.1 are presented in Table B.1.

Table B.1: Amount of biomass used for each experiment and the amount of biocarbon, condensate and gas produced.

Experiment	**Biomass**	**Biocarbon**	**Condensate**	**Gas**	**Losses**
$N_2N_2480.1$	727.2	214.5	330.6	-	-
$N_2N_2480.2$	692.4	208.2	316.4	137.5	30.3
CO_2N_2480	736.4	219.5	337.2	151.4	28.3
$CO_2CO_2480.1$	687.0	204.8	308.7	-	-
$CO_2CO_2480.2$	703.1	207.1	320.9	135.7	39.4
COCO480	695.2	205.3	318.5	130.8	40.6
N_2CO480	696.5	206.2	314.2	138.3	37.8
N_2N_2580	686.7	185.8	318.4	136.2	46.3
CO_2CO_2580	711.2	192.7	280.9	163.4	74.2

B.2 Yield and gas development

The gas development per time for the major (CO_2, CO and CH_4) and minor gases (C_2H_6, C_2H_2/C_2H_4 and H_2), accumulated amount of gas, and the gas development as function of internal temperature were calculated for all the experiments. The results are presented below. The biocarbon is referred to as charcoal.

Experiment			Biomass			Weight [g]
Reference T_{hold} 480°C (N_2N_2480)			Raw spruce chips			692.4
Heating rate [°C/min]			Hold temperature [°C]			Hold time [min]
13			480			180
Yield [g]			Yield [%]			Losses [%]
Charcoal	Condensate	Gas	Charcoal	Condensate	Gas	4.4
208.2	316.2	137.5	30.1	45.7	19.9	

Gas development

As function of time – major gases

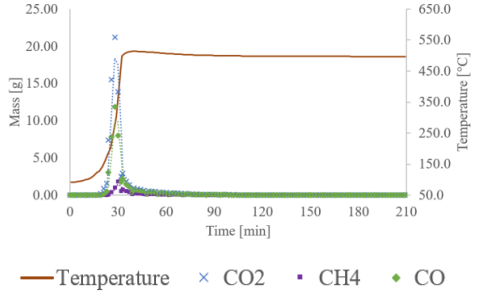

As function of time – minor gases

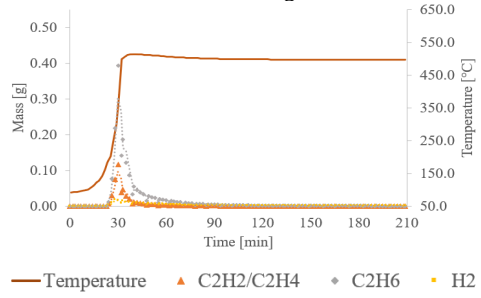

Accumulated – all gases

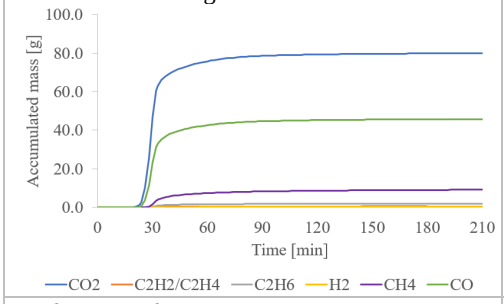

Accumulated – minor gases

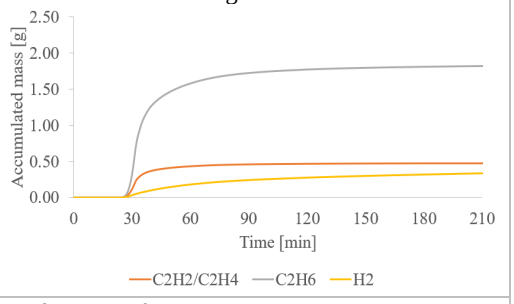

As function of temp. – all gases

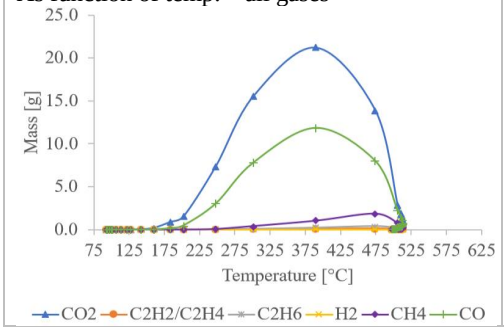

As function of temp. – Minor gases

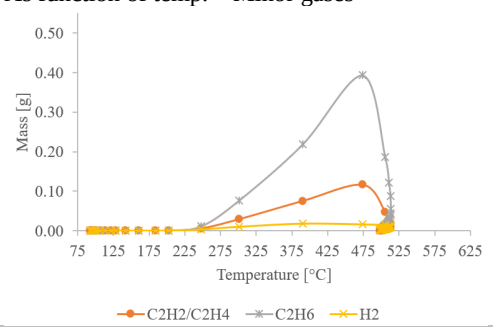

Experiment			Biomass			Weight [g]
CO_2 during heat-up ($CO_2N_2$480)			Raw spruce chips			736.4
Heating rate [°C/min]			Hold temperature [°C]			Hold time [min]
13			480			180
Yield [g]			Yield [%]			Losses [%]
Charcoal	Condensate	Gas	Charcoal	Condensate	Gas	3.8
219.5	337.2	151.4	29.8	45.8	20.6	

Gas development

As function of time – major gases

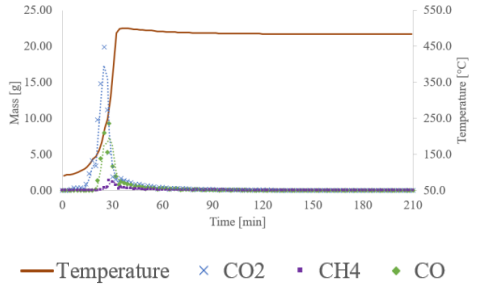

As function of time – minor gases

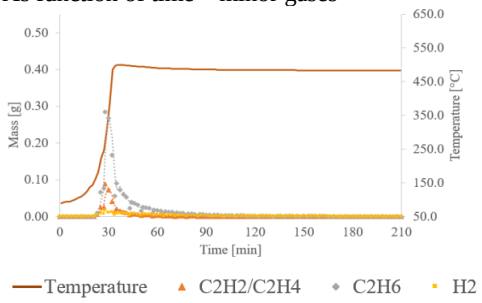

Accumulated – all gases

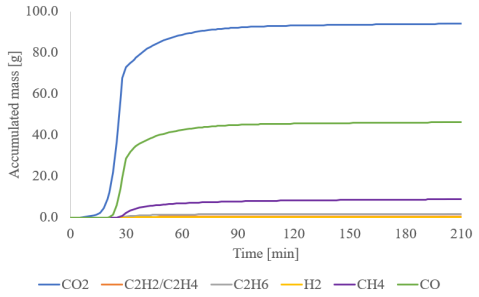

Accumulated – minor gases

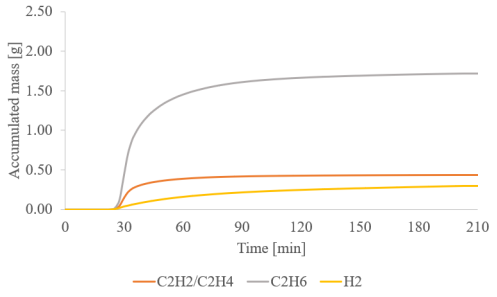

As function of temp. – all gases

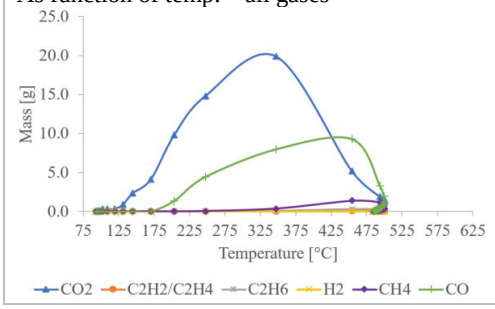

As function of temp. – Minor gases

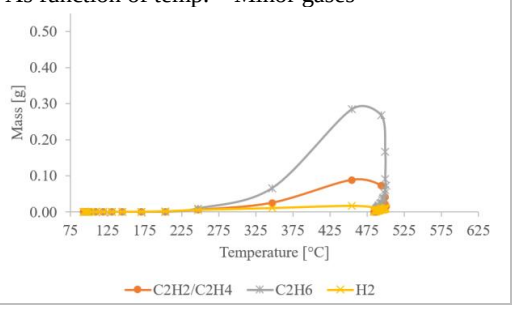

Experiment			Biomass			Weight [g]
CO_2 T_{hold} 480°C (CO_2CO_2480)			Raw spruce chips			703.1
Heating rate [°C/min]			Hold temperature [°C]			Hold time [min]
13			480			180
Yield [g]			Yield [%]			Losses [%]
Charcoal	Condensate	Gas	Charcoal	Condensate	Gas	5.6
207.1	320.9	135.7	29.5	45.6	19.3	
Gas development						

As function of time – major gases

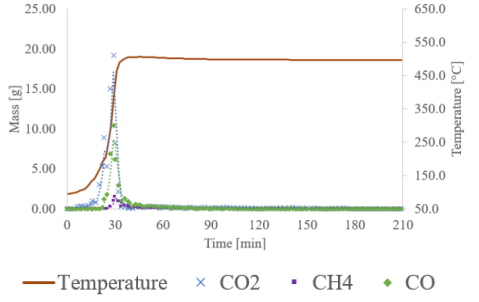

As function of time – minor gases

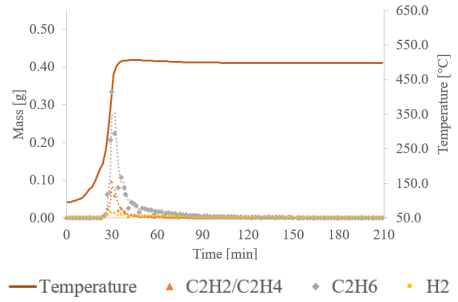

Accumulated – all gases

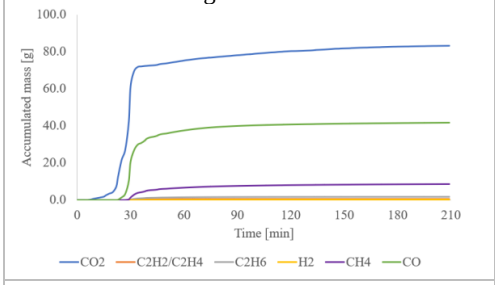

Accumulated – minor gases

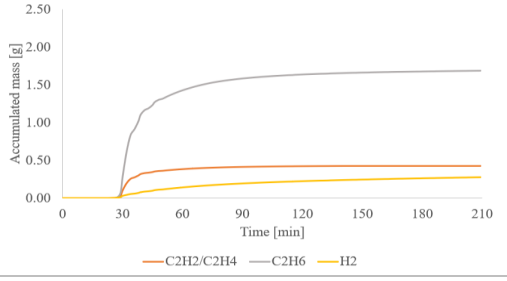

As function of temp. – all gases

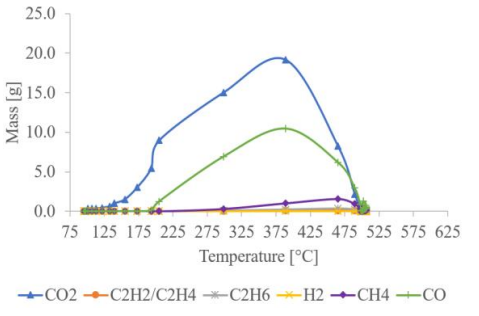

As function of temp. – Minor gases

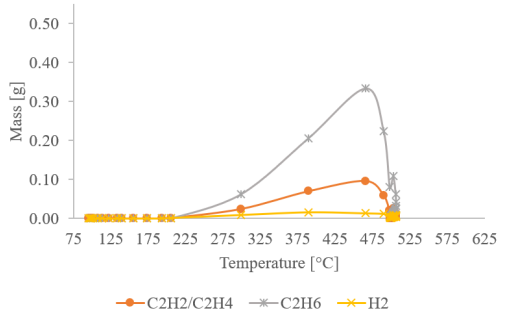

Experiment			Biomass			Weight [g]
CO T_{hold} 480°C (COCO480)			Raw spruce chips			695.2
Heating rate [°C/min]			Hold temperature [°C]			Hold time [min]
13			480			180
Yield [g]			Yield [%]			Losses [%]
Charcoal	Condensate	Gas	Charcoal	Condensate	Gas	5.8
205.3	318.5	130.8	29.5	45.8	18.8	

Gas development

As function of time – major gases

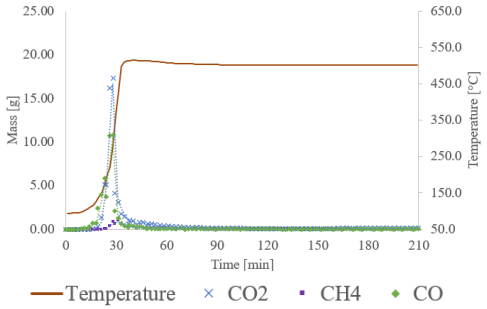

As function of time – minor gases

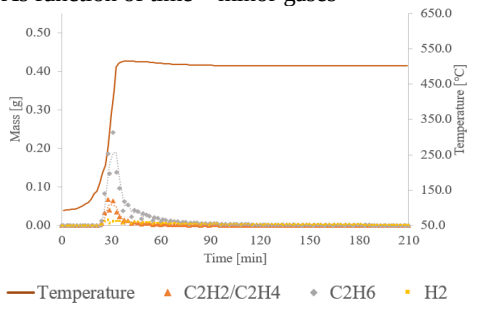

Accumulated – all gases

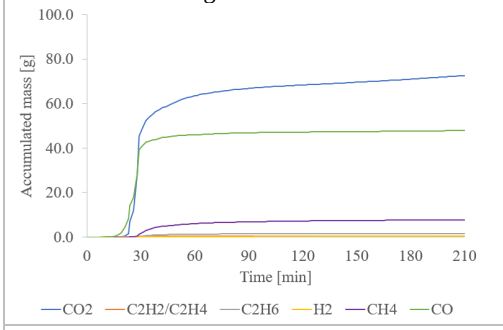

Accumulated – minor gases

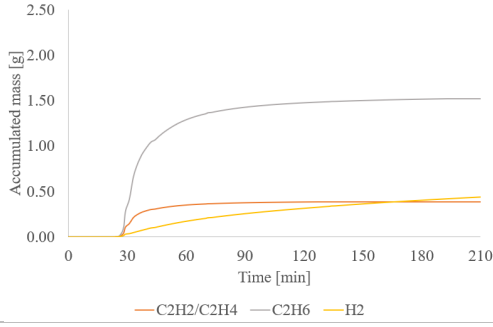

As function of temp. – all gases

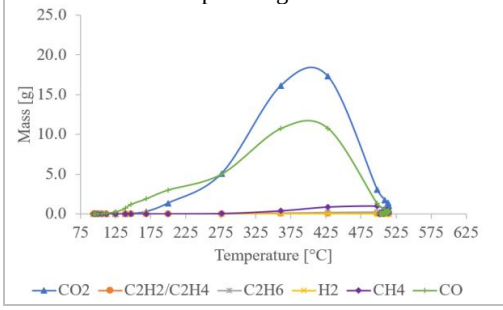

As function of temp. – Minor gases

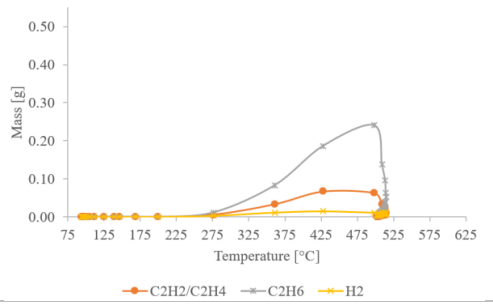

Experiment			Biomass			Weight [g]
CO during hold phase (N_2CO480)			Raw spruce chips			696.5
Heating rate [°C/min]			Hold temperature [°C]			Hold time [min]
13			480			140
Yield [g]			Yield [%]			Losses [%]
Charcoal	Condensate	Gas	Charcoal	Condensate	Gas	5.4
206.2	314.2	138.3	29.6	45.1	19.9	
Gas development						

As function of time – major gases

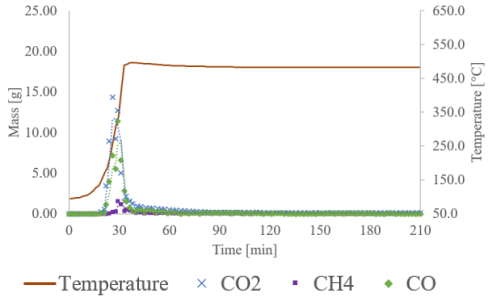

As function of time – minor gases

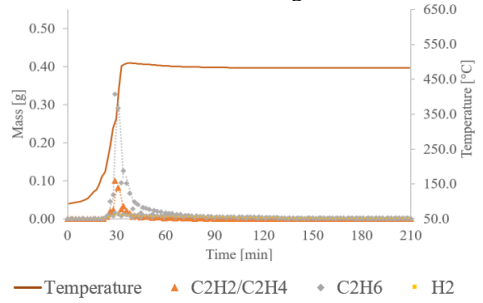

Accumulated – all gases

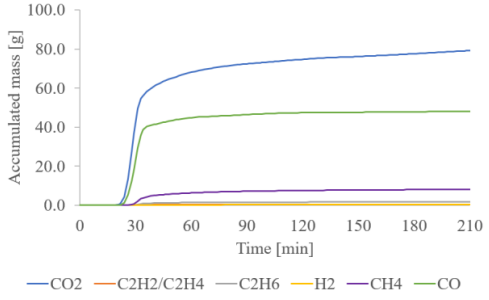

Accumulated – minor gases

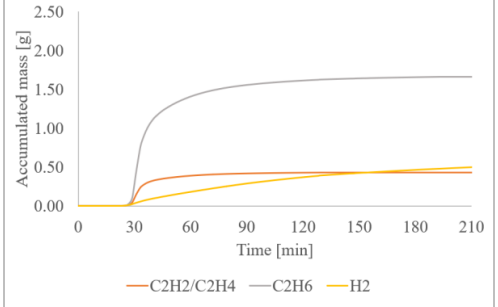

As function of temp. – all gases

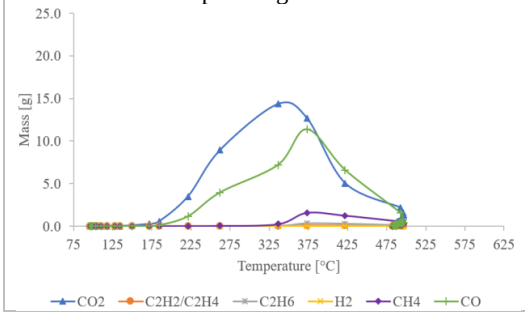

As function of temp. – Minor gases

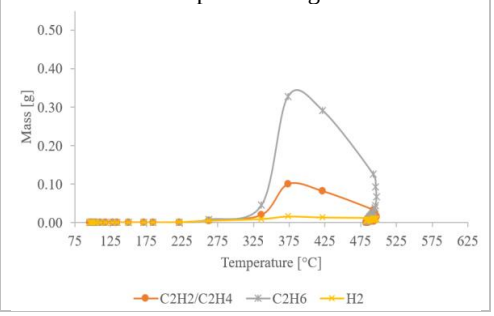

Experiment			Biomass			Weight [g]
Reference T_{hold} 580°C (N_2N_2580)			Raw spruce chips			686.7
Heating rate [°C/min]			Hold temperature [°C]			Hold time [min]
13			580			180
Yield [g]			Yield [%]			Losses [%]
Charcoal	Condensate	Gas	Charcoal	Condensate	Gas	6.7
185.8	318.4	136.2	27.1	46.4	19.8	

Gas development

As function of time – major gases

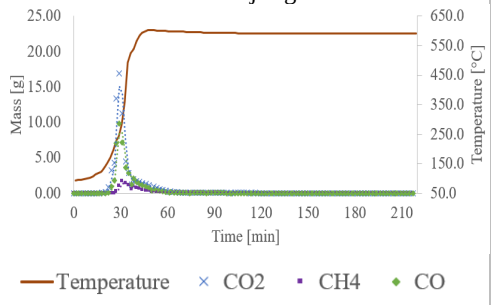

As function of time – minor gases

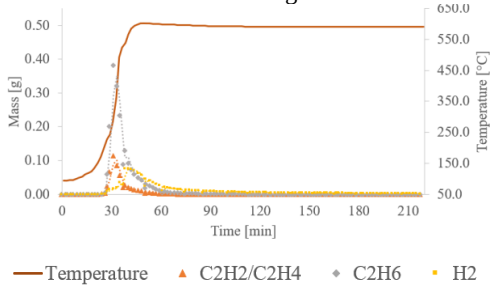

Accumulated – all gases

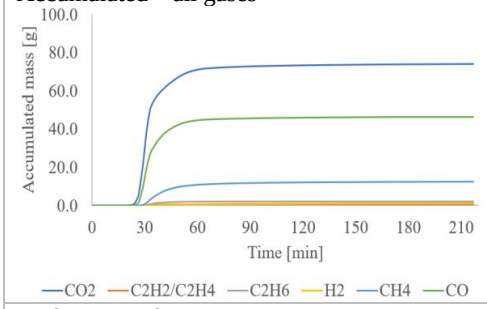

Accumulated – minor gases

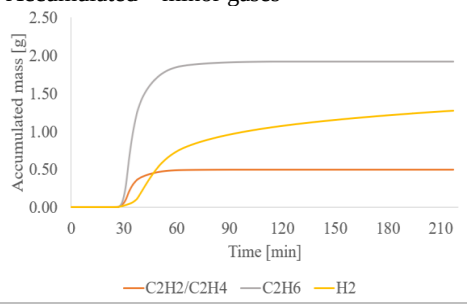

As function of temp. – all gases

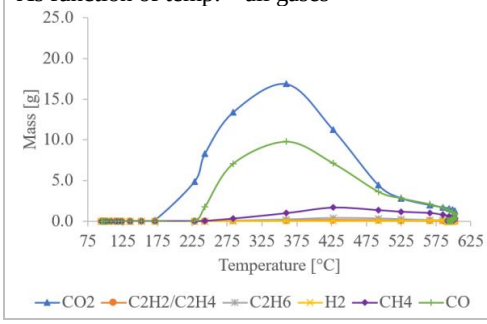

As function of temp. – Minor gases

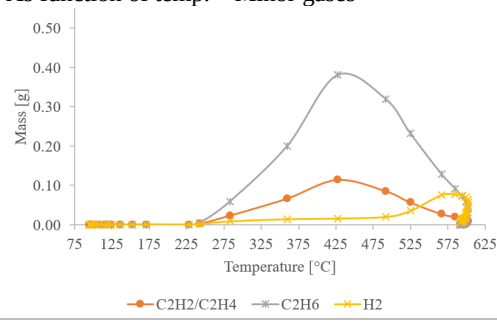

Experiment			Biomass			Weight [g]
CO_2 T_{hold} 580°C (CO_2CO_2580)			Raw spruce chips			686.7
Heating rate [°C/min]			Hold temperature [°C]			Hold time [min]
13			580			180
Yield [g]			Yield [%]			Losses [%]
Charcoal	Condensate	Gas	Charcoal	Condensate	Gas	10.4
192.7	280.9	163.4	27.1	39.5	23.0	
Gas development						

As function of time – major gases

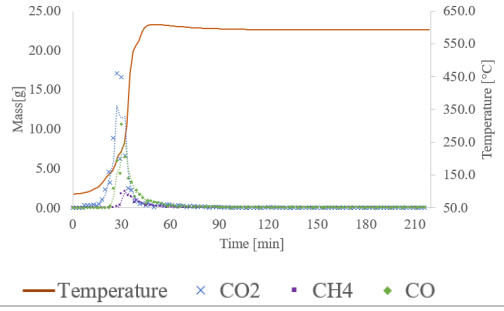

As function of time – minor gases

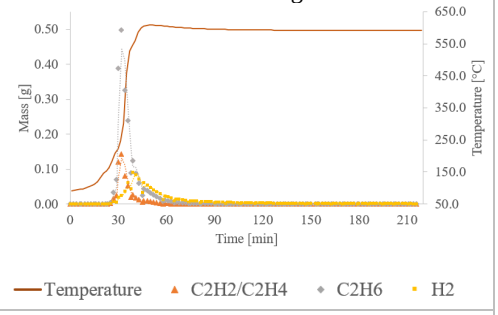

Accumulated – all gases

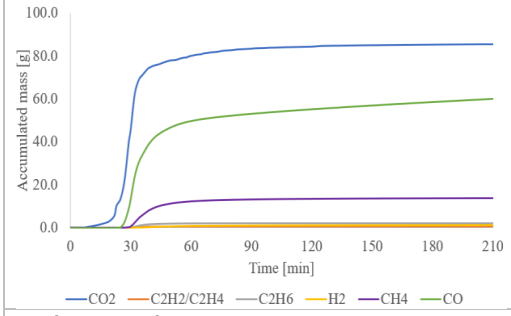

Accumulated – minor gases

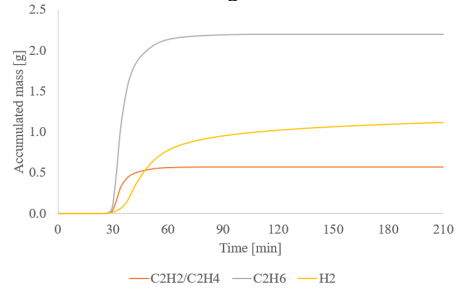

As function of temp. – all gases

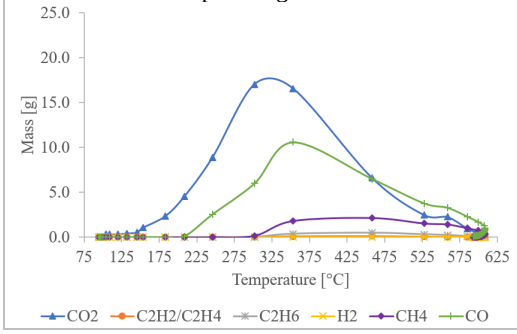

As function of temp. – Minor gases

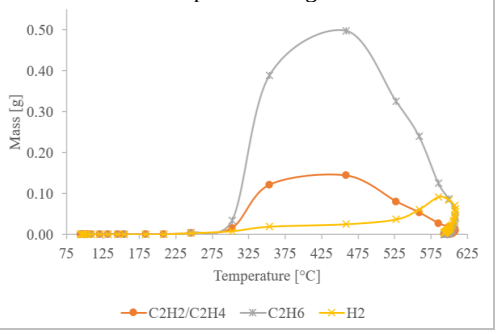

B.3 Proximate analysis

Raw data corresponding to Table 5.2 are presented in Table B.2.

Table B.2: Raw data obtained from the proximate analysis used to determine moisture, volatile, fixed carbon and ash content.

Sample	Dried biomass	N_2N_2480 $1^{st}/2^{nd}$	N_2N_2580	CO_2N_2480	CO_2CO_2480 $1^{st}/2^{nd}$	CO_2CO_2580	N_2CO480	$COCO480$
Mass raw sample [g]	0.913	0.947/1.139	1.036	0.987	0.947/1.047	1.052	1.108	0.996
	0.930	0.909/0.942	0.937	1.092	0.947/0.910	0.972	0.956	0.946
	0.934	0.922/0.945	0.911	0.940	0.978/1.074	0.996	0.922	0.934
Mass after drying at 105°C [g]	0.894	0.935/1.119	1.032	0.975	0.941/1.039	1.042	1.100	0.988
	0.908	0.898/0.930	0.935	1.079	0.941/0.899	0.962	0.950	0.939
	0.909	0.911/0.931	0.910	0.928	0.972/1.063	0.987	0.917	0.929
Mass after drying at 950°C [g]	0.130	0.716/0.905	0.914	0.775	0.821/0.870	0.885	0.930	0.821
	0.129	0.698/0.749	0.842	0.900	0.798/0.755	0.863	0.793	0.770
	0.126	0.704/0.750	0.800	0.813	0.798/0.893	0.936	0.761	0.760
Mass after drying at 750°C [g]	0.003	0.014/0.026	0.012	0.019	0.017/0.009	0.016	0.024	0.010
	0.002	0.014/0.017	0.010	0.021	0.014/0.009	0.015	0.019	0.010
	0.002	0.014/0.020	0.009	0.018	0.013/0.013	0.015	0.017	0.010